



8-2011

Continuously Variable Rotorcraft Propulsion System: Modelling and Simulation

Naveen Kumar Vallabhaneni
nvallabh@utk.edu

Recommended Citation

Vallabhaneni, Naveen Kumar, "Continuously Variable Rotorcraft Propulsion System: Modelling and Simulation." Master's Thesis, University of Tennessee, 2011.
https://trace.tennessee.edu/utk_gradthes/1033

This Thesis is brought to you for free and open access by the Graduate School at Trace: Tennessee Research and Creative Exchange. It has been accepted for inclusion in Masters Theses by an authorized administrator of Trace: Tennessee Research and Creative Exchange. For more information, please contact trace@utk.edu.

To the Graduate Council:

I am submitting herewith a thesis written by Naveen Kumar Vallabhaneni entitled "Continuously Variable Rotorcraft Propulsion System: Modelling and Simulation." I have examined the final electronic copy of this thesis for form and content and recommend that it be accepted in partial fulfillment of the requirements for the degree of Master of Science, with a major in Aerospace Engineering.

Hans August Desmidt, Major Professor

We have read this thesis and recommend its acceptance:

Xiaopeng Zhao, Kivanc Ekici

Accepted for the Council:

Dixie L. Thompson

Vice Provost and Dean of the Graduate School

(Original signatures are on file with official student records.)

CONTINUOUSLY VARIABLE ROTORCRAFT
PROPULSION SYSTEM:
MODELLING AND SIMULATION

A Thesis Presented for the
Master of Science
Degree
The University of Tennessee, Knoxville

Naveen Kumar Vallabhaneni
August 2011

All rights reserved.

DEDICATION

Dedicated to my parents.

ACKNOWLEDGEMENT

First and foremost, I would like to express my sincere thanks to my advisor Dr.Hans Desmidt. His guidance and patience during the course of my graduate experience have been invaluable. His discipline, attention to details, and emphasis on clear communication, are a few qualities that I hope, I have adopted during our association. I am grateful to Dr.Kivanc Ekici and Dr.Xiaopeng Zhao for serving on my research committee. This work was supported under NASA Grant #NNX07AC58A, with Technical Monitors Dr. Robert F. Handschuh and Dr. David G. Lewicki.

It gives me great joy to thank my family who has supported me in all my endeavors with love and pride. I am forever indebted to my friends and colleagues who have provided the memories of a lifetime.

ABSTRACT

This study explores the variable speed operation and shift response of a prototype of a continuously variable rotorcraft propulsion system. Here a Comprehensive Variable Speed Rotorcraft Propulsion system Modeling (CVSRPM) tool is developed and utilized to simulate the drive system dynamics in steady forward speed condition. This investigation attempts to build upon previous variable speed rotorcraft propulsion studies by:

- 1) Including fully nonlinear first principles based transient gas-turbine engine model
- 2) Including shaft flexibility
- 3) Incorporating a basic flight dynamics model to account for interactions with the flight control system.

Through exploring the interactions between the various subsystems, this analysis provides important insight into the continuing development of variable speed rotorcraft propulsion systems.

TABLE OF CONTENTS

| | |
|---|----|
| 1. INTRODUCTION AND LITERATURE SURVEY | 14 |
| 1.1 INTRODUCTION AND MOTIVATION..... | 14 |
| 1.2 VARIABLE RATIO TRANSMISSIONS..... | 2 |
| 1.3 RESEARCH OBJECTIVES AND SIGNIFICANCE..... | 2 |
| 2. GAS TURBINE ENGINE MODEL..... | 4 |
| 2.1 INTRODUCTION..... | 4 |
| 2.2 TRANSIENT GAS TURBINE ENGINE MODEL..... | 4 |
| 2.3 ENGINE NOMINAL DESIGN..... | 9 |
| 2.4 COMPRESSOR AND TURBINE DESIGN..... | 10 |
| 2.5 ANALYTICAL CALCULATION OF OFF-NOMINAL CHARACTERISTIC MAPS | 14 |
| 2.6 REPRESENTATION OF COMPRESSOR AND TURBINE MAPS IN COMPUTER PROGRAM..... | 22 |
| 2.7 ENGINE CLOSED-LOOP FUEL CONTROL..... | 24 |
| 2.8 TRANSIENT GAS TURBINE ENGINE SIMULATION | 25 |
| 3. IDEAL CVT SYSTEM/GEARBOX DYNAMIC MODEL | 30 |
| 3.1 INTRODUCTION..... | 30 |
| 3.2 SINGLE PATH DRIVELINE OF AN IDEAL CVT SYSTEM | 31 |
| 3.3 FORWARD FLIGHT ROTOR (PROPELLER) MODEL..... | 34 |
| 3.4 CONTROL SYSTEM | 36 |
| 4. RESULTS, CONCLUSIONS AND FUTURE SCOPE..... | 39 |
| 4.1 INTRODUCTION..... | 39 |
| 4.2 COMPREHENSIVE VARIABLE SPEED ROTORCRAFT PROPULSION SYSTEM MODEL | 39 |
| 4.3 RESULTS | 41 |
| 4.4 FUTURE SCOPE | 48 |
| 4.5 CONCLUSIONS | 48 |
| BIBLIOGRAPHY..... | 50 |
| CHAPTER 1..... | 51 |
| CHAPTER 2..... | 53 |
| CHAPTER 3..... | 53 |
| CHAPTER 4..... | 55 |
| APPENDIX..... | 56 |
| VITA..... | 92 |

LIST OF TABLES

| TABLE | PAGE |
|--|-------------|
| TABLE 1. NOMINAL DESIGN PARAMETERS..... | 9 |
| TABLE 2. COMPRESSOR DESIGN PARAMETERS..... | 13 |
| TABLE 3. FUEL CONTROL GAINS AND NOMINAL FUEL RATE..... | 24 |
| TABLE 4. ROTOR PARAMETERS..... | 36 |

LIST OF FIGURES

| | |
|---|----|
| FIGURE 1.1 SOME CURRENT ROTORCRAFT EMPLOYING A VARIABLE SPEED ROTOR..... | 1 |
| FIGURE 1.2 COMPREHENSIVE VARIABLE SPEED ROTORCRAFT PROPULSION SYSTEM ELEMENTS..... | 2 |
| FIGURE 2.1 TWO SPOOL GAS TURBINE ENGINE SYSTEM COMPONENTS AND ANALYSIS STATIONS. | 5 |
| FIGURE 2.2 PLENUM CHAMBER ELEMENT..... | 7 |
| FIGURE 2.3 COMBUSTION CHAMBER CONTROL VOLUME..... | 8 |
| FIGURE 2.4 EIGHT-STAGE AXIAL COMPRESSOR WITH IGV AND EGV AND CONSTANT MEAN RADIUS..... | 10 |
| FIGURE 2.5 COMPRESSOR STAGE AND FLOW VELOCITY TRIANGLES..... | 11 |
| FIGURE 2.6 COMPRESSOR HUB AND TIP RADIUS | 13 |
| FIGURE 2.7 ASSUMED FLOW ANGLE DEVIATIONS FOR OFF-NOMINAL OPERATION..... | 14 |
| FIGURE 2.8 CALCULATED COMPRESSOR PRESSURE RATIO CHARACTERISTIC MAP..... | 16 |
| FIGURE 2.9 CALCULATED COMPRESSOR EFFICIENCY CHARACTERISTIC MAP | 17 |
| FIGURE 2.10 PRESSURE RATIO CHARACTERISTIC MAPS WITH VARYING SCALING PARAMETER ε | 17 |
| FIGURE 2.11 GAS GENERATOR AND POWER TURBINE CONTROL VOLUMES..... | 18 |
| FIGURE 2.12 GAS GENERATOR TURBINE CHARACTERISTIC MAP..... | 20 |
| FIGURE 2.13 GAS GENERATOR TURBINE INPUTS FOR OFF NOMINAL CALCULATIONS..... | 21 |
| FIGURE 2.14 SIMULINK MODEL FOR GENERATION OF \dot{m} , PR , η FOR GIVEN Ω AND β LINE VALUES..... | 22 |
| FIGURE 2.15 LOOKUP TABLES AND CORRESPONDING PR , \dot{m} AND η_c VERSUS β LINES PLOTS..... | 23 |
| FIGURE 2.16 ENGINE WITH CLOSED LOOP PID CONTROL | 24 |
| FIGURE 2.17 GAS TURBINE ENGINE WITH FUEL CONTROL BLOCK..... | 25 |
| FIGURE 2.18 TWO SPOOL GAS TURBINE ENGINE SIMULATION BLOCK..... | 26 |
| FIGURE 2.19 COMPRESSOR SIMULATION BLOCK..... | 27 |
| FIGURE 2.20 INTER COMPRESSOR/COMBUSTION CHAMBER PLENUM..... | 27 |
| FIGURE 2.21 COMBUSTION CHAMBER SIMULATION BLOCK..... | 28 |
| FIGURE 2.22 GAS GENERATOR TURBINE SIMULATION BLOCK..... | 28 |
| FIGURE 2.23 INTER TURBINE PLENUM..... | 29 |

| | |
|--|----|
| FIGURE 2.24 POWER TURBINE SIMULATION BLOCK..... | 29 |
| FIGURE 3.1 SINGLE PATH DRIVELINE OF AN IDEAL CVT MODEL CONNECTED TO A GAS TURBINE ENGINE..... | 31 |
| FIGURE 3.2 SINGLE PATH CVT TORSIONAL DYNAMIC MODEL..... | 31 |
| FIGURE 3.3 CONTINUOUSLY VARIABLE TRANSMISSION BLOCK..... | 33 |
| FIGURE 3.4 PROPELLER IN FORWARD FLIGHT..... | 34 |
| FIGURE 3.5 ROTOR THRUST AND TORQUE SIMULATION BLOCK..... | 36 |
| FIGURE 3.6 COMPREHENSIVE VARIABLE SPEED ROTORCRAFT PROPULSION MODEL..... | 37 |
| FIGURE 3.7 FORWARD SPEED CONTROLLER BLOCK..... | 38 |
| FIGURE 3.8 BLADE PITCH CONTROLLER BLOCK..... | 38 |
| FIGURE 4.1 COMPREHENSIVE VARIABLE SPEED ROTORCRAFT PROPULSION SYSTEM MODEL..... | 40 |
| FIGURE 4.2 TWO SPEED HELICOPTER DRIVE SYSTEM SIMULATION MODEL..... | 40 |
| FIGURE 4.3 SLOWED ROTOR/STEADY CRUISE-SIMULATED MISSION PROFILE..... | 41 |
| FIGURE 4.4 SPEED RESPONSE FOR SLOWED ROTOR/STEADY CRUISE..... | 42 |
| FIGURE 4.5 TORQUE RESPONSE FOR SLOWED ROTOR/STEADY CRUISE..... | 43 |
| FIGURE 4.6 INDUCED VELOCITY AND BLADE PITCH RESPONSE..... | 44 |
| FIGURE 4.7 SLOWED ROTOR/HIGH-SPEED CRUISE SIMULATED MISSION PROFILE..... | 44 |
| FIGURE 4.8 INDUCED VELOCITY AND BLADE PITCH RESPONSE | 46 |
| FIGURE 4.9 TORQUE RESPONSE FOR SLOWED ROTOR/ HIGH-SPEED CRUISE..... | 47 |
| FIGURE 4.10 SPEED RESPONSE FOR SLOWED ROTOR/ HIGH-SPEED CRUISE..... | 48 |

NOMENCLATURE

| Symbols | Description |
|------------|-------------------------------------|
| A_1 | cross-sectional area at rotor inlet |
| A_2 | cross-sectional area at rotor exit |
| A_3 | cross-sectional area at stator exit |
| a | local speed of sound in a medium |
| C_1 | absolute velocity at rotor inlet |
| C_2 | absolute velocity at rotor exit |
| C_3 | absolute velocity at stator exit |
| C_{a_1} | axial velocity at rotor inlet |
| C_{a_2} | axial velocity at rotor outlet |
| C_{a_3} | axial velocity at stator outlet |
| c | rotor chord |
| c_D | blade section drag coefficient |
| c_p | specific heat at constant pressure |
| c_v | specific heat at constant volume |
| dD | blade drag force increment |
| dFT_{MR} | incremental main rotor thrust |
| dL | blade lift force increment |
| dTQ_{MR} | incremental main rotor torque |
| EGV | Exit guide vanes |
| e | error |
| FT_{MR} | total main rotor thrust |
| f | fuel-air ratio |
| IGV | Inlet guide vanes |
| J | rotational inertia |
| J_e | rotational inertia of engine |
| J_{g_1} | rotational inertia of CVT gear 1 |
| J_{g_2} | rotational inertia of CVT gear 2 |
| J_{MR} | rotational inertia of main rotor |
| K_{S_1} | torsional stiffness of shaft 1 |

| | |
|-----------------------|---|
| K_{s_2} | torsional stiffness of shaft 2 |
| kf_b | anti-windup gain |
| kf_d | derivative gain |
| kf_i | integral gain |
| kf_p | proportional gain |
| LHV | lower heating value |
| M | mass |
| Ma | mach number |
| \dot{m} | mass flow rate |
| $\widehat{\dot{m}}_f$ | fuel flow deviation |
| \dot{m}_{fn} | nominal fuel rate |
| N | Number of stages |
| N_b | number of blades |
| n (or) Ω | shaft rotational speed |
| PR | pressure ratio |
| P_a | ambient pressure |
| P_0 | stagnation pressure |
| P_{0_1} | inlet stagnation pressure of compressor |
| P_{0_2} | outlet stagnation pressure of compressor |
| P_{0_3} | outlet stagnation pressure of plenum 1 |
| P_{0_4} | outlet stagnation pressure of combustion chamber |
| P_{0_5} | outlet stagnation pressure of gas generator turbine |
| P_{0_6} | outlet stagnation pressure of plenum 2 |
| P_{0_7} | outlet stagnation pressure of power turbine |
| p | pressure |
| p_1 | plenum 1 |
| p_2 | plenum 2 |
| pt | power turbine |
| Q | heat added |
| R | gas constant |
| R_b | rotor radius |
| R_m | mean radius |
| r | blade radial location |
| r_c | overall compressor temperature ratio |
| T | system kinetic energy |
| T_e | engine(power turbine) torque |
| T_{0_1} | inlet stagnation temperature of compressor |
| T_{0_2} | outlet stagnation pressure of compressor |
| T_{0_3} | outlet stagnation temperature of plenum 1 |
| T_{0_4} | outlet stagnation temperature of combustion chamber |

| | |
|---------------------|--|
| T_{0_5} | outlet stagnation temperature of gas generator turbine |
| T_{0_6} | outlet stagnation temperature of plenum 2 |
| T_{0_7} | outlet stagnation temperature of power turbine |
| t | time |
| TQ_{MR} | total main rotor torque |
| U | mean line rotor speed |
| U | total strain energy |
| u | internal energy |
| V | volume |
| V_1 | relative velocity at rotor inlet |
| V_2 | relative velocity at stator inlet |
| V_3 | relative velocity at stator exit |
| \dot{W} | power |
| α_1 | flow angle at rotor inlet |
| α_2 | flow angle at rotor outlet |
| α_3 | flow angle at stator outlet |
| β | beta line value |
| β_1 | relative flow angle at rotor inlet |
| β_2 | relative flow angle at rotor exit |
| β_3 | relative flow angle at stator exit |
| β_c (or) PR | pressure ratio |
| γ | specific heat ratio = c_p / c_v |
| ΔT | temperature change |
| ΔT_0 | stagnation temperature rise |
| $\Delta\beta_{n,k}$ | rotor entrance flow deviation angle |
| δP | virtual work done by the system |
| η | isentropic efficiency |
| θ_p | blade pitch |
| λ_{ind} | induced flow ratio |
| μ_{ht} | hub-to-tip ratio |
| v_c | vehicle forward speed |
| v_{ind} | induced inflow velocity |
| ρ_{air} | air density |
| $\dot{\rho}$ | rate of change of density |
| σ | rotor solidity ratio |
| v_T | tangential blade speed |
| ϕ | total inflow angle |
| ϕ_0 | rotation at initial gear |
| $\hat{\phi}_1$ | rotation of shaft 1 |
| $\hat{\phi}_2$ | rotation of shaft 2 |

| | |
|--------------|---------------------------|
| ϕ_{MR} | main rotor(load) rotation |
| ϕ_e | engine rotation |
| ϕ_f | rotation at final gear |
| ϕ_{g_1} | CVT gear 1 rotation |
| ϕ_{g_2} | CVT gear 2 rotation |
| ϕ_{ind} | induced inflow angle |

Subscripts

| | |
|------------|--------------------|
| a | air |
| a (or) amb | ambient conditions |
| c | compressor |
| cc | combustion chamber |
| cool | cooling air |
| des | design-point |
| f | fuel |
| gg | gas generator |
| in | inlet |
| init | initial |
| n | nominal |
| off | off nominal |
| out | outlet |

1. INTRODUCTION AND LITERATURE SURVEY

1.1 INTRODUCTION AND MOTIVATION

According to a recent NASA-Army-Industry-University investigation, significant benefits to rotorcraft operational performance, effectiveness and acoustic signature could be gained through the ability to adjust main rotor speed to accommodate various flight conditions [1]. In particular, variable speed rotor technology is critical to the slowed-rotor compound configuration concepts and would offer significant benefits to future Heavy-Lift helicopter and tilt rotor configurations as well as variable diameter rotor concepts [2]. Current rotorcraft propulsion systems are designed around a fixed-ratio transmission without the capability to vary rotor speed except by engine speed adjustment. Figure 1 shows several examples of rotorcraft, which are required to adjust their rotor speeds over a certain portion of their operating, envelop. In these cases, the rotor RPM variations are archived through engine speed adjustments alone.



Figure 1.1 Some current rotorcraft employing a variable speed rotor (achieved with engine speed variations); (a) Bell-Boeing V-22, (b) A169 Humming Bird UA, (c) Eurocopter EC130

Since the specific fuel consumption of modern gas-turbine engines is optimum within a relatively narrow speed range, the ability to achieve a variable speed rotor through engine speed adjustment is limited [3]. Therefore, to fully benefit from variable rotor speed designs, some form of variable ratio transmission becomes necessary.

1.2 VARIABLE RATIO TRANSMISSIONS

Recently, there have been many investigations concerning variable ratio transmissions for rotorcraft [2-4]. We refer the reader to [3] for an extensive survey of variable speed transmission concepts. For rotorcraft applications, both two-speed transmission and traction-drive Continuously Variable Transmission (CVT) concepts have been explored. [3-5]. Also referenced are investigations on other applications, such as wind-turbines and automotive drivetrains [5-10]. The success of these investigations adds further motivation to develop and implement variable speed rotorcraft concepts. There have been numerous studies concerning various, ideally driven, propulsion system components. To note a few, [11-16] explored rotor blade dynamics and aeromechanics, [17-24] studied flexible driveshaft vibration and stability issues, and [25-28] explored closed-loop fuel control and modeling techniques for gas turbine engines. Also, many coupled rotorcraft engine/drivetrain/rotor system analyses have been conducted for constant rotor speed propulsion systems, [29-32].

1.3 RESEARCH OBJECTIVES AND SIGNIFICANCE

The overall goal of this program is to develop first principles-based, comprehensive rotorcraft propulsion system modeling and analysis tools to account for dynamical interactions between engine, rotor, gearbox and an ideal CVT system.

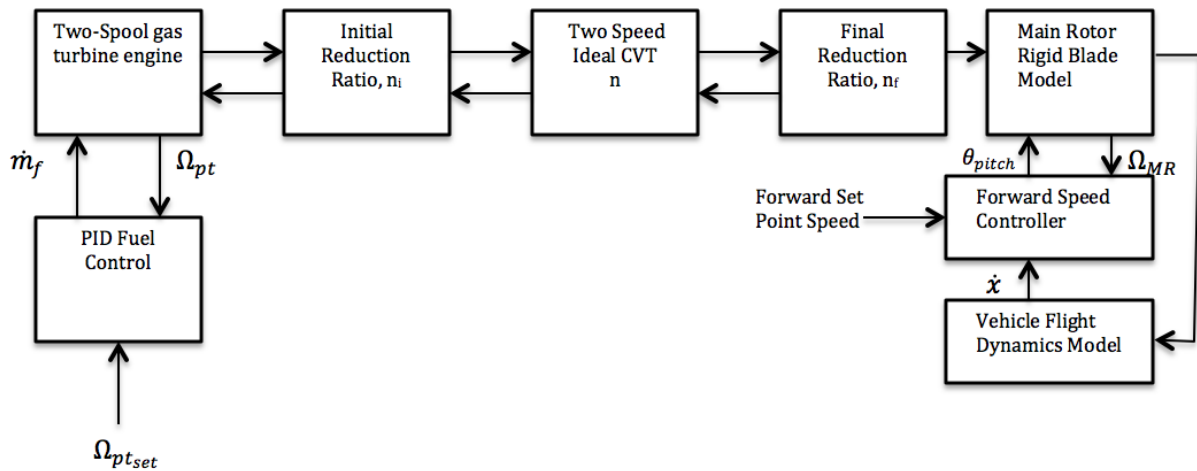


Figure 1.2 Comprehensive variable speed rotorcraft propulsion system elements

The variable speed rotorcraft propulsion system components and their interactions which are considered in this project are summarized in Figure 1.2. Through the comprehensive analysis, another goal is to gain insight into the complex system-level and component-level transient responses under a variety of variable speed operating conditions and gear shifting scenarios.

To fully benefit from the variable speed rotor concept and ensure efficient, reliable, highly loaded propulsion system designs, a complete understating of the effects of: (a) variable speed operation and (b) variable ratio transmissions designs on the overall propulsion system dynamics must be obtained. To address these issues, the objective of the proposed study is to analytically develop and experimentally validate a comprehensive dynamics model of a variable speed rotorcraft propulsion system including engine/transmission/rotor interactions. Incorporating recent developments such as, low-order turbine engine throttle response models, multi-segment flexible driveshaft models and variable ratio transmission concepts into a single analysis will advance the state of the art and yield new knowledge about the overall variable speed propulsion system dynamics.

By accounting for the various propulsion sub-system dynamic interactions, the proposed Comprehensive Variable Speed Rotorcraft Propulsion System Model (CVSRPM) will allow better performance prediction, give new design insights and enable system level optimization of (a) conventional constant speed helicopter propulsion systems and (b) novel variable speed rotorcraft propulsion systems. Furthermore, this research will create analytical and computational tools for analyzing the resulting non-linear, time-varying, comprehensive propulsion system model. Finally, given the current trend toward tandem, tilt-rotor, multi-rotor, and co-axial rotor/pusher-prop configurations with numerous cross-shafting and multi-path power flow arrangements (e.g. Boeing CH-47 and V-22, Sikorsky X-2 High Speed Lifter and Heavy Lift quad tilt rotor concepts), the CVSRPM code can be utilized to investigate and compare these different configurations for fixed and variable speed design cases under a variety of operating conditions.

2. GAS TURBINE ENGINE MODEL

2.1 INTRODUCTION

In order to simulate the variable speed operation of the rotorcraft driveline, a gas turbine engine model has been developed. In general the gas turbine will undergo transient operations due to startups, changing loads, and sudden shutdowns. Here the main focus is to capture the effects due to sudden load changes which will be encountered during gear changes.

In the area of transient gas turbine engine modeling several researchers have explored techniques based on linearization models about the nominal operating conditions. Here the model Jacobian is estimated and the engine response about the nominal is computed [1, 2]. However, such approaches are not valid for significant deviations about nominal which could be expected during severe or sudden operational load changes. More recently engine models based on the fully nonlinear aero-thermal relations have been developed [3 - 9]. In these models, the nonlinear aero-thermal equations have been solved using various Newton-Raphson based methods. Such iterative solving procedures have been further explored by [10] where it was found that the iterative nature was problematic for real-time simulations due to slow convergence times. To address this, others have proposed non-iterative simulations techniques based on forward substitution methods [11]. Still others have utilized simplified compressor and turbine models which do not rely on engine maps allowing explicit solutions without the need for iteration at the expense of reduced simulation fidelity [12].

The gas turbine engine model developed in this investigation is a nonlinear mechanical-aero-thermal model with lumped representation of the gas turbine components. The solution approach is based on non-iterative forward substitution similar to [11] together with a new analytical method to explicitly compute the compressor and turbine performance maps. One key feature for a transient model is that the mass flow through each component is not the same. For example, at any instant the compressor and turbine could induce different mass flows depending on the instantaneous upstream and downstream pressures across each component. To account for this plenum chamber elements are included between each component to accommodate these transient differential mass flows and density changes. The mechanical-aero-thermal equations are implemented in the Matlab® Simulink™ environment for use as a module in the comprehensive variable speed drive system simulation.

2.2 TRANSIENT GAS TURBINE ENGINE MODEL

To simulate the effect of the engine and fuel control system dynamics during variable speed rotor operation, a generic twin spool gas turbine model is developed. The components of this model are shown in Figure 2.1. The components included in this analytical model are axial compressor, combustor, gas-generator turbine, power turbine and two mass accumulators (plenums). The torque balances between the compressor and gas generator turbine as well as between the power turbine and the load have also been included and the physical and thermodynamic laws [6] have been utilized to describe the system dynamics. This analytical model is then implemented in the MATLAB/Simulink environment. The thermodynamic model is based on the standard idealized Joule/Brayton cycle [1]. The main assumptions made in this analytical model can be summarized as follows:

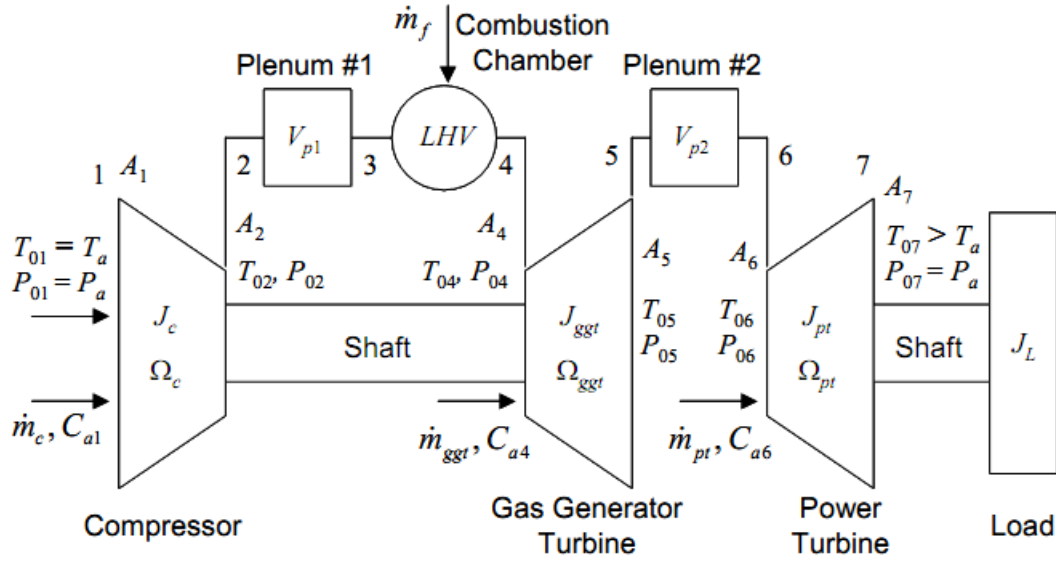


Figure 2.1 Two spool gas turbine engine system components and analysis stations.

Engine Model Assumptions:

- 1) The air mass flows through the system are all 1-dimensional at the mean line.
- 2) Air with ideal gas law behavior is assumed to have constant properties.
- 3) All expansion and compression is adiabatic.
- 4) All power transfer occurs in the rotor stages, the stators do no work (only transform between kinetic energy and static pressure).
- 5) Mass flow rates inside compressor, turbines and combustion chamber is constant.
- 6) Instantaneous compressor and turbine mass flow rates determined via off-nominal compressor and turbine maps.
- 7) No air bleed occurs from the compressor.
- 8) The combustion is modeled as isobaric heat addition.
- 9) Power turbine exit pressure is same as atmospheric pressure.
- 10) Flow is choked in Gas Generator and Power Turbines.

The power required to drive the compressor is

$$\dot{W}_c = \dot{m}_c c_p (T_{02} - T_{01}) \quad (1)$$

Where \dot{m}_c is the compressor air mass flow rate, c_p is the specific heat of air and T_{01} and T_{02} are the stagnation temperatures at the compressor entrance and exit respectively. Furthermore the stagnation temperature ratio is related to the compressor pressure ratio by

$$\frac{T_{02}}{T_{01}} = 1 + \frac{1}{\eta_c} \left[\left(\frac{P_{02}}{P_{01}} \right)^{\frac{\gamma-1}{\gamma}} - 1 \right] \quad (2)$$

Where η_c is the compressor isentropic efficiency, γ is the specific heat ratio, and P_{01} and P_{02} are the stagnation pressures at the compressor entrance and exit respectively. Based on (1) and (2), the torque required to drive the compressor is

$$TQ_c = J_c \dot{\Omega}_c + \dot{m}_c c_p \frac{T_{01}}{\Omega_c \eta_c} \left[\left(\frac{P_{02}}{P_{01}} \right)^{\frac{\gamma-1}{\gamma}} - 1 \right] \quad (3)$$

Where Ω_c the compressor rotation speed and J_c the compressor rotational inertia. Also, in the above equations the stagnation temperature and pressures at the compressor entrance are assumed to be the ambient atmospheric pressure, $P_{01} = P_a$, and temperature $T_{01} = T_a$ values. Furthermore compressor pressure ratio, $PR_c = P_{02}/P_{01}$, and efficiency, η_c , are related to \dot{m}_c and Ω_c via the compressor characteristic maps,

$$PR_c = f_{cP}(T_{01}, P_{01}, \dot{m}_c, \dot{\Omega}_c) \text{ and } \eta_c = f_{c\eta}(T_{01}, P_{01}, \dot{m}_c, \Omega_c) \quad (4)$$

In this study, the compressor pressure and efficiency maps are generated numerically based on the nominal compressor design values as detailed in section 2.3.

To drive the compressor and the load, separate gas generator and power turbines are present in the two spool gas turbine engine (Figure 1). The power generated from these turbines is

$$\dot{W}_{ggt} = \dot{m}_{ggt} c_p (T_{04} - T_{05}) \quad (5)$$

$$\dot{W}_{pt} = \dot{m}_{pt} c_p (T_{06} - T_{07}) \quad (6)$$

Where \dot{m}_{ggt} and \dot{m}_{pt} are gas generator and power turbine mass flows respectively and T_{04}, T_{05}, T_{06} and T_{07} are turbine entrance and exit stagnation temperatures as defined in Fig: 2.1.

Furthermore, the turbine pressure ratios, $PR_{ggt} = P_{04}/P_{05}$ and $PR_{pt} = P_{06}/P_{07}$ and isentropic efficiencies η_{ggt} and η_{pt} are related to mass flows and the rotation speeds via the characteristic maps

$$PR_t = f_{p,t}(T_{0in,t}, P_{0out,t}, \dot{m}_t, \dot{\Omega}_t) \text{ and } \eta_t = f_{\eta,t}(T_{0in,t}, P_{0out,t}, \dot{m}_t, \Omega_t) \quad (7)$$

Where subscript “t” represents indicates either “ggt” for gas generator turbine or “pt” for power turbine. Here since the gas generator turbine and the compressor are on a common shaft, we have $\Omega_c = \Omega_{ggt}$. Finally the torque balance between the compressor and the gas generator turbine is

$$(J_c + J_{ggt}) \dot{\Omega}_c = \frac{1}{\Omega_c} (\dot{W}_{ggt} - \dot{W}_c) \quad (8)$$

And the torque balance between the power turbine and load is

$$(J_{pt} + J_L) \dot{\Omega}_{pt} = \frac{1}{\Omega_{pt}} (\dot{W}_{pt} - \dot{W}_L) \quad (9)$$

Where \dot{W}_L is the power consumed by the load and J_{ggt}, J_{pt} and J_L are rotational inertias of the turbines and the load respectively.

During steady state operation assuming that the mass flow rate of the fuel is negligible, the mass flow rates through the compressor and turbines are equal, $\dot{m}_c = \dot{m}_{ggt} = \dot{m}_{pt}$. Unlike in steady state conditions during transient operating conditions the mass flow rate in the compressor and combustion chamber may vary due to change in applied load, fuel flow rate and shaft speed. To account for this variance a plenum is introduced between a compressor and a combustion

chamber (A plenum is placed downstream of a compressor or upstream of a combustion chamber) to balance the unsteady mass flow within a compressor and combustion chamber. Similarly another plenum is placed between gas generator turbine and power turbine to attain a uniform the mass flow rate.

The plenum chambers are modeled as ideal mass accumulators with no losses or heat transfer. Figure 2.2 shows a schematic of the plenum chamber element with input and output mass flow rates \dot{m}_{in} and \dot{m}_{out} generated by the upstream and downstream compressor and turbine sub-systems. Due to the differential mass flows, the rate of change of air density inside a plenum, ρ_p , is given

$$\dot{\rho}_p = \frac{\dot{m}_{in} - \dot{m}_{out}}{V_p} \quad (10)$$

Where V_p is the plenum chamber volume. Furthermore, through differentiation of the ideal gas law and assuming adiabatic compression, the following differential equation for plenum chamber pressure P_p is obtained

$$\dot{P}_p(t) = \frac{\gamma(\dot{m}_c - \dot{m}_{ggt})}{M_p(t)} P_p(t) \quad \text{with } M_p(t) = \int (\dot{m}_c - \dot{m}_{ggt}) dt + M_{p,init} \quad (11)$$

Here M_p is the mass of the air accumulating inside the plenum and $M_{p,init}$ is the initial air mass.

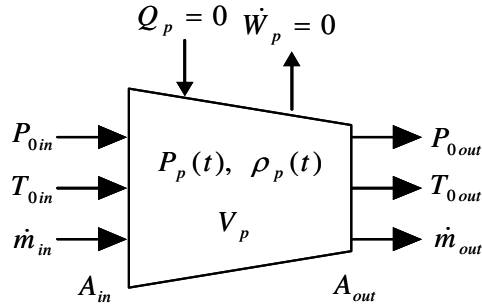


Figure 2.2: Plenum chamber element.

It is assumed that the plenum pressure is uniform such that input and output pressure $P_{in} = P_p$ and $P_{out} = P_p$ equal the internal plenum pressure. Furthermore, based on energy conservation inside the plenum we have

$$\frac{d(C_p M_p T_{0p})}{dt} = C_p \dot{m}_{in} T_{0in} - C_p \dot{m}_{out} T_{0out} \quad (12)$$

Where T_{0in} , and T_{0out} are entrance and exit stagnation temperatures and T_{0p} is the internal plenum stagnation temperature. Using (1)-(3) the exit stagnation temperate can be approximated as

$$T_{out} \approx \frac{1}{\dot{m}_{out}} [\dot{m}_{in} T_{0in} - \frac{V_p}{R} \dot{P}_p] \quad (13)$$

If there are no pressure losses and energy accumulation inside the plenum is neglected,

$$P_{0in} = P_{0out} \quad (14)$$

$$T_{0in} = T_{0out} \quad (15)$$

Finally, the combustion chamber (entrance station 3, exit station 4 in Fig. 1) is modeled as a pure isobaric heat addition process. With heat addition, Q_{cc} , based on an idealized combustion model

$$Q_{cc} = \dot{m}_f LHV \quad (16)$$

Where \dot{m}_f is the fuel mass flow rate and LHV is the fuel lower heating value.

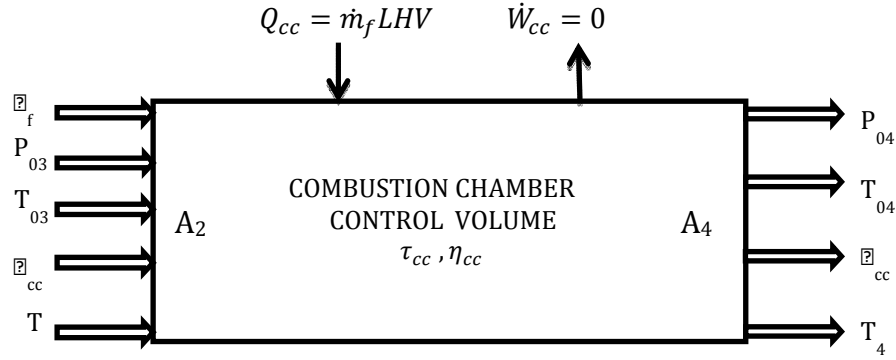


Figure 2.3: Combustion Chamber control volume

As a result of an energy balance and the input stagnation temperature, T_{03} the combustion Chamber exit stagnation temperature T_{04} is determined as a solution to

$$\tau_{cc} \frac{dT_{04}}{dt} = \dot{m}_{cc} c_p (T_{03} - T_{04}) + \dot{m}_f LHV \quad (17)$$

Where τ_{cc} is the combustion chamber time-constant and \dot{m}_{cc} is the air mass flow through the combustion chamber which equals the gas generator mass flow $\dot{m}_{cc} = \dot{m}_{ggt}$. Furthermore, the combustion chamber exit stagnation pressure, P_{04} , is computed from the input stagnation pressure P_{03} using,

$$P_{04} = \eta_{cc} P_{03} \quad (18)$$

Where $\eta_{cc} < 1$ represents the combustion chamber pressure drop. Also, at steady-state the combustion chamber temperature rise $\Delta T_{0cc} = T_{04} - T_{03}$ is

$$\Delta T_{0cc} = f \frac{LHV}{c_p} \text{ with } f = \frac{\dot{m}_f}{\dot{m}_{cc}} \quad (19)$$

Where f is the fuel-air ratio

2.3 ENGINE NOMINAL DESIGN

Next the overall engine design is determined by the choice of several nominal operating parameters. These parameters, selected based on the NASA LCTR-2 heavy lift concept [13, 14] are summarized in table 1. Here the subscript “n” refers to nominal conditions.

Table 1. Engine Nominal Design Parameters

| | | | |
|-----------------------------|-----------------------------------|--|------------------------------------|
| Ambient Temperature | $T_a=288^\circ \text{ K}$ | Ambient Pressure | $P_a=1.023 \text{ bar}$ |
| Output Power | $\dot{W}_{Ln} = 7500 \text{ Hp}$ | Compressor Mass Flow | $\dot{m}_{cn} = 13.5 \text{ kg/s}$ |
| Compressor Speed | $\Omega_{cn}=17,500 \text{ RPM}$ | Flow Axial Velocity | $C_{an}=150 \text{ m/s}$ |
| Power Turbine Speed | $\Omega_{ptn}=12,500 \text{ RPM}$ | Compressor inlet hub-to-tip ratio | $\mu_{ht} = 0.35$ |
| Compressor Pressure Ratio | $\beta_{cn} = 28$ | Combustion Chamber Pressure Drop Coefficient | $\eta_{cc} = 0.90$ |
| Number of Compressor Stages | $N_c = 8$ | Fuel Lower Heating Value | $LHV = 43.1 \text{ MJ/kg}$ |

Assuming 100% isentropic compression efficiency at nominal conditions ($\eta_{cn} = 1$) we have

$$T_{02n} = T_a \beta_{cn}^{\frac{\gamma-1}{\gamma}} \quad \text{and} \quad \Delta T_{0cn} = T_a [\beta_{cn}^{\frac{\gamma-1}{\gamma}} - 1] \quad (20)$$

Where $\Delta T_{0cn} = T_{02n} - T_a$ is the nominal stagnation temperature rise in the compressor. Under steady-state conditions we have

$$\dot{W}_{ggt} = \dot{W}_c \quad \text{and} \quad \dot{W}_{pt} = \dot{W}_L \quad (21)$$

Thus using (1),(5),(16),(18) and (19) the required combustion chamber rise at nominal operating conditions is

$$\Delta T_{0cn} = \frac{\dot{W}_{Ln} - T_a c_p \dot{m}_{cn} (1 - \eta_{cc}^{\frac{1-\gamma}{\gamma}})}{c_p \dot{m}_{cn} [1 - (\beta_{cn} \eta_{cc})^{\frac{1-\gamma}{\gamma}}]} \quad (22)$$

And the nominal gas generator and power turbine temperature drops are

$$\Delta T_{0ggtn} = T_a (\beta_{cn}^{\frac{\gamma-1}{\gamma}} - 1) \quad \text{and} \quad \Delta T_{0ptn} = \frac{\dot{W}_{Ln}}{c_p \dot{m}_{cn}} \quad (23)$$

Finally the nominal fuel flow rate and fuel/air ratio are

$$\dot{m}_{fn} = \frac{\dot{m}_{cn} c_p \Delta T_{0ccn}}{LHV} \quad \text{and} \quad f_n = \frac{\dot{m}_{fn}}{\dot{m}_n} \quad (24)$$

2.4 COMPRESSOR AND TURBINE DESIGN

The compressor design is based on a multi-stage constant mean radius design. Figure 2.4 shows the 8 stage ($N_c = 8$) axial compressor modeled in this study which also includes an inlet guide vane (IGV) stage and an exit guide vane (EGV) stage.

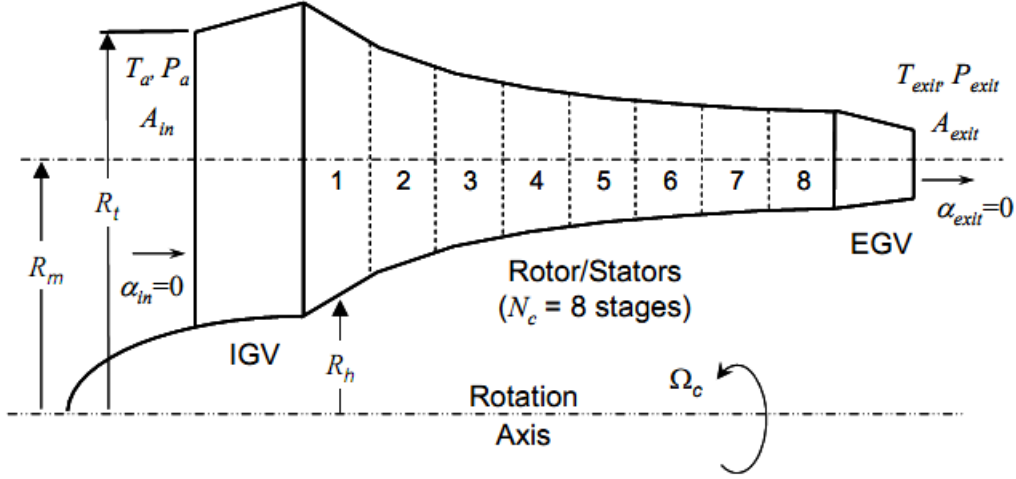


Figure 2.4: Eight-stage axial compressor with IGV and EGV and constant mean radius.

Figure 2.5 shows a typical rotor/stator stage and the corresponding air flow velocity triangles. Here U_c is the mean line rotor speed of the compressor

$$U_c = R_m \Omega_c \quad (25)$$

Where R_m is the compressor mean radius. As shown in Fig.5, C_1 , C_2 and C_3 are the absolute velocities and α_1 , α_2 and α_3 are the corresponding flow angles. Also V_1 , V_2 and V_3 and β_1 , β_2 and β_3 are the flow velocities and flow angles relative to the rotor. Here the stage axial flow velocities C_{a1} , C_{a2} and C_{a3} are

$$\begin{aligned} C_{a1} &= C_1 \cos \alpha_1 \\ C_{a2} &= C_2 \cos \alpha_2 \\ C_{a3} &= C_3 \cos \alpha_3 \end{aligned} \quad (26)$$

Here the entrance flow angle α_1 is equal to the upstream stage exit angle. Based on the flow velocity triangles, the flow angles also satisfy

$$\frac{U_c}{C_{a1}} = \tan \alpha_1 + \tan \beta_1, \quad \frac{U_c}{C_{a2}} = \tan \alpha_2 + \tan \beta_2 \quad \text{and} \quad \frac{U_c}{C_{a3}} = \tan \alpha_3 + \tan \beta_3 \quad (27)$$

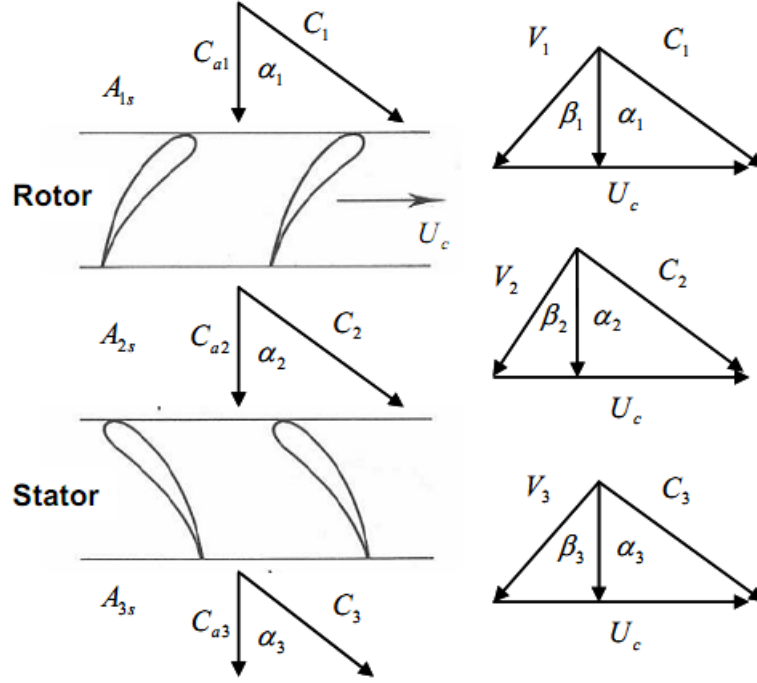


Figure 2.5: Compressor stage and flow velocity triangles

Furthermore, the rotor entrance, rotor exit and stator exit stagnation temperatures T_{01s} , T_{02s} and T_{03s} are

$$T_{01s} = T_{1s} + \frac{C_1^2}{2c_p}, \quad T_{02s} = T_{2s} + \frac{C_2^2}{2c_p} \quad \text{and} \quad T_{03s} = T_{3s} + \frac{C_3^2}{2c_p} \quad (28)$$

With corresponding flow temperatures T_{1s} , T_{2s} and T_{3s} . Also, the compressor mass flow rate, \dot{m}_c , which is equivalent at every stage, satisfies

$$\dot{m}_c = \rho_1 A_{1s} C_{a1} = \rho_2 A_{2s} C_{a2} = \rho_3 A_{3s} C_{a3} \quad (29)$$

Where ρ_1 , ρ_2 and ρ_3 are the flow densities and A_{1s} , A_{2s} and A_{3s} are stage cross-section areas. In each stage, the rotor increases the energy of the flow by increasing the swirl velocity. The power added in each compressor stage is

$$\dot{W}_{cs} = \dot{m}_c c_p \Delta T_{0s} = \dot{m}_c U_c (C_{a2} \tan \alpha_2 - C_{a1} \tan \alpha_1) \quad (30)$$

Where $\Delta T_{0s} = \Delta T_{02s} - \Delta T_{01s}$ is the stage stagnation temperature rise. After each rotor the swirl velocity is reduced by the stators. However, the stators do not add energy to the flow thus $\Delta T_{03s} = \Delta T_{02s}$. Likewise, neither do the IGV or EGV stages.

Based on the total compressor stagnation temperature rise ΔT_{0n} in (18), the nominal stage stagnation temperature rise, ΔT_{0sn} , for each stage is designed to be identical, therefore

$$\Delta T_{0sn} = \frac{\Delta T_{0cn}}{N} \quad (31)$$

Where N is the number of stages and the stagnation temperature at the k^{th} stage is

$$\Delta T_{01sn,k} = T_a + (k - 1)\Delta T_{0sn} \text{ and } \Delta T_{02sn,k} = \Delta T_{03sn,k} = T_a + k\Delta T_{0sn} \quad (32)$$

The compressor stage cross-sectional areas A_{1s} , A_{2s} and A_{3s} are determined such that the axial flow velocities though each stage remain constant at the nominal operating condition. Thus, at nominal conditions we have

$$C_{an} = C_{a1} = C_{a2} = C_{a3} \quad (33)$$

In this case, the nominal design axial flow speed is selected as $C_{an} = 150m/s$. Using (30)-(33), the nominal flow angles for the N_c identical stages are

$$\alpha_{1n} = \alpha_{IGV}, \quad \alpha_{2n} = \tan^{-1}\left[\frac{\Delta T_{0sn}}{U_{cn}C_{an}} + \tan \alpha_{1n}\right], \quad \alpha_{3n} = \alpha_{1n} = \alpha_{IGV} \quad (34)$$

Where α_{IGV} is the IGV exit angle which is used as the free design variable (within limits). Note, for identical stages, since the stator exit angle is the same as rotor entrance angle of the next stage, we have $\alpha_{3n} = \alpha_{1n}$. Also, using (27) together with (33), β_{1n} , β_{2n} and β_{3n} can be determined. Here the range of allowable α_{IGV} is determined by checking the so called De Haller number[1].

Next, using, (28), (29), (31) and (34), together with the ideal gas law expression for density and the adiabatic compression relations starting from the compressor inlet, the compressor cross-section areas at the k^{th} stage are

$$A_{1s,k} = \frac{\dot{m}_{cn}RT_a^{\frac{\gamma}{\gamma-1}}}{C_{an}P_aT_{1sn,k}^{\frac{1}{\gamma-1}}}, \quad A_{2s,k} = \frac{\dot{m}_{cn}RT_a^{\frac{\gamma}{\gamma-1}}}{C_{an}P_aT_{2sn,k}^{\frac{1}{\gamma-1}}} \text{ and } A_{3s,k} = \frac{\dot{m}_{cn}RT_a^{\frac{\gamma}{\gamma-1}}}{C_{an}P_aT_{3sn,k}^{\frac{1}{\gamma-1}}}, \quad k = [1 - N_c] \quad (35)$$

Where R is the ideal gas constant. Finally, the compressor mean radius is

$$R_m = \sqrt{\frac{A_{1s,1}}{4\pi} \frac{1+\mu_{ht}}{1-\mu_{ht}}} \quad (36)$$

Where $\mu_{ht} = R_{tip}/R_{hub}$ is the hub-to-tip ratio at the inlet, which is a geometric design variable. Here, similar to [13, 14] for the LCTR-2 engine concept, the hub-to-tip ratio is selected as $\mu_{ht} = 0.35$. The resulting compressor stage hub and tip radii for this design are show in Figure 2.6, and the corresponding compressor stage angles are summarized in Table 2. Furthermore, the gas generator angles as well as the rotational inertias computed based on the component mean radius values are also given in Table 2. These tabulated absolute and relative angles are calculated using (27),(33) and (34) using the design parameters i.e. exit angle of the inlet guide vane of 37° and adjusting the exit angle of exit guide vanes to 0° independent of the exit angle of the compressor and assuming that all stages are identical and the stagnation temperature raise in each stage is the same.

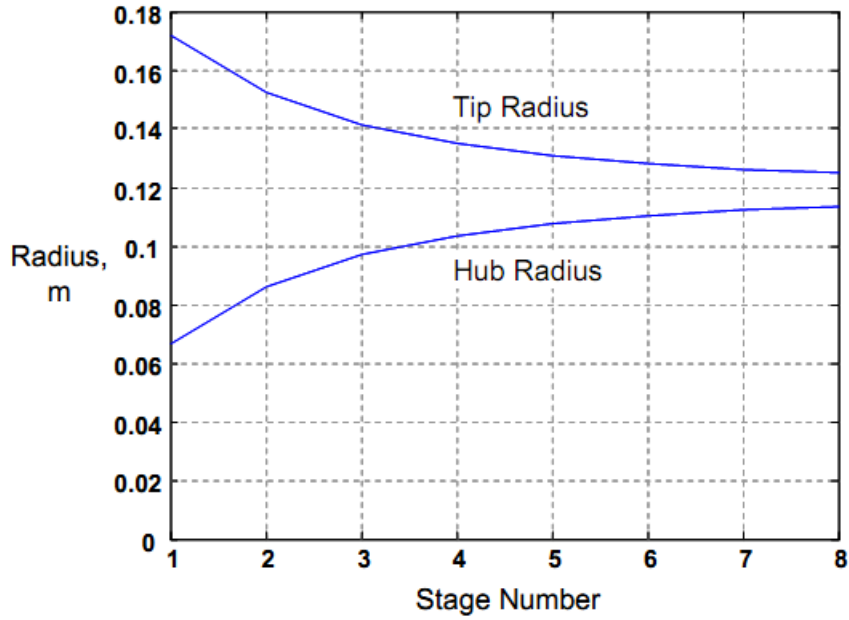


Figure 2.6: Compressor hub and tip radius

TABLE 2: COMPRESSOR DESIGN PARAMETERS

| | Temperature Raise | Absolute Angles | Relative Angles | Mean Radius(m) | Rotational Inertia (Kg-m ²) |
|------------|-------------------------------|---|--|-----------------|---|
| Compressor | $\Delta T_{0_{cn}} = 458.21K$ | $\alpha_{1n} = 37^\circ$ $\alpha_{2n} = 62.44^\circ$ $\alpha_{3n} = 37^\circ$ | $\beta_{1n} = 55.34^\circ$ $\beta_{2n} = 15.83^\circ$ $\beta_{3n} = 55.34^\circ$ | $R_{mc} = 0.11$ | $J_c = 0.6414$ |

2.5 ANALYTICAL CALCULATION OF OFF-NOMINAL CHARACTERISTIC MAPS

Under transient conditions such as during gear ratio changes or during sudden main rotor power demands, the engine will undergo deviations about the nominal design operating point which is regulated by the engine fuel control. Therefore, it is necessary to model the off-nominal operation of compressor and turbine units. The off-nominal characteristics are typically described by compressor and turbine maps which show pressure ratio and isentropic efficiency as a function of mass flow for a given rotational speed as shown in (4) and (7). These maps can either be obtained experimentally or estimated analytically. In this investigation, compressor map data was not available, therefore a novel procedure is developed to analytically generate these maps for a given compressor design.

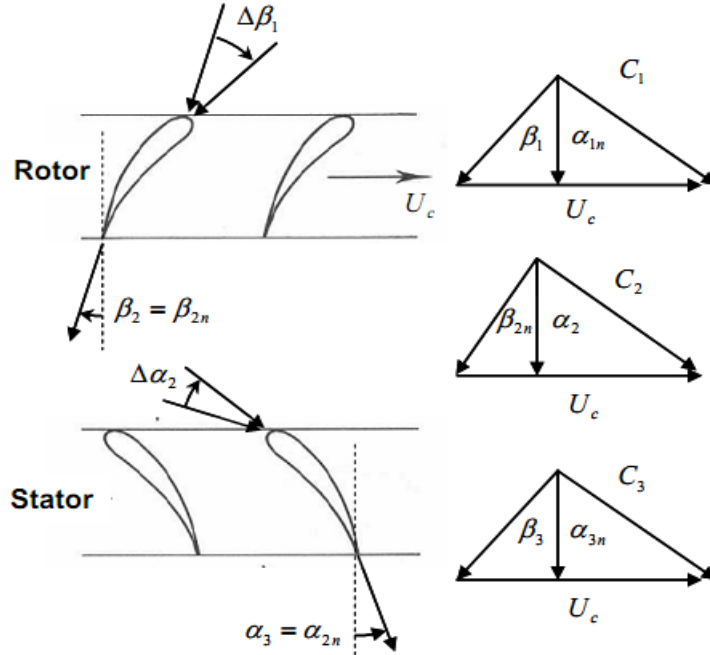


Figure 2.7: Assumed flow angle deviations for off-nominal operation

Since the stage areas and blade angles are fixed, the constant axial velocity condition (33) is only valid at the nominal operating point. For off-nominal operation, the axial velocity and the flow angles will deviate from nominal and vary from stage to stage. However, as discussed in [1], since the flow exiting a rotor or stator is essentially attached to the blade, the exit flow deviation angles are negligible compared to the entrance flow deviation angles (See Figure 2.7). Based on this assumption, the k^{th} stage flow angles in the cascade are

$$\begin{aligned}
 \alpha_{1,k} &= \alpha_{3,k-1} & \beta_{1,k} &= \beta_{1,n} + \Delta\beta_{1,k} \\
 \alpha_{2,k} &= \alpha_{2,n} + \Delta\alpha_{2,k} & \beta_{2,k} &= \beta_{2,n} \\
 \alpha_{3,k} &= \alpha_{3n} & \beta_{3,k} &= \beta_{3,n} + \Delta\beta_{3,k}
 \end{aligned}
 \quad [k = 1 - N_c] \quad (37)$$

Where $\Delta\alpha_{2,k}$, $\Delta\beta_{1,k}$ and $\Delta\beta_{3,k}$ are the flow deviation angles during off-nominal operation. Also, since the initial entrance angle into the cascade is equal to the fixed exit angle of the IGV we have

$$\alpha_{1,k} = \alpha_{3,k-1} = \dots \alpha_{1,1} = \alpha_{IGV} \quad (38)$$

Next, in order to compute the velocities and corresponding stagnation temperatures and pressures in a given stage, the stage entry conditions (which are equal to the exit conditions of

the previous stage) are assumed to be known. In this way the results from stage k can be utilized in the computation of stage $k + 1$ in the cascade. Starting with stage work and mass flow expressions in (29) and (30) and utilizing (26)-(28) together with the ideal gas law relations, we arrive at the following polynomial equation for the k^{th} stage turbine exit axial velocity $C_{a2,k}$.

$$C_{a2,k}^{\gamma+1} + a_1 C_{a2,k}^{1-\gamma} + a_2 = 0 \quad (39-a)$$

With Coefficients

$$a_1 = -(U_c^2 - 2C_{a1,k}U_c \tan \alpha_{1n} + 2c_p T_{01s,k}) \cos(\beta_{2n})^2 \quad (39-b)$$

$$a_2 = 2C_p \cos(\beta_{2n})^2 \left(\frac{\dot{m}_c R}{P_{01s,k} A_{2s,k}} \right)^{\gamma-1} T_{01s,k}^{\gamma} \quad (39-c)$$

for $[k = 1 - N_c]$ with

$$C_{a1,k} = C_{a3,k-1}, T_{01s,k} = T_{03s,k-1}, P_{01s,k} = P_{03s,k-1} \quad (40)$$

Likewise utilizing the fact that $U_c = 0$ in the stator section (or equivalently that $T_{03s,k} = T_{02s,k}$) we obtain the following polynomial equation for stator exit axial velocity $C_{a3,k}$.

$$C_{a3,k}^{\gamma+1} + b_1 C_{a3,k}^{1-\gamma} + b_2 = 0 \quad (41-a)$$

With coefficients

$$b_1 = -2c_p T_{02s,k} \cos(\alpha_{3n})^2 \quad (41-b)$$

$$b_2 = -2c_p \cos(\alpha_{3n})^2 \left(\frac{\dot{m}_c R}{P_{02s,k} A_{3s,k}} \right)^{\gamma-1} T_{02s,k}^{\gamma} \quad (41-c)$$

For $k = [1 - N_c]$, the cascade computation is initialized at the first stage $k=1$, for a given ambient inlet condition T_a and P_a , mass flow rate, \dot{m}_c , and rotation speed, Ω_c . The subsequent stages are computed using the output of the previous stage as input for the next stage. Here the k^{th} stage rotor exit stagnation pressure $P_{02s,k}$ is computed as

$$P_{02s,k} = P_{01s,k} [\eta_{s,k} \left(\frac{T_{02s,k}}{T_{01s,k}} - 1 \right) + 1]^{\frac{\gamma}{\gamma-1}} \quad \text{with } \eta_{s,k} = 1 - \varepsilon \left| \frac{\Delta\beta_{1,k}}{\beta_{1n}} \right| \quad (42)$$

Where $\eta_{s,k}$ is the stage isentropic efficiency with scaling parameter ε . Here $\eta_{s,k}$ varies in proportion to the rotor entrance flow deviation angle which is directly computed from the stage input conditions based on the (29).

$$\Delta\beta_{1,k} = \tan^{-1} \left[\frac{U_c}{C_{a1,k}} - \tan \alpha_{1n} \right] - \beta_{1n} \quad (43)$$

Thus at nominal conditions we have $\Delta\beta_{1,k} = 0$ and $\eta_{s,k}=1$. Finally, it is assumed that the stator stage is lossless, therefore, since $T_{03s,k} = T_{02s,k}$, the stator exit stagnation pressure $P_{03s,k}$ is just

$$P_{03s,k} = P_{02s,k} \quad (44)$$

After performing the cascade calculations (39)-(44) and proceeding through to the final stage $k = N_c$. The overall compressor pressure and temperature ratios β_c and r_c are

$$\beta_c = \frac{P_{02}}{P_{01}} = \frac{P_{03s,N_c}}{P_a} \quad \text{and} \quad r_c = \frac{T_{02}}{T_{01}} = \frac{T_{03s,N_c}}{T_a} \quad (45)$$

And the overall isentropic efficiency is

$$\eta_c = \frac{\beta_c^{\frac{\gamma-1}{\gamma}} - 1}{r_c - 1} \quad (46)$$

By performing this analysis over a range of mass flows and compressor rotation speeds we numerically obtain the compressor pressure and efficiency characteristic maps. Figure 2.8 shows the calculated pressure ratio characteristic corresponding to the design given in Tables 1 and 2.

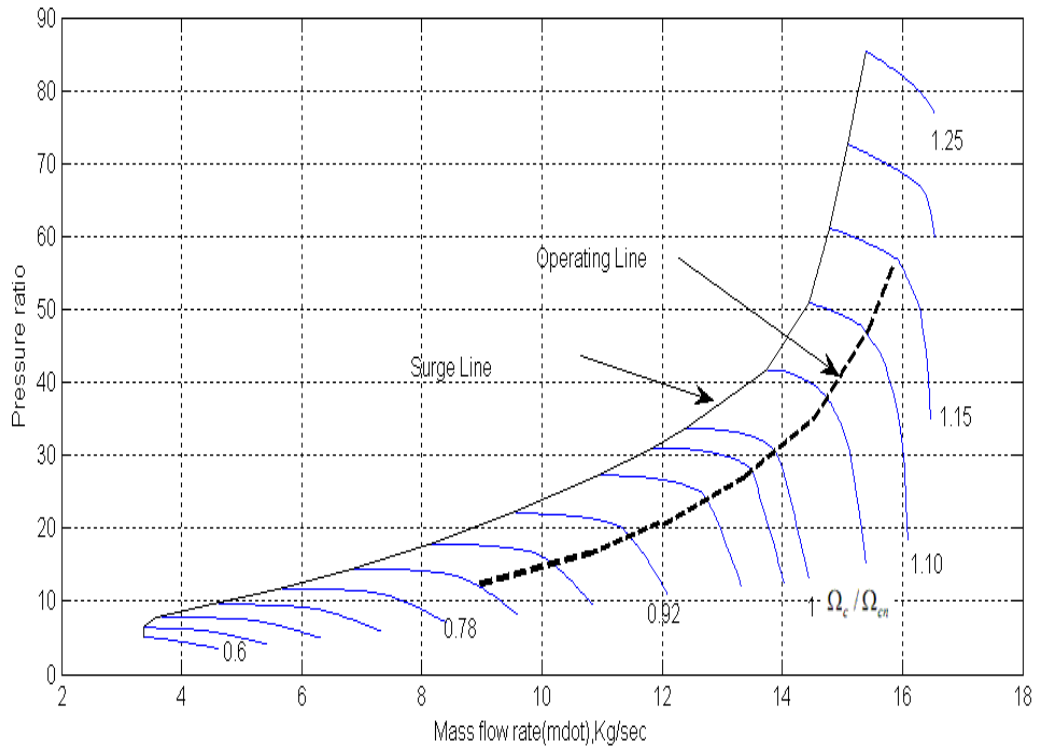


Figure 2.8: Calculated Compressor pressure ratio characteristic map

Here, the surge line is determined by the location of maximum pressure ratio for a given rotation speed Ω_c . Figure 2.8 also shows the resulting steady-state operating line calculated based on the engine simulation model (See section 2.8). In addition to the pressure ratio, the corresponding calculated isentropic efficiency characteristic is shown in Figure 2.9. Note $\eta_c = 1$ at the nominal operation.

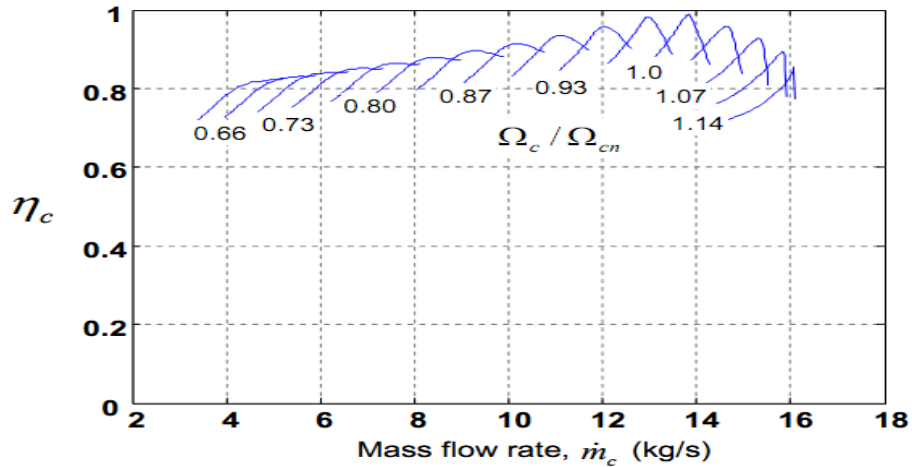


Figure 2.9: Calculated compressor efficiency characteristic map

These maps are computed for the particular engine design and then stored digitally as lookup tables for use in the transient engine simulation (See section 2.7). Finally, Figure 2.10 shows the computed pressure ratio characteristic map with varying values of scaling parameter ε (1,0.8,0.6 and 0.4) represented in (42).Scaling parameter $\varepsilon=0.6$ has been used during the model design.

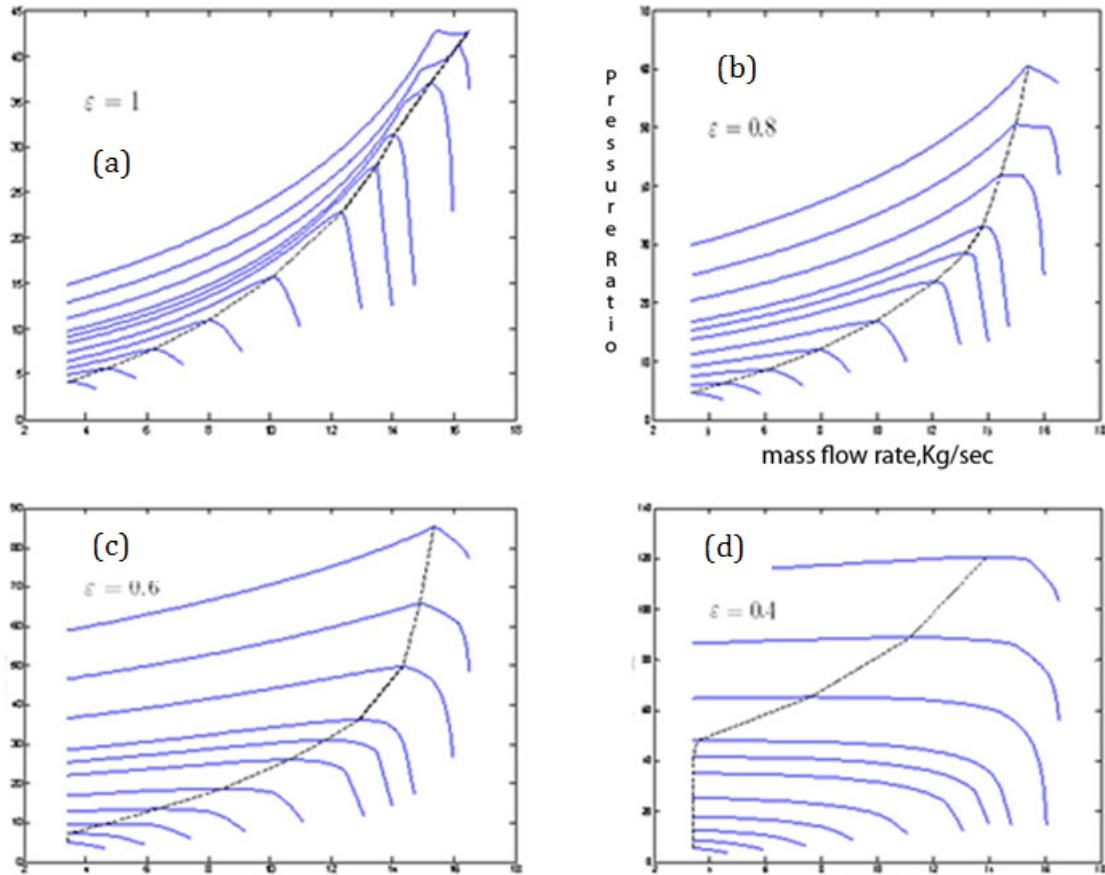


Figure 2.10 : Pressure ratio characteristic map with varying values of scaling parameter ε

a) $\varepsilon = 1$ b) $\varepsilon = 0.8$ c) $\varepsilon = 0.6$ d) $\varepsilon = 0.4$

GAS GENERATOR AND POWER TURBINE:

To drive the compressor and load, separate gas generator and power turbine are used in this two spool gas turbine engine. The power generated from these turbines is given in (5) and the inlet and exit stagnation temperatures are calculated using (6) Figure 2.11 represents the gas generator and power turbine control volumes.

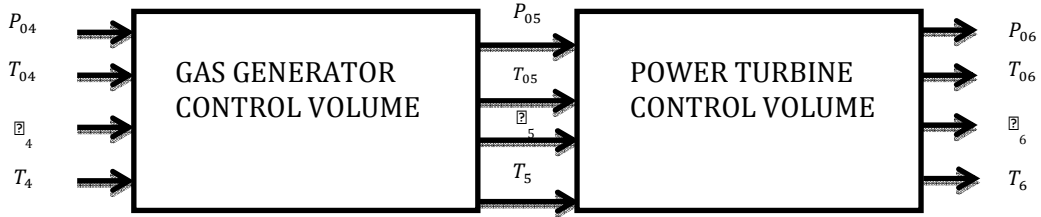


Figure 2.11: Gas Generator and Power Turbine control volumes.

Furthermore the turbine pressure ratios based on isentropic expansion in the turbines are

$$\frac{P_{04}}{P_{05}} = \left(\frac{T_{04}}{T_{05}}\right)^{\frac{\gamma}{\gamma-1}} \quad \text{and} \quad \frac{P_{06}}{P_{07}} = \left(\frac{T_{06}}{T_{07}}\right)^{\frac{\gamma}{\gamma-1}} \quad (47)$$

And the turbine mass flows are computed based on the assumption that both turbines are operating in the condition of choking flow. Therefore

$$\dot{m}_{ggt} = \lambda \frac{A_4 P_{04}}{\sqrt{T_{04}}} \quad \text{and} \quad \dot{m}_{pt} = \lambda \frac{A_6 P_{06}}{\sqrt{T_{06}}} \quad (48)$$

With

$$\lambda = \sqrt{\frac{\gamma}{R} \left(1 + \frac{\gamma-1}{2}\right)^{\frac{\gamma+1}{1-\gamma}}} \quad (49)$$

TURBINE CHARACTERISTIC MAP:

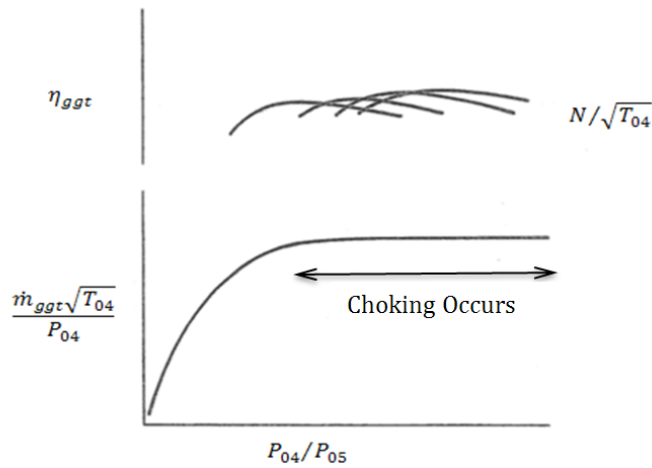


Figure 2.12: Gas Generator Turbine Characteristic Map

(Note: Parameters will be $\frac{\sqrt{T_{0_5}} \dot{m}}{P_{0_4}}, \frac{P_{0_4}}{P_a}, \frac{N_{pt}}{\sqrt{T_{0_4}}}, \eta_{pt}$ for a power turbine)

Figure 2.12 represents a sample gas generator turbine characteristic map. It is often found that turbines do not exhibit any significant variation in non-dimensional flow with non-dimensional speed. In off-design performance calculations it can be assumed that mass flow function can be represented by a single curve as shown in figure 2.12. Also while solving for off design performance calculations the inlet and exhaust losses are assumed to be negligible.

CHOKING IN A TURBINE:

In Compressible flows Mach number M , is defined as

$$M = \frac{C}{a} \quad (50)$$

Where a is local speed of sound in a medium. For a perfect gas it is given by

$$a = \sqrt{\gamma RT} \quad (51)$$

In an ideal isentropic flow of a perfect gas in the absence of work and body forces, for a constant specific heat

$$\frac{T_0}{T} = 1 + \frac{C^2}{2C_p} \quad (52)$$

which, with the definition of Mach number, becomes

$$\frac{T_0}{T} = 1 + \frac{\gamma - 1}{2} M^2 \quad (53)$$

For a perfect gas with constant specific heat the stagnation temperature and pressure are related by

$$\frac{P_0}{P} = \left(\frac{T_0}{T} \right)^{\frac{\gamma}{\gamma - 1}} \quad (54)$$

So, equation (54) can be written as

$$\frac{P_0}{P} = \left(1 + \frac{\gamma - 1}{2} M^2 \right)^{\frac{\gamma}{\gamma - 1}} \quad (55)$$

$$\frac{\rho_0}{\rho} = \left(1 + \frac{\gamma - 1}{2} M^2 \right)^{\frac{1}{\gamma - 1}} \quad (56)$$

For any flow of a perfect gas these relations can be used to relate the local conditions (T, P, ρ) to the local stagnation conditions (T_0, P_0, ρ_0) . The mass flow per unit area is:

$$\frac{\dot{m}}{A} = \rho C \quad (57)$$

Using Equations (50), (51) and (53), velocity is expressed as

$$C_4 = M \sqrt{\frac{\gamma R T_{04}}{1 + \frac{\gamma-1}{2} M^2}} \quad (58)$$

since

$$C = \frac{C_a}{\cos(\alpha_n)} \quad (59)$$

Where C_a is the axial velocity and α_n is the nominal inlet angle(0 in this case).

Using expression (56) and (58) we may write the mass flow rate as

$$\frac{\dot{m}}{a} = \frac{P_0 \sqrt{\gamma}}{\sqrt{R T_0}} M \left(\frac{1}{1 + \frac{\gamma-1}{2} M^2} \right)^{\frac{\gamma+1}{2(\gamma+1)}} \quad (60)$$

For a given fluid and inlet state(T_0, P_0) it is known that mass flow per unit area is maximum at $M=1$. The maximum flow per unit area from equation (60) is

$$\frac{\dot{m}}{A} = \frac{P_0 \sqrt{\gamma}}{\sqrt{R T_0}} \left(\frac{2}{\gamma+1} \right)^{\frac{\gamma+1}{2(\gamma-1)}} \quad (61)$$

$$\text{(or)} \quad \frac{\dot{m}}{A} = \frac{P_0 \lambda}{\sqrt{T_0}} \quad (62)$$

where λ is a constant($\lambda=0.0404$) and is given by

$$\lambda = \sqrt{\frac{\gamma}{R}} \left(\frac{2}{\gamma+1} \right)^{\frac{\gamma+1}{2(\gamma-1)}} \quad (63)$$

Unlike in the case of a compressor the turbine map is not used in off-design performance calculations. It is assumed that turbine is CHOKED and at every instant of time the different off-nominal parameters can be calculated using:

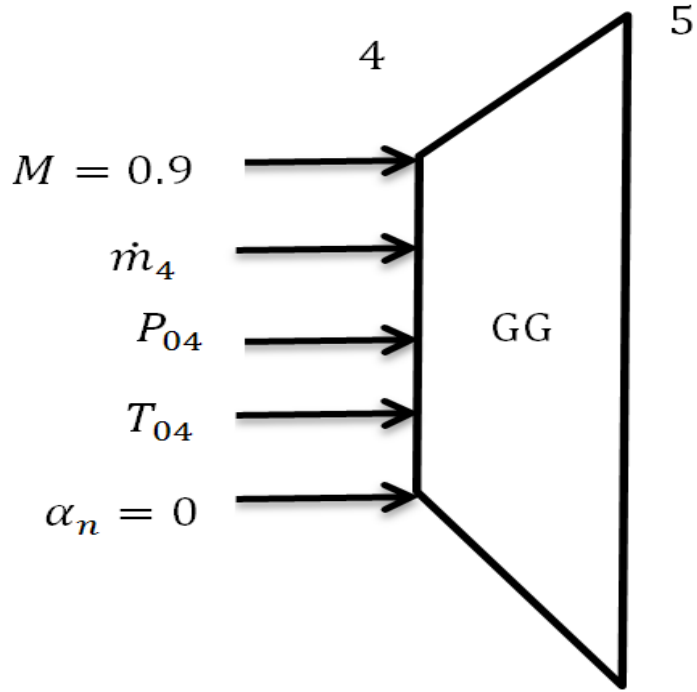


Figure 2.13: Gas generator turbine inputs for off nominal calculations.

INLET:

$$C_4 = M \sqrt{\frac{\gamma R T_{04}}{1 + \frac{\gamma-1}{2} M^2}}$$

$$C_{a_4} = C_4 \cos(\alpha_{n_4})$$

$$T_4 = T_{0_4} - \left(\frac{C_4^2}{2C_p} \right)$$

$$P_4 = P_{0_4} \left(\frac{T_4}{T_{0_4}} \right)^{\frac{\gamma}{\gamma-1}}$$

$$\rho_4 = \frac{P_4}{RT_4}$$

$$A_4 = \frac{\dot{m}_{ggt}}{\rho_4 C_{a_4}}$$

$$M_4 = \frac{C_4}{\sqrt{\gamma R T_4}}$$

OUTLET:

$$C_5 = \frac{C_{a_5}}{\cos(\alpha_{n_5})}$$

$$C_5 = \frac{C_{a_5}}{\cos(\alpha_{n_5})}$$

$$T_5 = T_{0_5} - \left(\frac{C_5^2}{2C_p} \right)$$

$$P_5 = P_{0_5} \left(\frac{T_5}{T_{0_5}} \right)^{\frac{\gamma}{\gamma-1}}$$

$$\rho_5 = \frac{P_5}{RT_5}$$

$$A_5 = \frac{\dot{m}_{pt}}{\rho_5 C_{a_5}}$$

$$M_5 = \frac{C_5}{\sqrt{\gamma R T_5}}$$

(64)

2.6 REPRESENTATION OF COMPRESSOR AND TURBINE MAPS IN COMPUTER PROGRAM

The compressor or turbine characteristic maps in standard format shown in Fig2.8 and 2.9 cannot be used directly in the computer program. Hence these maps are converted into a good numerical representation. It is not possible to read the compressor map parameters with give speed Ω_c and pressure ratio P_{02}/P_{01} , as there might be two values for the mass flow parameter \dot{m}_c at a given pressure ratio. It is also not possible to determine the efficiency η_c from the compressor map at a given speed and mass flow parameter \dot{m}_c , because at some parts of the compressor map the speed lines can be vertical. Hence there might be two values for the pressure ratio P_{02}/P_{01} at a single value of mass flow parameter \dot{m}_c .

Hence we introduce new coordinates called BETA (β) lines as a solution for this problem. This allowed an independent map reading using the shape of the parameter lines with the β line and speed parameter Ω_c . The auxiliary coordinates (β lines) can be selected with only two conditions. First there are no intersections between the β lines within the range of interest and secondly the β lines are equally spaced. The β lines will have any number of lines with each line having a parameter number starting from 1. β lines can be straight lines or parabolic lines. Three-dimensional lookup tables were created to represent the compressor characteristics. These tables represent the compressor mass flow parameter \dot{m}_c versus rotational speed parameter Ω_c , the pressure ratio P_{02}/P_{01} versus rotational speed parameter Ω_c and the compressor efficiency η_c versus rotational speed parameter Ω_c . If the values of any parameter with β line parameter are specified, the program searches and picks the other two parameters from these lookup tables. Figure 2.14 represents the SIMULINK block used in program. Linear interpolation technique was used to estimate the parameters lying at intermediate points.

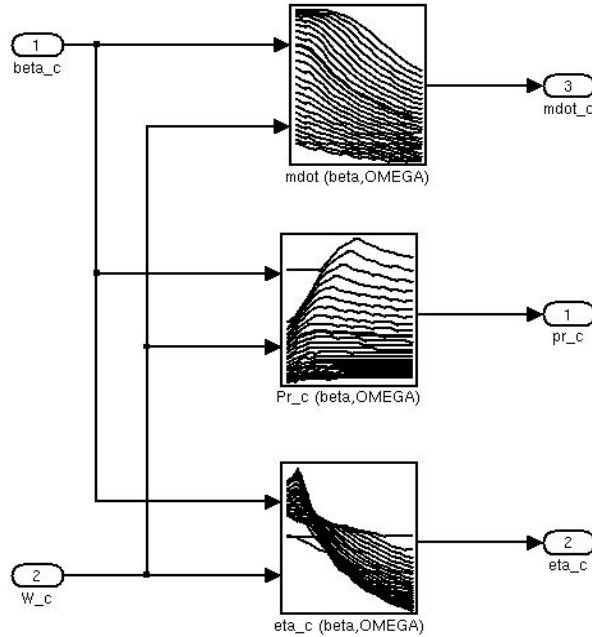


Figure 2.14: A sample SIMULINK model for generation of \dot{m} , π , η values for given Ω and β line values

Furthermore the compressor mass flow rate \dot{m}_c , pressure ratio π and efficiency characteristics η_c are computed by beta maps with functional dependencies,

$$\begin{aligned}\pi &= f_{pr}(T_a, P_a, \Omega_c, \beta) \\ \dot{m}_c &= f_m(T_a, P_a, \Omega_c, \beta) \\ \eta_c &= f_\eta(T_a, P_a, \Omega_c, \beta)\end{aligned}\quad (65)$$

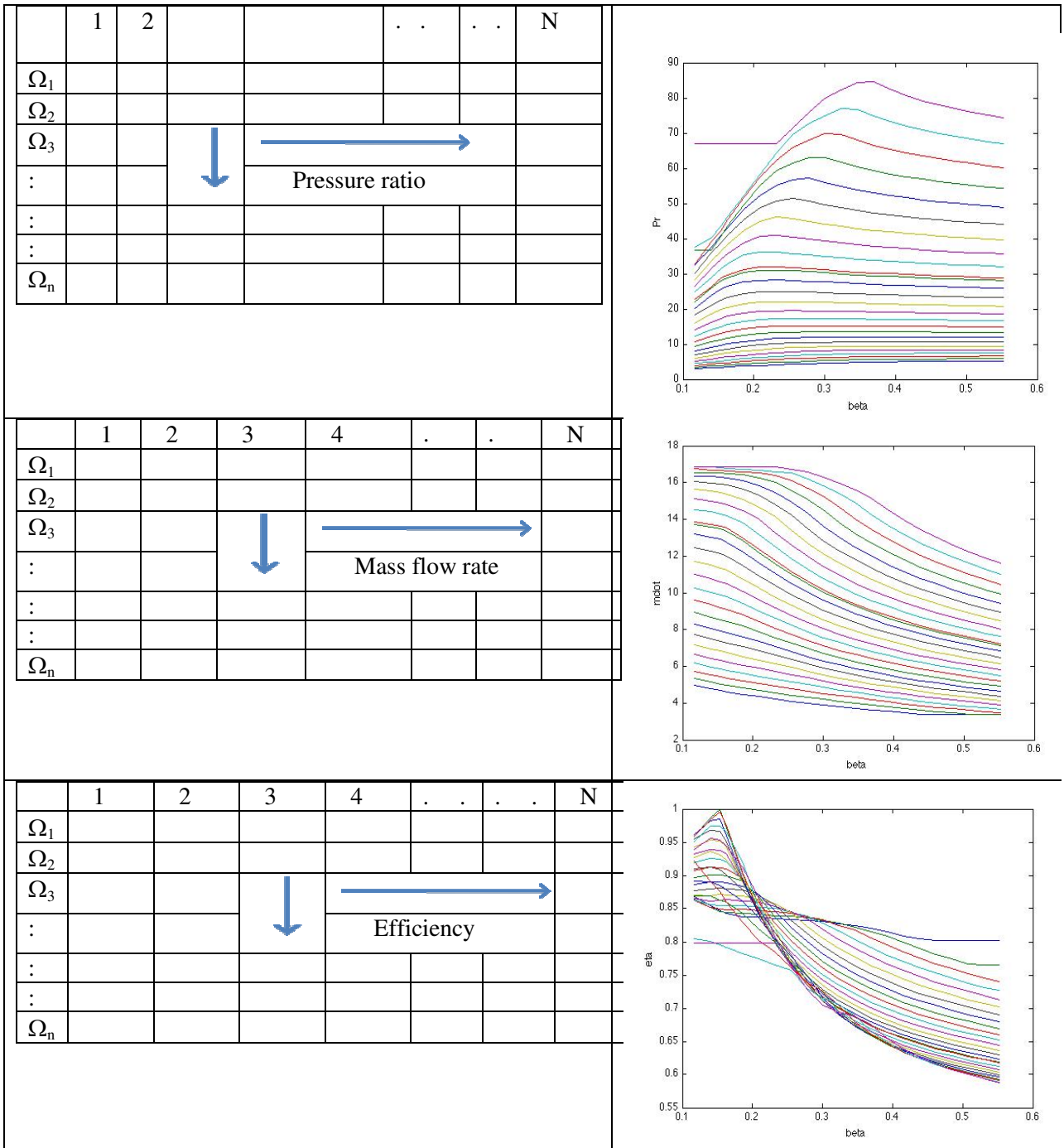


FIGURE 2.15: Lookup tables and corresponding PR, \dot{m} , and η versus β lines plots.

2.7 ENGINE CLOSED-LOOP FUEL CONTROL

To maintain the engine output shaft set-point speed during operation, a closed-loop fuel controller is required to regulate the fuel flow into the combustion chamber. A schematic of this arrangement is depicted in Figure 2.16.

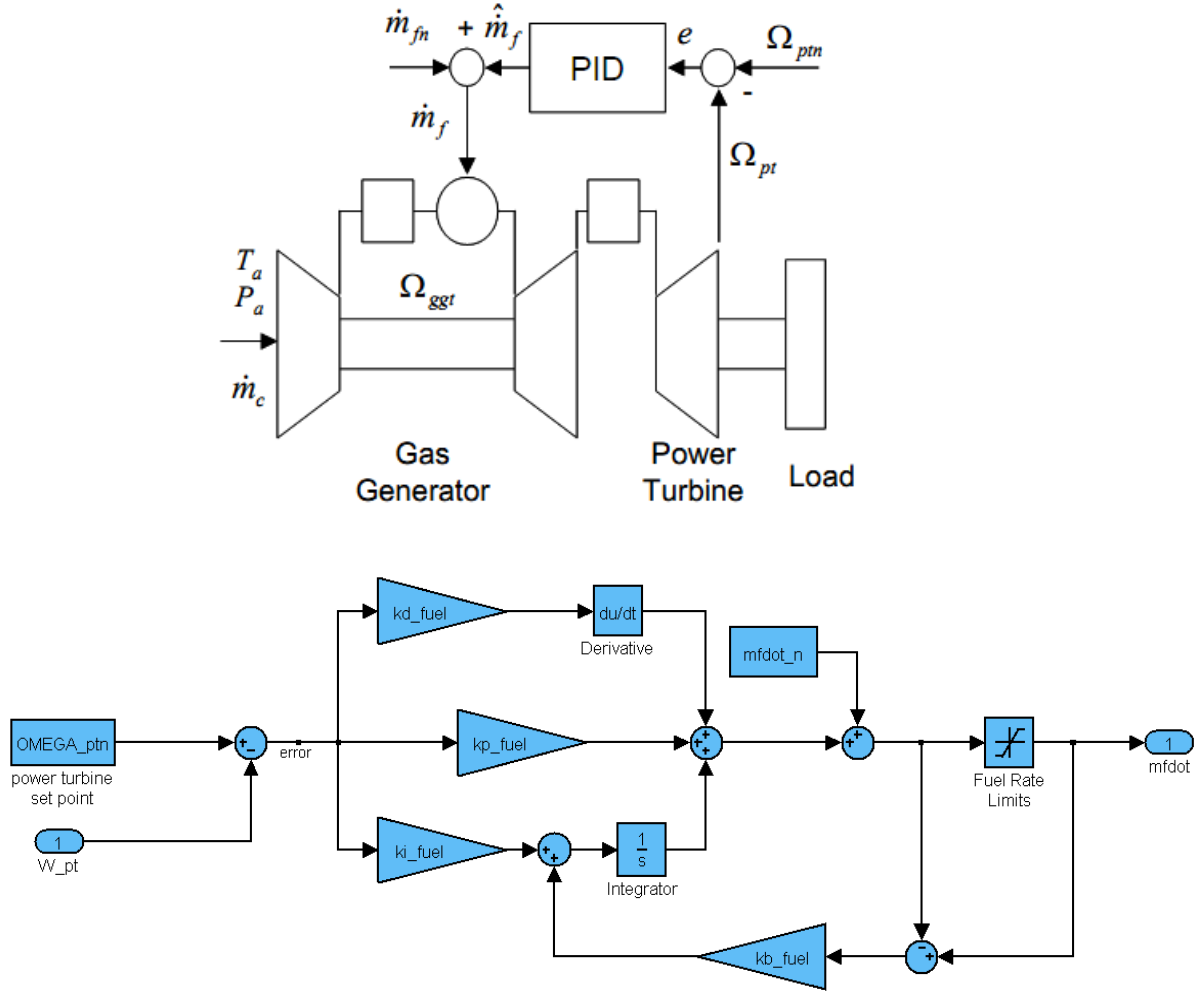


Figure 2.16: Engine with closed loop PID fuel control block

Here the Proportional Integral Derivative (PID) control law

$$\widehat{m}_f = kf_p e + kf_d \dot{e} + kf_i \int e dt \quad \text{With } e = \Omega_{pt} - \Omega_{ptn} \quad (66)$$

Is utilized for this purpose with net instantaneous fuel flow into the combustion chamber

$$\dot{m}_f = \widehat{m}_f + \dot{m}_{fn} \quad (67)$$

Where the PID control, with control gains kf_p , kf_d , kf_i and kf_b determines the fuel flow deviation \widehat{m}_f About the nominal fuel rate \dot{m}_{fn} in order to regulate the power turbine set-point speed error e to zero, where kf_b is the anti-windup gain. The stability and performance

characteristics of the closed-loop engine system is strongly affected by the gain values kf_p , kf_d , kf_b and kf_i . Table 2.3 summarizes the fuel control gains and nominal fuel rate corresponding to the engine design in this simulation.

Table 3: Fuel Control gains and Nominal fuel rate

| | | | |
|-------------------|--|--------------------------------|----------------------------------|
| Nominal Fuel Rate | \dot{m}_{fn} $= 0.2107 \text{ kg/sec}$ | | |
| PID Control Gains | Proportional gain | Integral gain | Derivative Gain |
| | $kf_p = 4e - 3 \text{ kg}$ | $kf_i = 1e - 2 \text{ kg/sec}$ | $kf_d = 4e - 5 \text{ kg - sec}$ |
| | Anti-windup gain (back calculating gain) = 100 | | |

2.8 TRANSIENT GAS TURBINE ENGINE SIMULATION

The dynamic simulation model of the gas turbine consists of a mixed set of ordinary differential and nonlinear algebraic equations. During each simulation time step, the mass flow through each component (compressor, gas generator turbine and power turbine) is interpolated using the numerically generated characteristic maps for the instantaneous rotation speed and upstream and downstream pressure states. As was shown in [11] a non-iterative solution to the equations can be obtained through forward substitution provided that the equations are solved in the proper sequence. Here equations are arranged in order to explicitly generate the output values by forward substitution. At each time step, the differential equations are integrated by means of an explicit scheme, thus obtaining the new values of the system plenum pressures, fuel control input and shaft rotational speeds. As was shown in [11] when the equations are ordered in accordance with the stream direction of the gas turbine model this results in the proper solution order. Figures 2.17 –2.21 summarize the non-iterative transient gas turbine engine simulation model which is implemented in the Mat lab® Simulink™ environment.

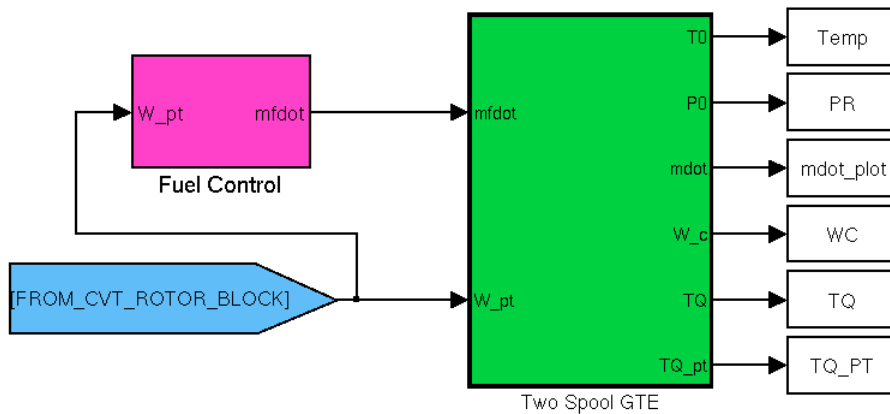


Figure 2.17: Gas Turbine Engine with fuel control block

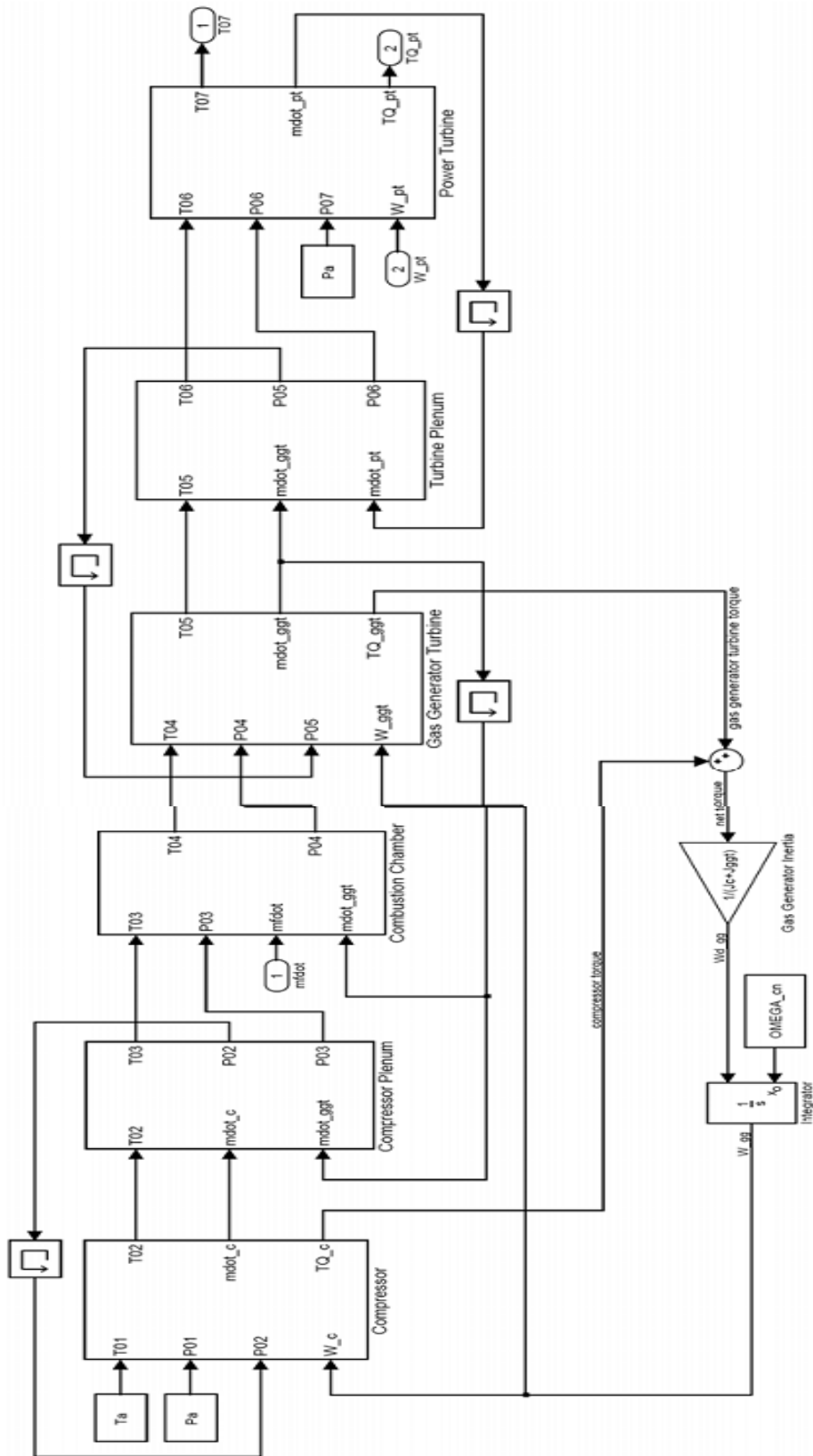


Figure 2.18: Two Spool gas turbine engine simulation block

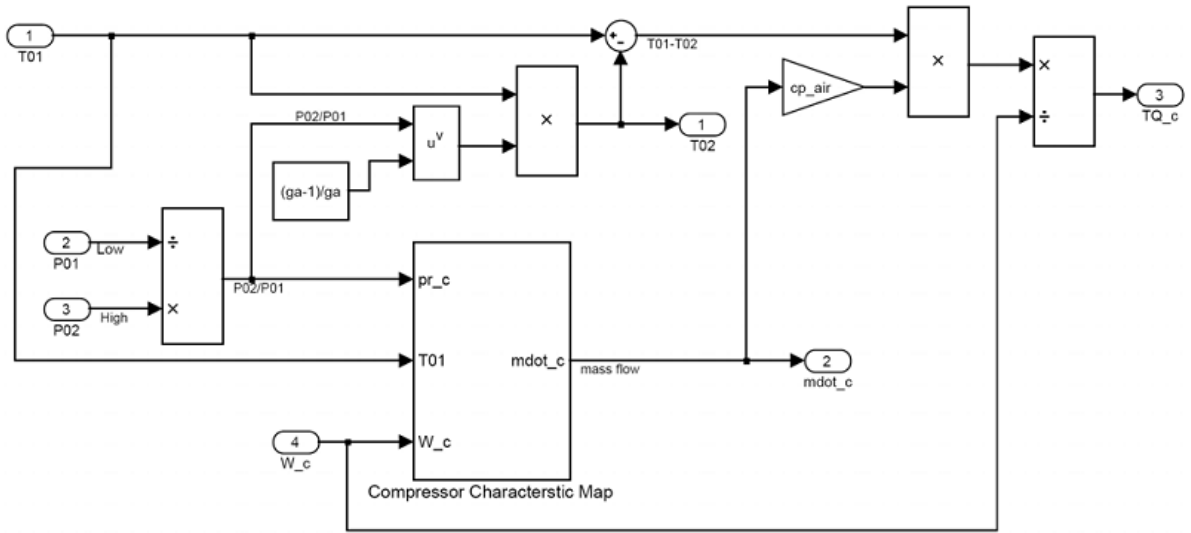


Figure 2.19 : Compressor Simulation Block

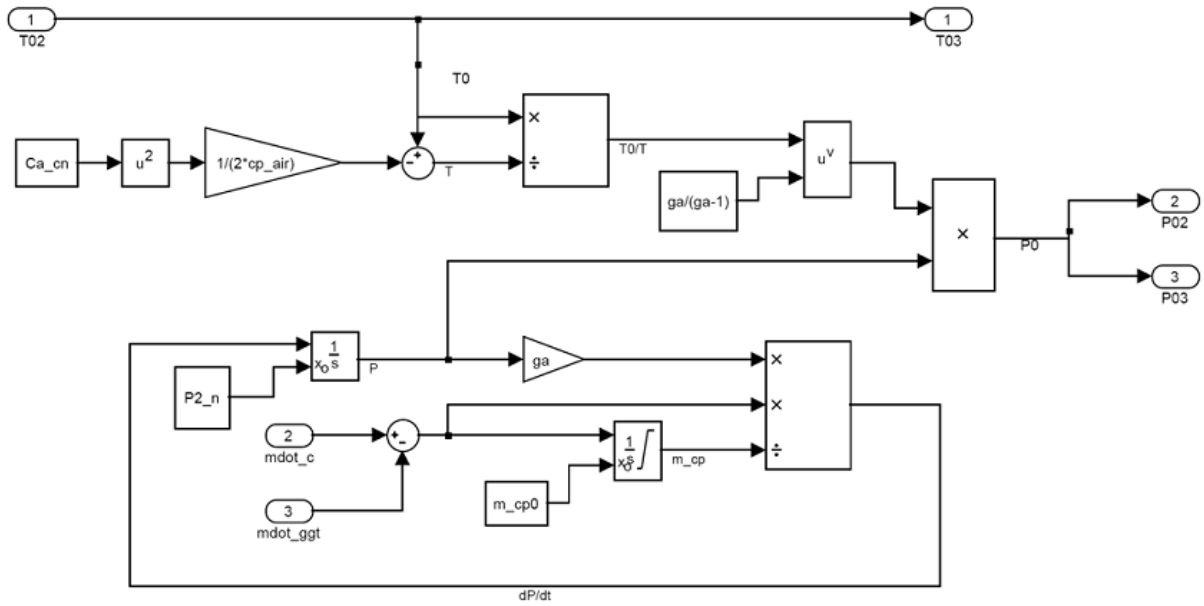


Figure 2.20 : Inter compressor/combustion chamber plenum

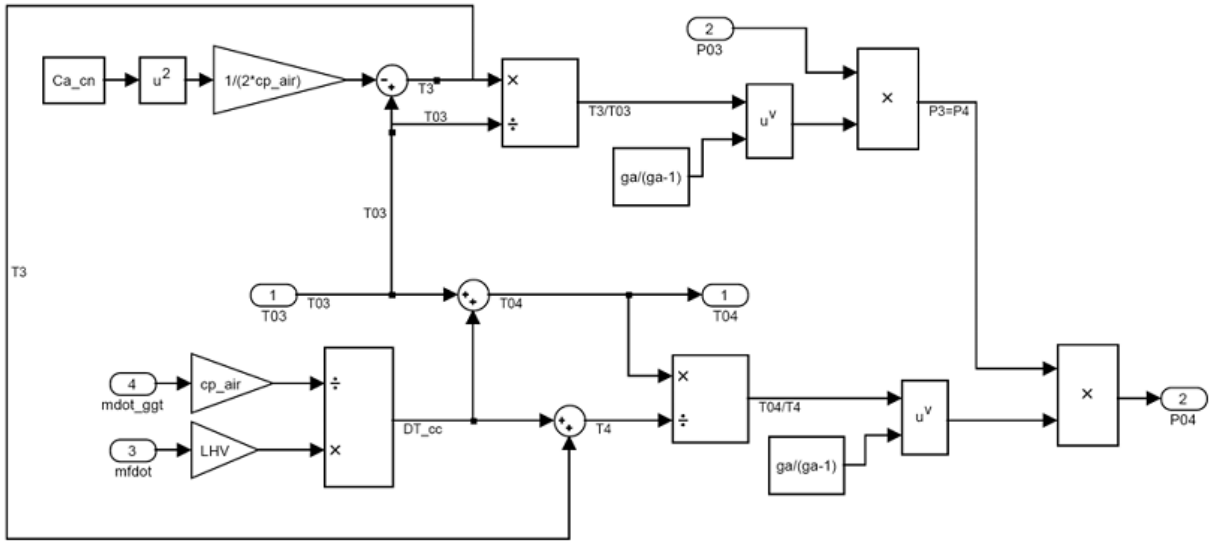


Figure 2.21: Combustion chamber simulation block

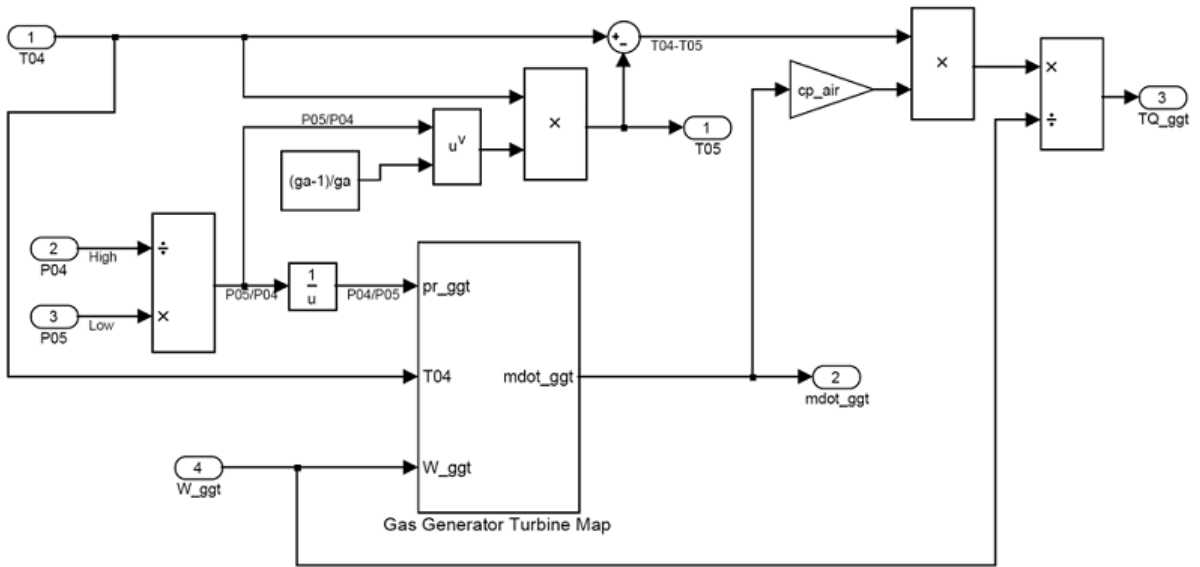


Figure 2.22: Gas generator turbine simulation block

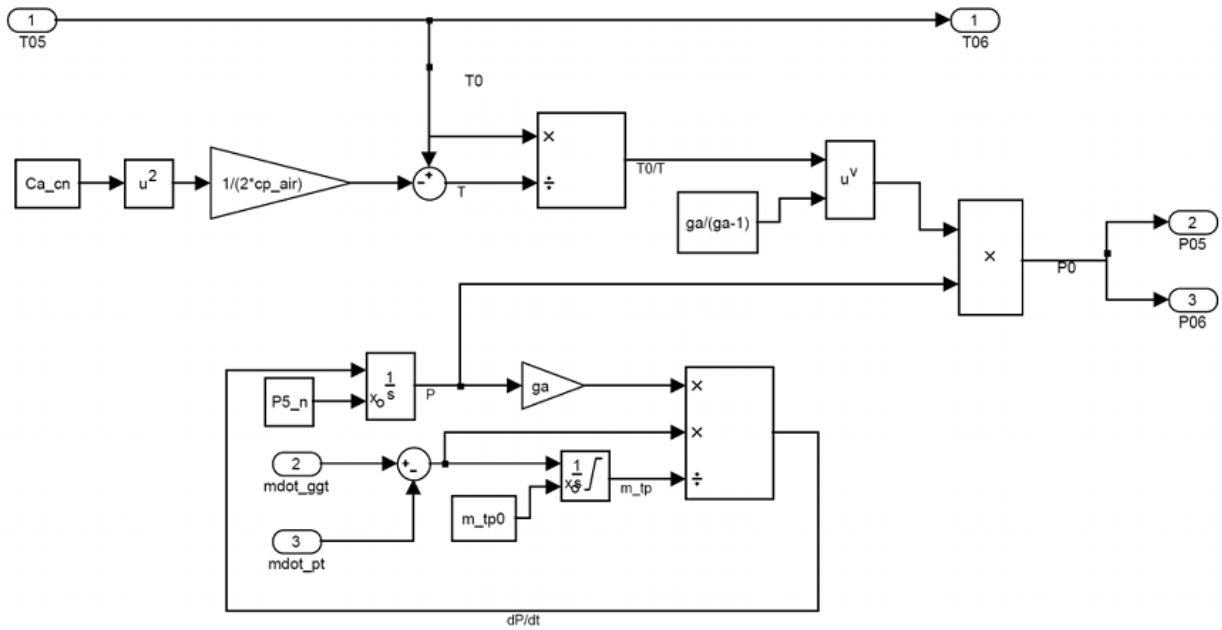


Figure 2.23: Inter turbine plenum

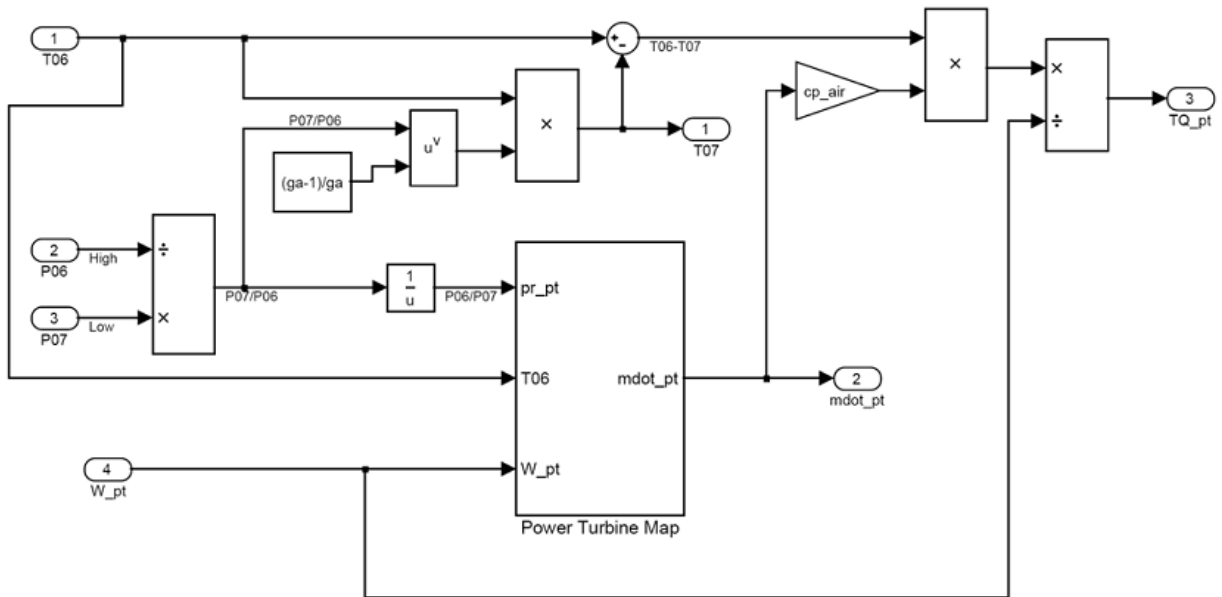


Figure 2.24 Power turbine simulation block

3. IDEAL CVT SYSTEM/GEARBOX DYNAMIC MODEL

3.1 INTRODUCTION

Aircraft sizing design studies have identified that a two-speed rotor configuration is required [1-2]. Rotor speed at cruise is required to be reduced, possibly down to 50% of hover speed, to keep rotor blade advancing tip speeds reasonable. One early study of a multi-speed rotorcraft drive system consisted of a high speed traction drive variator and a planetary differential gear unit [3]. A unit was tested and performed as designed. However, the mechanical efficiency was lower than that of a conventional drive system. Also, the use of traction drives for a main drive path is not an accepted practice for U.S. rotorcraft manufacturers. Previous studies have been sponsored by NASA to investigate multi-speed drive systems [4-5]. These studies looked at earlier tilt rotor applications where 15% speed reduction for cruise was required. Dual path configurations and compound planetary configurations looked promising. However, a major concern of the shifting process as well as drive system weight penalties resulted from the studies. An electro-mechanical infinitely variable transmission, comprising a pair of planetary trains interconnected with two electric machines and clutches has been proposed [6]. Again, the mechanical efficiency suffered as well as the added complexity of two planetary systems. A unique concept called a per cyclic continuously variable speed transmission is being investigated [7]. It uses per cyclic kinematics to achieve single speed reduction ratios between 1.05:1 and 50:1 with variable speed capability in one hardware stage. This concept, however, had yet to be tested. In summary, the results from previous studies indicate that the incorporation of multi-speed concepts in rotorcraft application is not a trivial process and adds complexity and weight. Thus, further research and development in this area is required, such as described in [8]. In addition, dynamic modeling of multi-speed drive systems can help define the characteristics and limitations of the drive systems and the shifting process.

Since very few multi-speed rotorcraft studies have been published, very little work on dynamic modeling for multi-speed rotorcraft drive systems has been done. There has been, however, numerous publications on dynamic modeling of automotive drive systems. Much of the work addresses the automatic transmission shifting control with emphasis on maximizing fuel economy and maintaining performance [9-15]. For these, the typical system being modeled is the gasoline combustion engine, torque convertor, multi-speed gearbox, tires and vehicle dynamics, as well as throttle and shifting controls. Dynamic speed, gear ratio, and torque are amongst the parameters predicted. This strategy has been applied to hybrid powertrains [16-17], continuously variable transmissions [18-22], and even heavy trucks and tanks for the military [23-27]. The modeling in the automotive field has had much success in improving drive train development. The approach and some modeling tools can be extended to the rotorcraft arena. However, specifics of integration of the gas turbine engine, multi-speed drive systems and the dynamics of the rotor and rotorcraft vehicle have yet to be addressed in the rotorcraft application.

3.2 SINGLE PATH DRIVELINE OF AN IDEAL CVT SYSTEM

To predict the shift response of an ideal CVT system, a torsional dynamics model including gear, CVT, shaft and load inertias, as well as shaft torsional flexibilities is developed.

CVT SYSTEM DESCRIPTION:

A schematic of single path driveline of an ideal CVT model is shown in Fig. 3.1 and the kinematics are summarized in equations (1-3) and by the kinematic diagram in Fig 3.2.

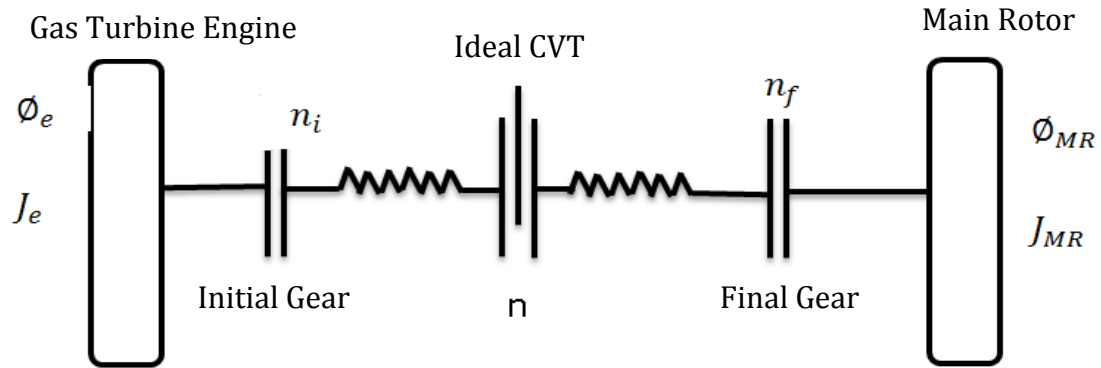


Figure 3.1: Single path driveline of an ideal CVT model connected to a Gas Turbine Engine.

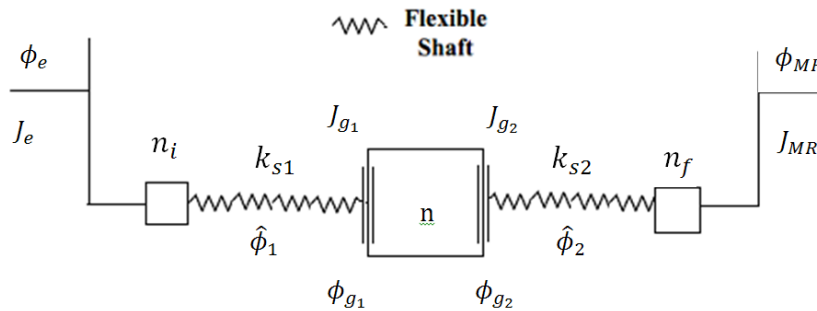


Figure 3.2: Single path CVT torsional dynamic model

$$\begin{aligned}
\phi_0(t) &= n_i \phi_e(t) \\
\phi_{MR}(t) &= n_f \phi_f(t) \\
\phi_{g_1}(t) &= \widehat{\phi}_1(t) + \phi_0(t) \\
\phi_f(t) &= \widehat{\phi}_2(t) + \phi_{g_2}(t) \\
\dot{\phi}_{g_2}(t) &= n \dot{\phi}_{g_1}(t)
\end{aligned} \tag{1}$$

Here, ϕ_e is the engine rotation, ϕ_{MR} is the main rotor(load) rotation, ϕ_{g_1} and ϕ_{g_2} are CVT gear rotations ϕ_0 and ϕ_f are initial and final rotations and $\widehat{\phi}_1$ and $\widehat{\phi}_2$ are rotations of shafts with torsional stiffness K_{s_1} and K_{s_2} respectively.

The system kinetic energy can be expressed as:

$$T = \frac{J_e}{2} [\dot{\phi}_e(t)]^2 + \frac{J_{g_1}}{2} [\dot{\phi}_{g_1}(t)]^2 + \frac{J_{g_2}}{2} [\dot{\phi}_{g_2}(t)]^2 + \frac{J_{MR}}{2} [\dot{\phi}_{MR}(t)]^2 \tag{2}$$

Where $J_e, J_{g_1}, J_{g_2}, J_{MR}$ are rotational inertias of Engine(Power Turbine), CVT gears and Main Rotor(load) respectively. Furthermore, the total strain energy is

$$U = \frac{K_{s_1}}{2} [\phi_{g_1}(t) - \phi_0(t)]^2 + \frac{K_{s_2}}{2} [\phi_f(t) - \phi_{g_2}(t)]^2 \tag{3}$$

Where K_{s_1} and K_{s_2} are torsional stiffness values of shafts on either side of CVT block(see Fig 1). Finally the virtual work done by the system torques is

$$\delta P = T_e \delta \phi_e(t) - T_{MR} \delta \phi_{MR} \tag{4}$$

Where T_e is Engine(Power Turbine) torque and T_{MR} is Main Rotor(Load) torque. After applying Euler-Lagrange equations to (3.2)-(3.3)

$$\frac{d}{dt} \left[\frac{\partial T}{\partial \dot{q}} \right] - \frac{\partial T}{\partial q} + \frac{\partial U}{\partial q} = Q \tag{5}$$

the following equations of motion are obtained

$$M \ddot{q} + C \dot{q} + K q = Q_{T_e} T_e + Q_{T_{MR}} T_{MR} \tag{6}$$

with the corresponding generalized vector

$$q = [\phi_e \quad \widehat{\phi}_1 \quad \widehat{\phi}_2 \quad \phi_e \quad \dot{\widehat{\phi}}_1 \quad \dot{\widehat{\phi}}_2]^T \tag{7-a}$$

$$q = [\phi_e \quad \widehat{\phi}_1 \quad \widehat{\phi}_2]^T \tag{7-b}$$

Here the system mass and stiffness matrices M and K, are

$$M = \begin{bmatrix} J_e + (J_{g_1} + (J_{g_2} + J_{MR}n_f^2)n^2)n_i^2 & n_i(J_{g_1} + (J_{g_2} + J_{MR}n_f^2)n^2) & J_{MR}n_f^2n_in \\ n_i(J_{g_1} + (J_{g_2} + J_{MR}n_f^2)n^2) & (J_{g_1} + (J_{g_2} + J_{MR}n_f^2)n^2) & J_{MR}n_f^2n \\ J_{MR}n_f^2n_in & J_{MR}n_f^2n & J_{MR}n_f^2 \end{bmatrix} \quad (8-a)$$

$$Cnd = n \begin{bmatrix} 2(J_{g_2} + J_{MR}n_f^2)n_i^2n & 2(J_{g_2} + J_{MR}n_f^2)n_in & J_{MR}n_f^2n_i \\ 2(J_{g_2} + J_{MR}n_f^2)n_in & 2(J_{g_2} + J_{MR}n_f^2)n & J_{MR}n_f^2 \\ J_{MR}n_f^2n_i & J_{MR}n_f^2 & 0 \end{bmatrix} \quad (8-b)$$

$$K = \begin{bmatrix} 0 & 0 & 0 \\ 0 & K_{S_1} & 0 \\ 0 & 0 & K_{S_2} \end{bmatrix} \quad (8-c)$$

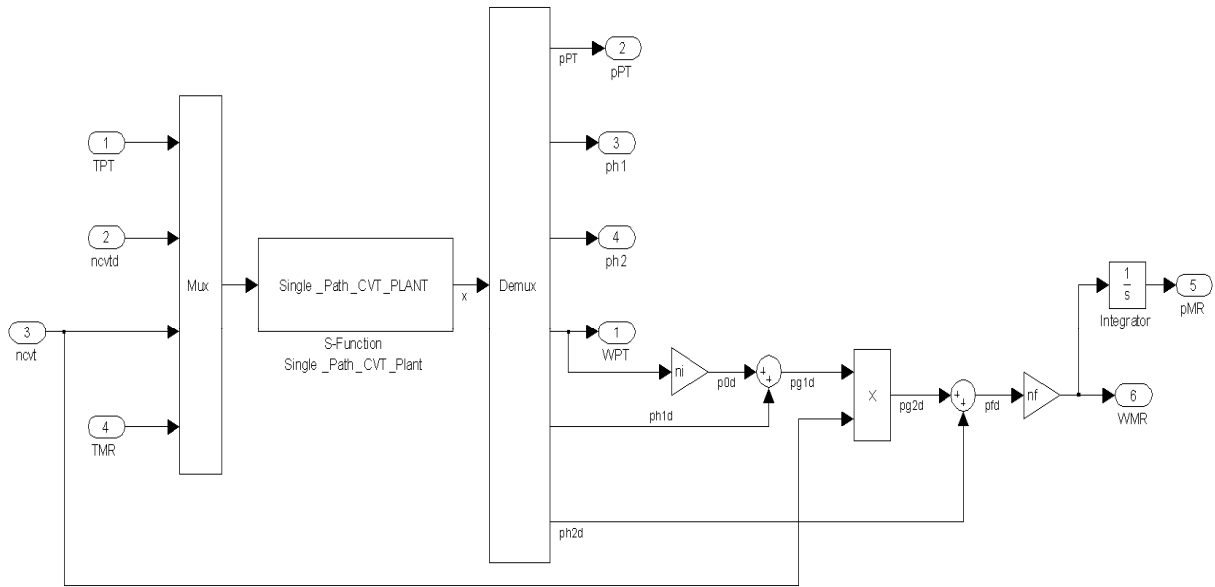


Figure 3.3: Continuously variable transmission block

3.3 FORWARD FLIGHT ROTOR (PROPELLER) MODEL

To include the rotor torque and resulting thrust for the tilt rotor in forward flight airplane mode with vehicle speed a rigid propeller model based on a standard blade element theory approach with quasi—steady aerodynamics is utilized (see Fig.1). Here the incremental rotor thrust and torque at blade radial location are expressed as

(9)

where and are blade lift and drag force increments along with the number of blades .

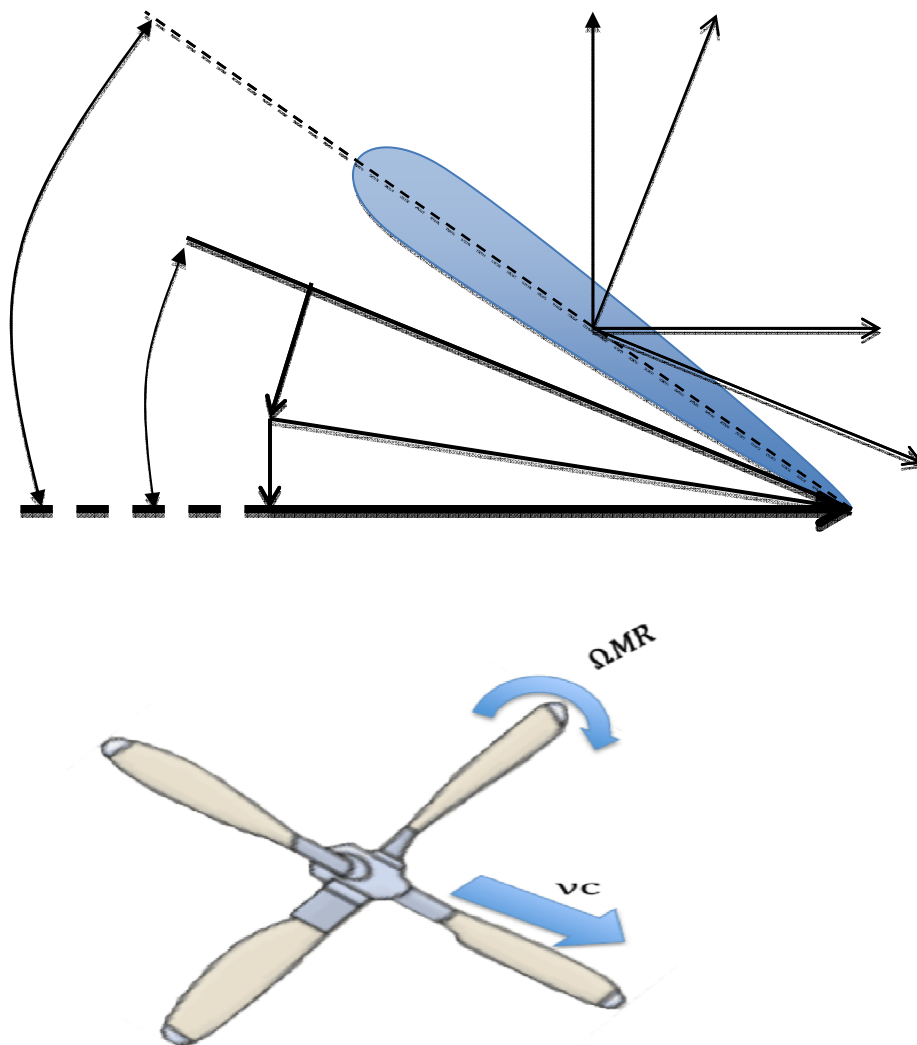


Fig:3.4 Propeller in forward flight.

Based on the tangential blade speed $\mathbf{v}_T = \boldsymbol{\Omega}_{MR}\mathbf{r}$, together with v_c , and the inflow velocity v_{ind} , the total inflow angle ϕ , is

$$\phi = \phi_c + \phi_{ind} \quad (10-a)$$

$$\phi_c = \tan^{-1} \left[\frac{v_c}{\Omega_{MR}r} \right] \quad \text{and} \quad \phi_{ind} = \frac{v_{ind}}{\sqrt{v_c^2 + \Omega_{MR}^2 r^2}} \quad (10-b)$$

where the induced inflow angle, ϕ_{ind} is assumed small as shown in Fig 3.4 Now, assuming uniform induced inflow velocity v_{ind} together with uniform blade pitch θ_p , the following expression for total rotor thrust is obtained as

$$FT_{MR} = \frac{\rho_{air} a_{cL} c N_b \Omega_{MR}}{2} \int_0^{R_b} \Psi_c (\phi_c + \phi_{ind} - \theta_p) (v_c \phi_{ind} - r \Omega_{MR}) r dr \quad (11)$$

Similarly the corresponding rotor torque is

$$TQ_{MR} = \frac{\rho_{air} c_D c N_b \Omega_{MR}}{2} \int_0^{R_b} \Psi_c (r \Omega_{MR} - v_c \phi_{ind}) r^2 dr - \frac{\rho_{air} a_{cL} c N_b \Omega_{MR}}{2} \int_0^{R_b} \Psi_c (\phi_c + \phi_{ind} - \theta_p) (v_c + r \Omega_{MR} \phi_{ind}) r^2 dr \quad (12)$$

Both with

$$\Psi_c = \sqrt{1 + \frac{v_c^2}{\Omega_{MR}^2 r^2}} \quad (13)$$

With air density ρ_{air} , rotor radius R_b and rotor chord c . Also c_D is the blade section drag coefficient and a_{cL} is the blade section lift coefficient slope.

Next by equating the thrust expression in (3) with an expression based on momentum theory we obtain the following equation for the induced flow ratio λ_{ind}

$$a_\lambda \lambda_{ind}^2 + b_\lambda \lambda_{ind} + c_\lambda = 0 \quad (14-a)$$

With coefficients

$$a_\lambda = 48 \ln \left[\frac{\gamma_c}{\lambda_c} \right] \lambda_c^2 + 6 a_{cL} \sigma \ln \left[\frac{1+\gamma_c}{\lambda_c} \right] \lambda_c - 24 \quad (14-b)$$

$$b_\lambda = 24 \sin^{-1} \left[\frac{1}{\lambda_c} \right] \lambda_c^3 + 6 a_{cL} \sigma \ln \left[\frac{\gamma_c}{\lambda_c} \right] \lambda_c^2 + \dots \\ (-24 \gamma_c + 6 a_{cL} \sigma \tan^{-1} \lambda_c - 6 a_{cL} \sigma \theta_p) \lambda_c - 3 a_{cL} \sigma \quad (14-c)$$

$$c_\lambda = a_{cL} \sigma \left(\pi - 2\theta_p - \ln \left[\frac{1+\gamma_c}{\lambda_c} \right] \right) \lambda_c^3 - 2 a_{cL} \sigma \gamma_c \tan^{-1} [\lambda_c] \lambda_c^2 \\ - a_{cL} \sigma \gamma_c \lambda_c + 2 a_{cL} \sigma \gamma_c (\gamma_c^2 \theta_p - \tan^{-1} [\lambda_c]) \quad (14-d)$$

With induced and forward speed inflow ratios

$$\lambda_{ind} = \frac{v_{ind}}{R_b \Omega_{MR}}, \quad \lambda_c = \frac{v_c}{R_b \Omega_{MR}} \quad \text{and} \quad \gamma_c = \sqrt{1 + \lambda_c^2} \quad (15)$$

and rotor solidity ratio

$$\sigma = \frac{cN_b}{\pi R_b} \quad (16)$$

Based on (14)-(16), the induced velocity v_{ind} , is determined from the roots of (14-a). Using this result in (11) and (12), the rotor thrust and torque values can be computed for a given rotor speed, forward speed and blade pitch angle as shown in the rotor thrust and torque simulation block in Fig. 3.5

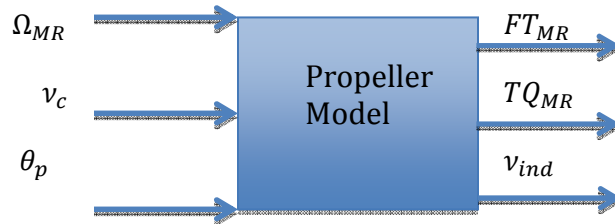


Figure 3.5: Rotor thrust and torque simulation block

Rotor parameters used in this investigation are summarized in Table 3.

TABLE 4. ROTOR PARAMETERS

| Parameter | Value |
|------------------------------------|------------------------------------|
| Number of Blades, N_b | 4 |
| Rotor radius, R_b | 9.91 m |
| Rotor solidity ratio, σ | 0.13 |
| Blade mass, m_b | 372 Kg |
| Rotor rotational Inertia, J_{MR} | $4.874 \times 10^4 \text{ Kg m}^2$ |
| Section Lift Coefficient, c_D | 0.012 |
| Section drag Coefficient, a_{cL} | 5.056 |

3.4 CONTROL SYSTEM

The variable speed rotorcraft transmission system consists of two major control systems. The in-flight maneuvers as regulated by these two different close-loop control systems (i.e., the engine fuel control and blade pitch forward speed control). Using these variable speed transient system response is computed.

ENGINE FUEL CONTROL SYSTEM:

A PID based Power Turbine speed controller with an anti-windup gain is used to regulate the power turbine speed.

BLADE PITCH CONTROL SYSTEM:

A PID based main rotor blade pitch controller is used to regulate the rotor thrust to track a desired forward set point speed (controls main rotor pitch θ_{pitch})

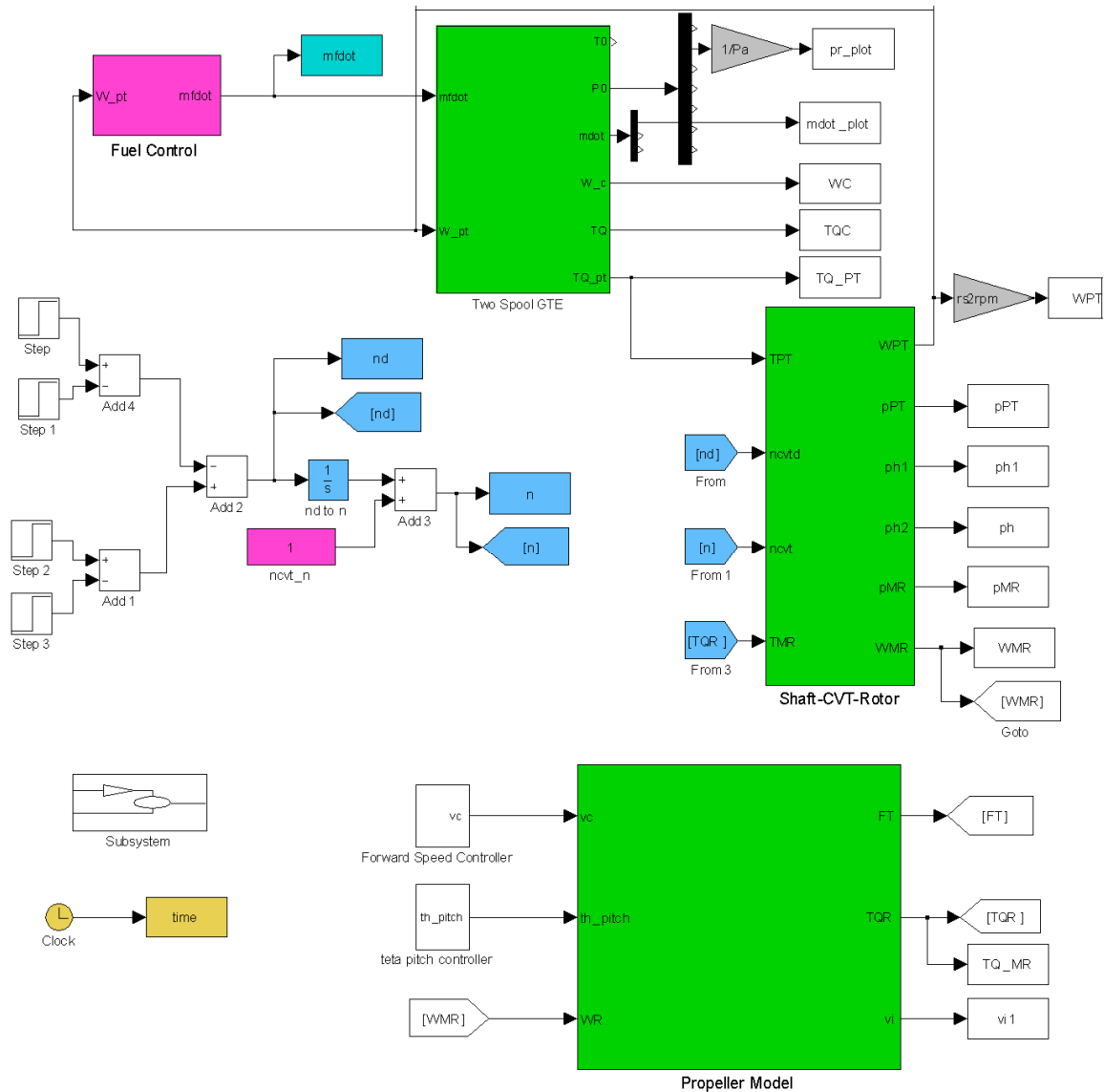


Figure 3.6: Comprehensive Variable Speed Rotorcraft Propulsion Model

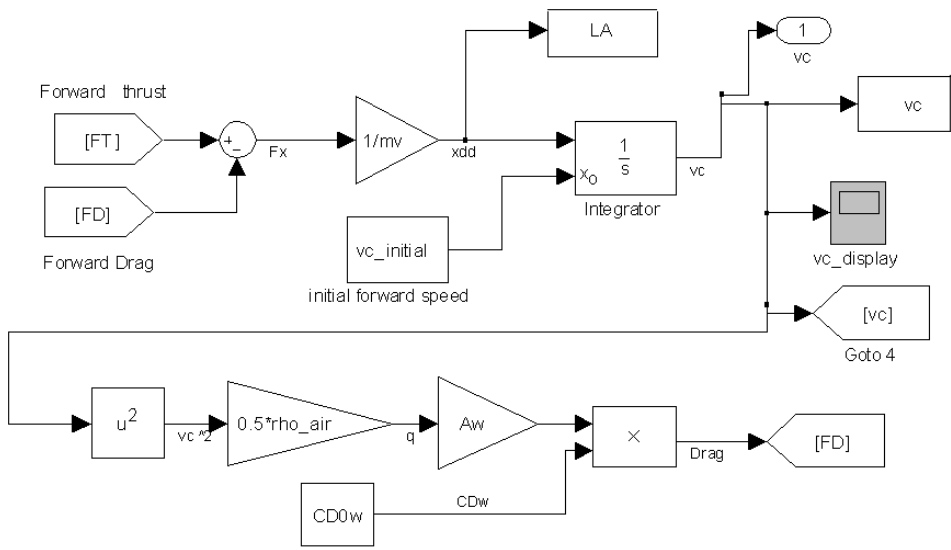


Figure 3.7: Forward Speed Controller Block

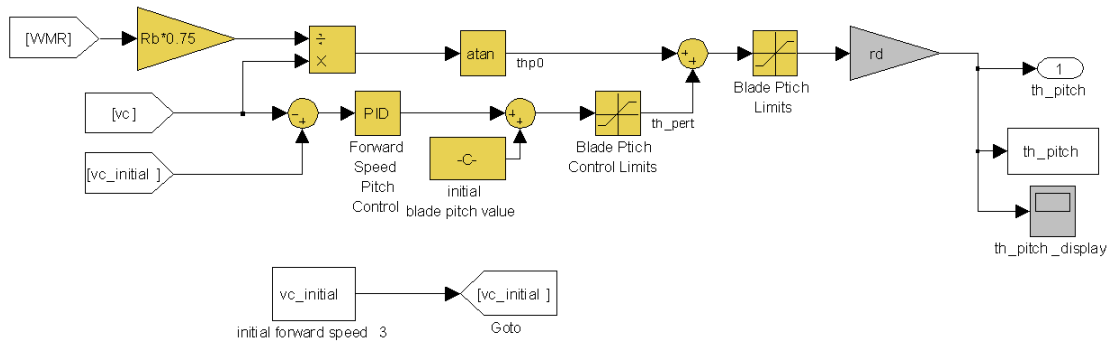


Figure 3.8: Blade Pitch Controller Block

4. RESULTS, CONCLUSIONS AND FUTURE SCOPE

4.1 INTRODUCTION

One of the main goals of this project is to develop a comprehensive first principles-based drive-system modeling tool to predict the complex transient dynamic response of variable speed rotorcraft propulsion systems including engine, transmission and rotor dynamic interactions. By accounting for the various propulsion sub-system dynamic interactions, this new Comprehensive Variable Speed Rotorcraft Propulsion System Modeling (CVSRPM) tool enables performance prediction to give future design insights and enable system level understanding.

According to a recent NASA-Army-Industry-University investigation, significant benefits to rotorcraft operational performance, effectiveness and acoustic signature could be gained through the ability to adjust main rotor speed to accommodate various flight conditions [1]. In particular, variable speed rotor technology is critical to the slowed-rotor compound configuration concepts and would offer significant benefits to future Heavy-Lift helicopter and tilt rotor configurations as well as variable diameter rotor concepts [2]. Current rotorcraft propulsion systems are designed around a fixed-ratio transmission without the capability to vary rotor speed except by engine speed adjustment. Since the specific fuel consumption of modern gas-turbine engines is optimum within a relatively narrow speed range, the ability to achieve a variable speed rotor through engine speed adjustment is limited [3]. Therefore, to achieve effective variable rotor speed designs, utilizing a variable ratio transmission in the rotorcraft propulsion system becomes necessary.

Furthermore, another goal is to exercise this newly developed computational tool to explore the behavior of various variable ratio rotorcraft drive-system configurations and ratio changing strategies under simulated operational conditions. To address these goals, a comprehensive rotorcraft propulsion system simulation tool based on the sub-system models developed in Chapter II-III is constructed. Simulations are then performed for several different drive system configurations to evaluate their variable speed performance characteristics.

4.2 COMPREHENSIVE VARIABLE SPEED ROTORCRAFT PROPULSION SYSTEM MODEL

The comprehensive dynamic simulation tool assembled in this project is based combining several of the key rotorcraft driveline sub-system models developed so far in Chapters II and III. Figure 1 shows a schematic of the overall CVSRPM architecture along with the various sub-system model interaction paths. Specifically, the main elements and assumptions included in this comprehensive, variable speed, drive system simulation tool are as follows;

- Two-spool gas turbine engine transient dynamics model and closed-loop PID fuel

controller to regulate power turbine speed (from Chapter I).

- Ideal CVT gearbox model (from Chapter III).
- Torsionally flexible shafting.
- A single DOF flight dynamics model for fuselage drag and vehicle forward flight dynamics.

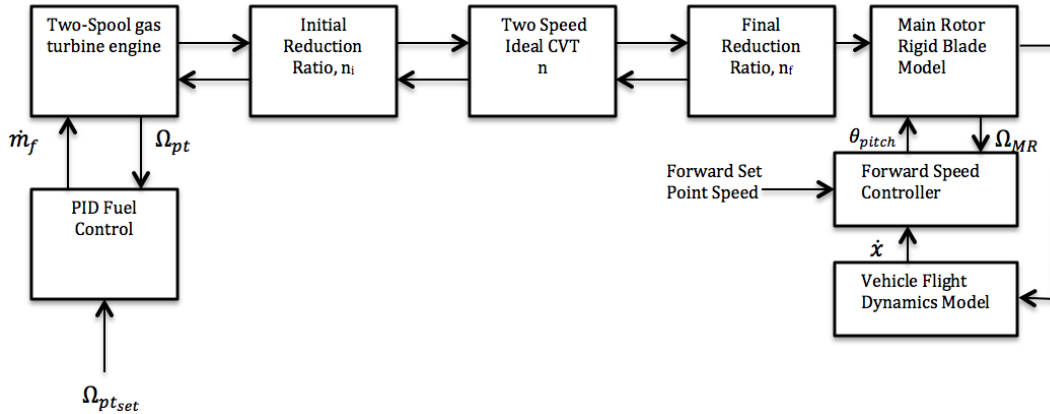


Figure 4.1: Comprehensive Variable Speed Rotorcraft Propulsion System Model

The comprehensive dynamic simulation code is implemented under the Matlab® Simulink™ software environment. Here, each sub-system block of the CVSRPM code as shown in Figure 4.1 is detailed in the Appendix. Figure 4.2 gives a schematic of the two-speed helicopter drive system simulation model implemented with the CVSRPM code.

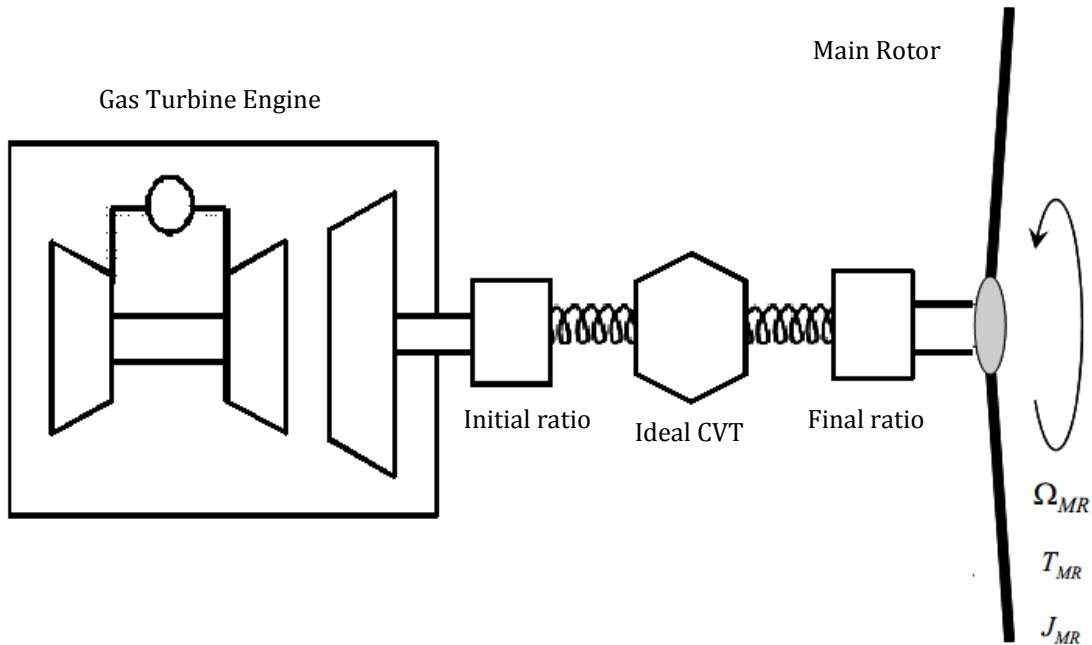


Figure 4.2: Two speed helicopter drive system simulation model

4.3 RESULTS

In this section the developed Comprehensive Variable Speed Rotorcraft Propulsion System Model (CVSRPM) is used to investigate the variable speed operational behavior of a rotorcraft with a Single Path Driveline and Ideal CVT system. The two cases considered are

- A) Constant forward speed and a varying rotor speed.**
- B) Varying forward speed with varying rotor speed**

In each case the system executes an in-flight maneuver as regulated by two different close-loop control systems (i.e., the engine fuel control and blade pitch forward speed control) and the resulting variable speed transient system response is computed.

A) Constant forward speed and a varying rotor speed

The simulated mission profile in Fig:4.3 is the slowed rotor/steady cruise scenario. This variable rotor RPM maneuver essentially consists of a downshift followed by an upshift, all with a constant set-point cruise speed v_c (300 knots), for three different shift rates. ($\Delta t = 5 \text{ sec}, 10 \text{ sec}, 15 \text{ sec}$).

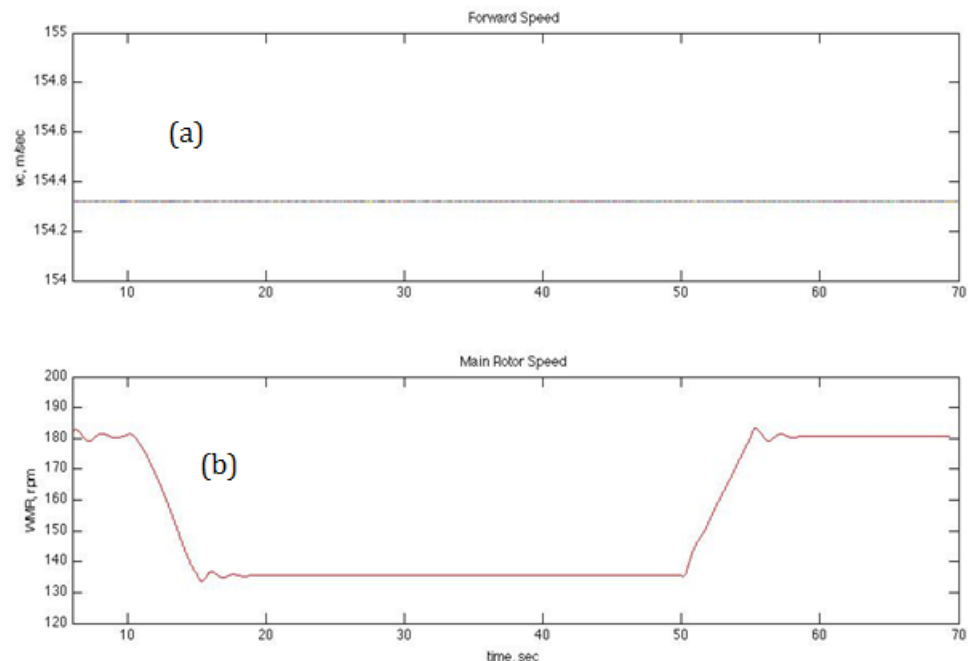


Figure 4.3: Slowed rotor/steady cruise-simulated mission profile.
(a) Forward Speed (b) Main Rotor Speed

The resulting system response is detailed in Figures 4.4-4.6. Here the helicopter is initially operating at 100% rotor speed, then at $t=10$ sec, the downshift is initiated.

Figure:4.4(a) shows corresponding response of the power turbine speed which is strongly influenced by the choice of fuel control gains. Figure:4.4(b) shows corresponding response of the main rotor speed which shows an essentially linear RPM decrease and a slight RPM dip can be observed due to system torsional compliances.

Next at $t=50$ sec, the upshift command is initiated. Here the process is essentially the reverse of the downshift and the corresponding rotor speed and engine speed responses are also well behaved.

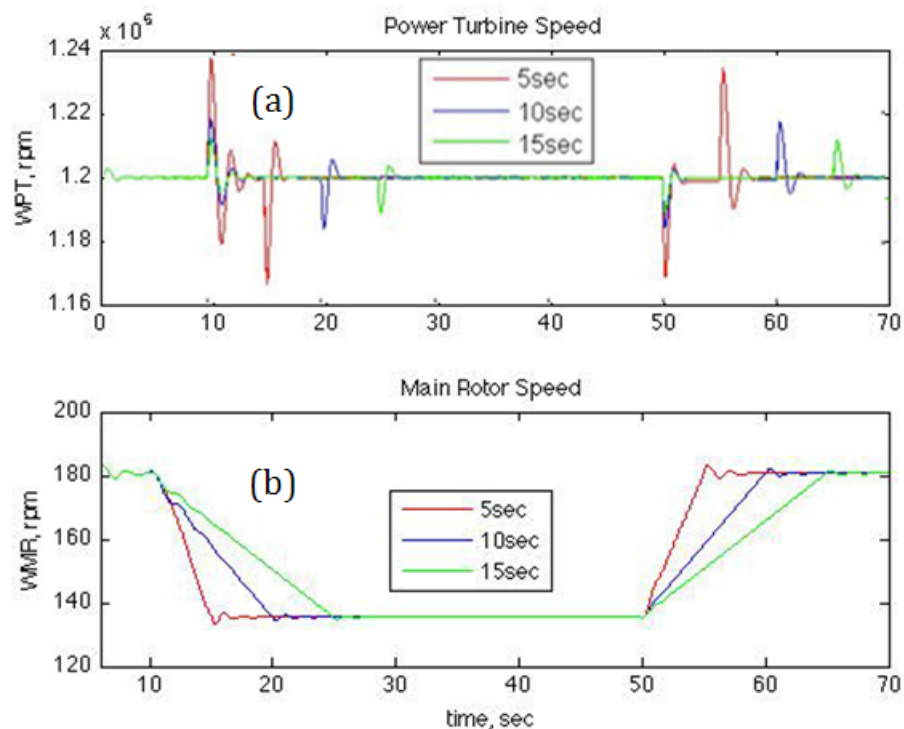


Figure 4.4: Two Speed Helicopter drive system response for slowed rotor/steady cruise; (a)Engine Power Turbine Speed (b)Main Rotor Speed

Further insight can be gained by observing Fig:4.5 which shows the system Torque responses. The engine output torque, shown in Fig:4.5(a) , is seen to have significant transients during both the downshift and the upshift events. Due to the magnitude of the engine torque increase, this cannot be explained by the effect of the main rotor blade pitch control.

Next it can be observed that the main rotor torque Fig:4.5(b) actually increases as a result of the lower rotor RPM. At first pass this seems counter intuitive; however, the rotor torque increase is a result of the pitch controller trying to maintain a constant rotor thrust. As the rotor RPM drops, the pitch controller

must add more collective blade pitch to generate the thrust, thereby increasing the rotor drag torque. The blade pitch control is shown in Fig:4.6(c).

An interesting observation is that the power dissipated during the downshift is significantly more than during the rotor upshift. One explanation for this is that a significant portion of the main rotors kinetic energy is being dissipated during the rotor speed downshift.

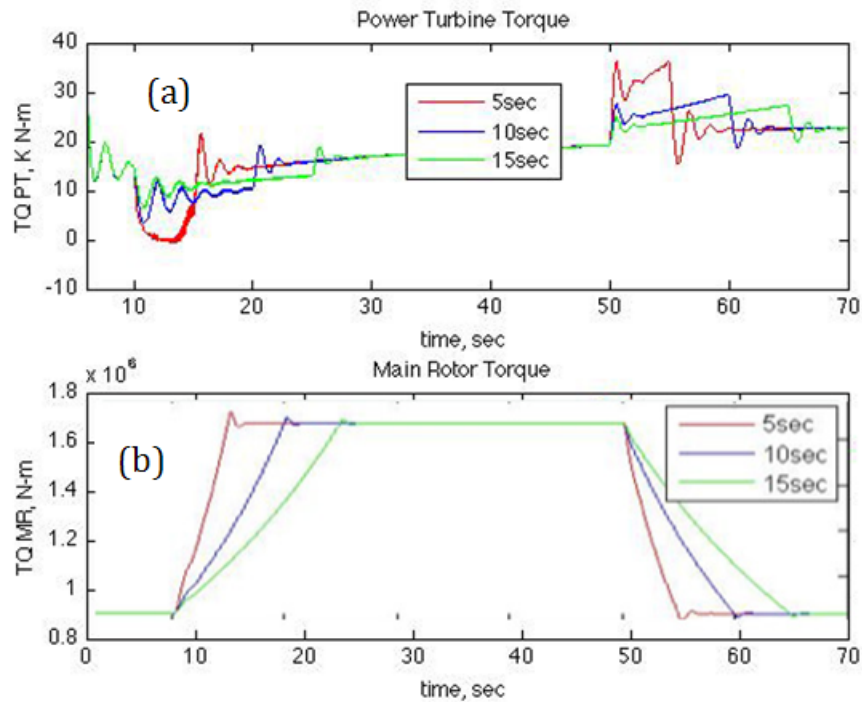


Figure 4.5: Two Speed Helicopter drive system response for slowed rotor/steady cruise; (a) Engine output Torque (b) Main Rotor Torque

Finally Fig:4.6 summarizes the corresponding helicopter flight parameters during the slowed rotor/steady cruise simulation. Here the induced velocity and blade collective pitch are plot against time during the upshift and downshift scenarios.

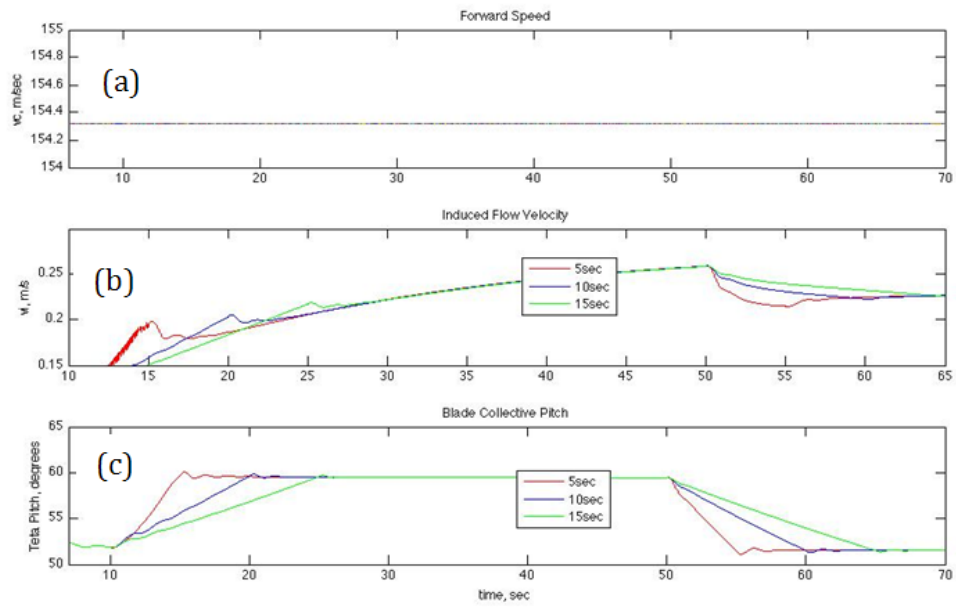


Figure 4.6: Two Speed Helicopter drive system response for slowed rotor/steady cruise; (a)Forward speed (b) Rotor Induced Flow (c)Blade pitch Input

B) Varying forward speed with varying rotor speed

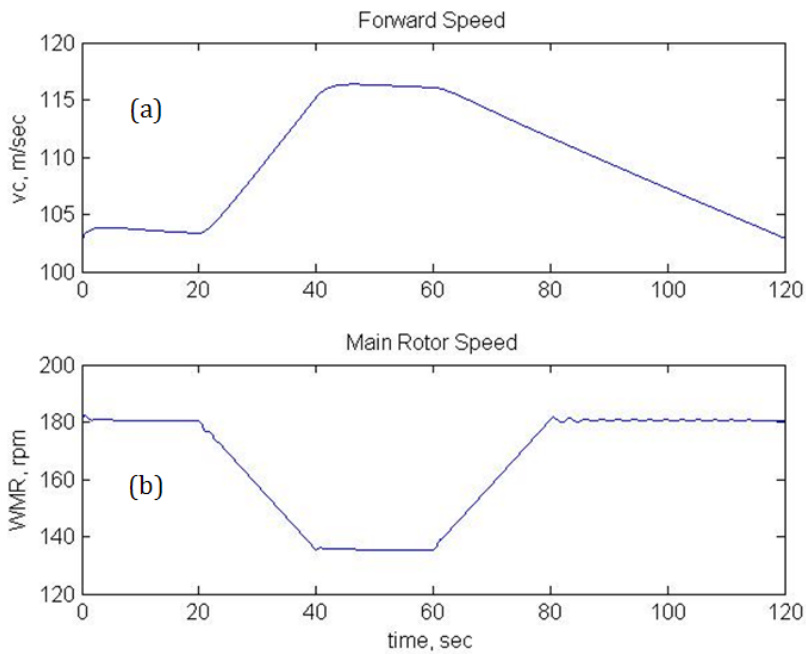


Figure 4.7: Slowed rotor/high-speed cruise - simulated mission profile
 (a)Forward Speed (b) Main Rotor Speed

The simulated mission profile for the variable speed rotor case is the scenario where in the system increases the forward speed and then reduces forward speed simultaneously reducing and increasing the main rotor speed as shown in Fig 4.7. This is the mission profile discussed in [4] for the LCTR-2 for when it is operating in forward-flight airplane mode. Specifically, in order to reduce the blade tip Mach number and associated losses, the rotor (propeller in the case of forward flight) is slowed to permit a higher forward flight cruising speed. In this case, at the start of the speed change maneuver, the rotor speed, Ω_{MR} is reduced from 180 RPM to 140 RPM (a 22 % reduction) while the forward speed set-point v_c is simultaneously commanded to increase from 200 to 225 knots. This mission profile was simulated in the model over a 120 second time span. The resulting two speed tilt rotor system response is detailed in Figures 4.8 –4.10.

Here the helicopter is initially operating at 100% rotor speed in forward flight airplane mode, then, at $t = 20$ seconds, maneuver is initiated. The forward speed set-point is ramped linearly from 200 to 225 knots over a 20 second time span. The resulting forward speed is shown in Fig. 4.8(a). Here it is seen that the forward speed controller, based on adjusting the blade pitch, is very effective in tracking the desired vehicle forward speed profile. The corresponding blade pitch control input and the induced velocity output is shown in Fig.4.10. In the downshift case (forward speed acceleration phase) the decreasing blade pitch influences the Main rotor torque to go down. During the 20 second speed increase from 200 to 225 knots the passengers would experience a maximum horizontal g of approximately 0.15. It can be observed that during upshift phase (forward speed deceleration phase) the shifting has been during a larger time step ($t=60$ sec) unlike the downshift phase (forward speed acceleration phase), where $t=20$ sec. This was done to avoid negative torques occurring at a lower time steps (i.e., $t < 60$ sec). To have flat deceleration rate we can have auxiliary devices like wing flaps or air-brakes. The fluctuations occurring during the power turbine speed and torque is due to the fuel flow gains.

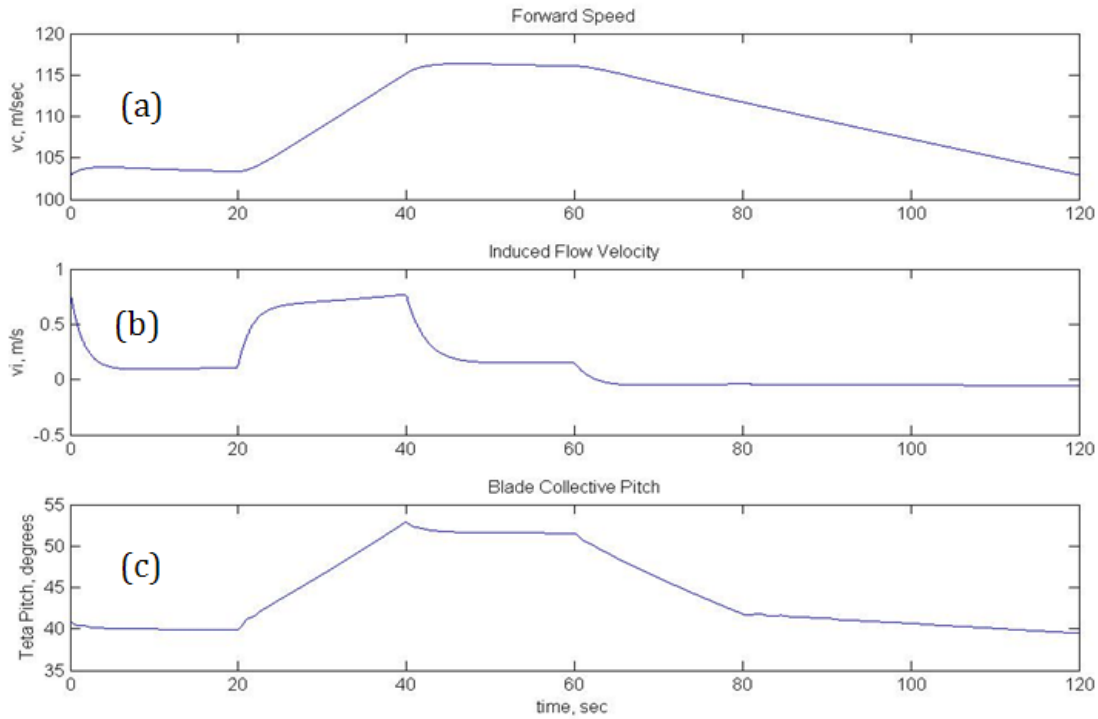


Figure 4.8: Two-speed rotor response for slowed rotor/high-speed cruise;
 (a) Forward speed (b) Induced velocity (c) Blade pitch input.

Upon observing Figs. 4.9 – 4.10, it is immediately found that, unlike the constant forward speed case considered in the last section, the downshift and upshift responses are not symmetric. In the following we will discuss each phase:

Downshift phase (forward speed acceleration phase) :

Figure 4.9(a) and (b) shows the corresponding engine and main rotor speeds. During the downshift (forward speed acceleration phase) the power turbine experiences a strong dip in speed near the end of the transition. The rotor speed also follows this transient speed drop (see Fig. 4.9(b)). Once again, similar to the (previous case in the last section), as the rotor speed drops, the forward speed control demands more blade pitch in order to satisfy the forward speed set-point. The previous case was less severe since the forward speed was constant. In this case, extra thrust is demanded to produce the required forward speed acceleration. This could be mitigated by placing more stringent constraints on the forward speed acceleration rate. Here, this is also seen by examining the rotor torque and the engine torque values in Fig. 4.10(a)-(b). Lower rotor speed means higher blade pitch angles and larger torque.

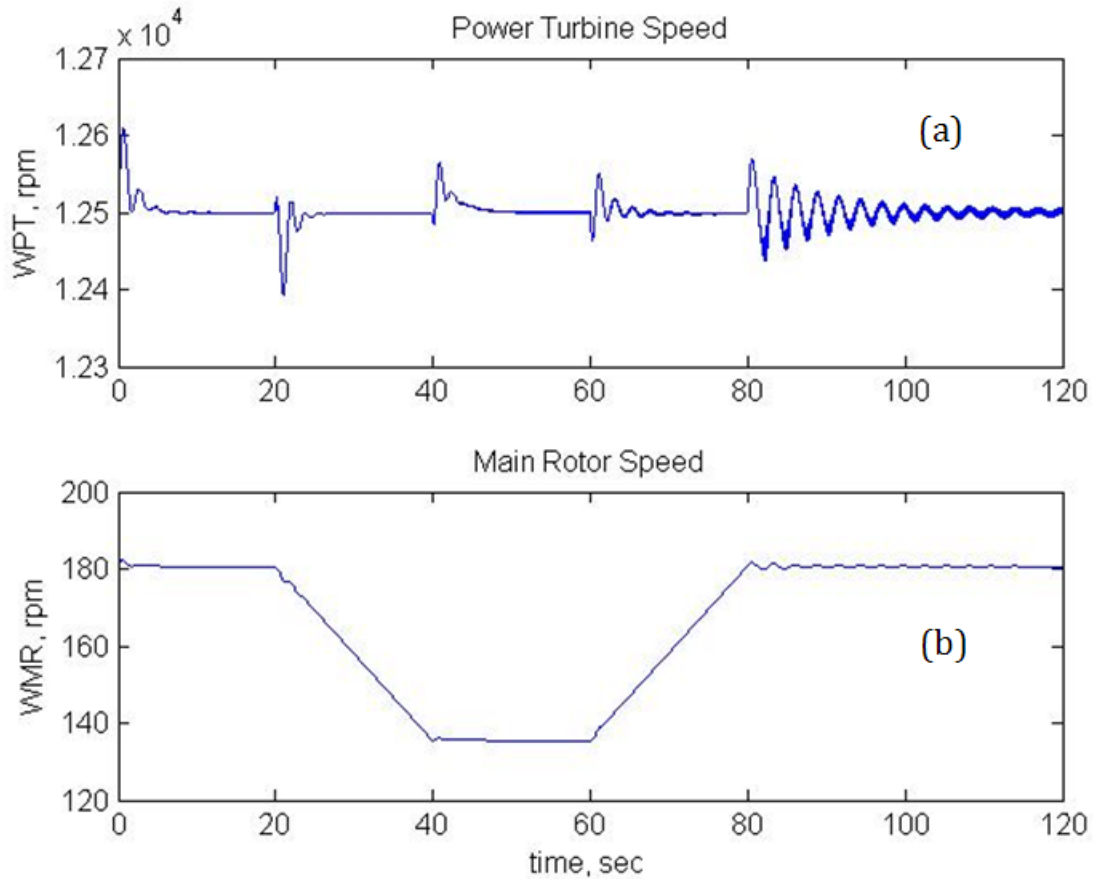


Figure 4.9 : Two-speed rotor response for slowed rotor/high-speed cruise; (a) engine power turbine response; (b) main rotor speed

Upshift phase (forward speed deceleration phase) :

When the upshift phase begins the forward speed control is commanded to begin decelerating the vehicle from 225 to 200 knots. During this phase, the blade collective pitch controller lowers the collective pitch, Fig 4.8(c). In this condition the forward air velocity drives the main rotor and the rotor experiences “wind milling”, Figs 4.9(b) and 4.10 (b). Hence, the motor output torques also becomes close to zero, Fig 4.10 (a). As a result of this rapid unloading of the engine, the power turbine RPM increases above the set-point before the fuel control is able to bring the speed back down, Fig. 4.9(a).

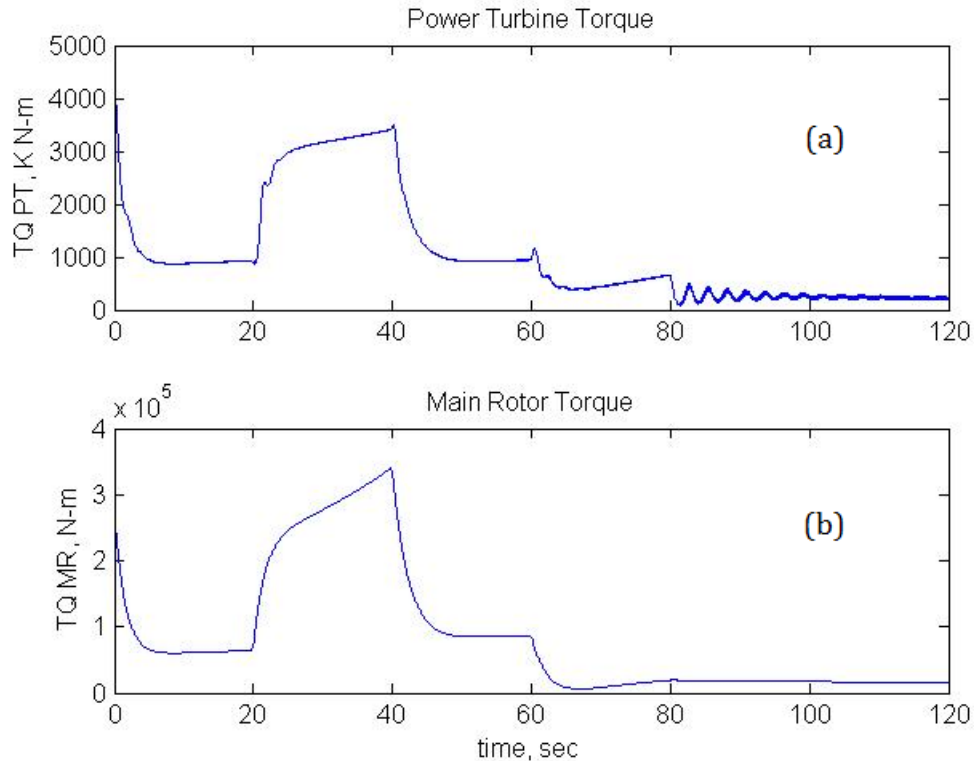


Figure 4.10 : Two-speed rotor response for slowed rotor/high-speed cruise; (a) engine power turbine torque (b) main rotor torque

4.4 FUTURE SCOPE

In the current CVSRPM the fuel flow rate is only function of the nominal fuel flow rate value i.e., the fuel flow saturates once the amount of fuel flown reaches 150% of the nominal fuel flow rate and also there is no limit on the compressor rotation speed. Hence in the future the case of including a compressor speed governor in the current model can be studied. Also the case of actual fuel flow rate being monitored depending on the variation of compressor speed or exit temperature of the combustion chamber can be studied.

4.5 CONCLUSIONS

This study explores the variable speed operation and transient shift response of a prototype of a two speed ideal CVT rotorcraft system based on the NASA LCTR-2 in forward flight airplane mode. Here a Comprehensive Variable Speed Rotorcraft Propulsion System Modeling (CVSRPM) tool developed is utilized to simulate the drive system dynamics under steady cruise condition. This research attempts to build upon previous variable speed rotorcraft propulsion studies by 1) Including a fully

nonlinear transient gas turbine engine model 2)by including shaft flexibility 3) By incorporating a basic flight dynamics model to account for interactions with the flight control system. Through exploring these interactions between various subsystems this analysis provides important insights into the continuing development of variable speed rotorcraft propulsion technology. Given the current trend toward tandem, tilt-rotor, multi-rotor, and co-axial rotor/pusher-prop configurations with numerous cross-shafting and multi-path power flow arrangements (e.g. Boeing CH-47 and V-22, Sikorsky X-2 High Speed Lifter and Heavy Lift quad tiltrotor concepts), It is hoped that the analysis tools and results presented from the CVSRPM code will be utilized as a guide for investigating and evaluating new configurations and designs for fixed and variable speed rotorcraft under a variety of operating conditions.

BIBLIOGRAPHY

CHAPTER 1

- [1] W. Johnson, G. K. Yamauchi and M.E. Watts “NASA Heavy Lift Rotorcraft Systems Investigation.” NASA 213467, December 2005.
- [2] Z. Saribay, A. Lemanski, M. Elmoznino, “Pericyclic Non-Traction Continuously Variable Speed Transmission (P-CVT): Rotorcraft Applications”, AHS International 62nd Annual Forum and Technology Display, Phoenix, AZ, May 9 – 11, 2006
- [3] J. Kish, "Vertical Lift Drive System Concept Studies Variable Speed/Two-Speed Transmissions," NASA CR -2002-211564, 2002.
- [4] Tatsuhiko, Goi, Kawakami, Koji, and Yamakawa, Eiichi, Advanced Technology Institute of Commuter Helicopter, Ltd, (ATIC), Kakamingahara, Japan, “Variable Rotor Speed Transmission With High Speed Traction Drive”, Presented at the American Helicopter Society 55th Annual Forum, Montreal, Quebec, Canada. May 25-27, 1999.
- [5] Kluger, M.A., et al., "An Overview of Current CVT Mechanisms, Forces and Efficiencies," SAE Technical Paper Series, 970687, 1997.
- [6] Davis, K., J. Frisk, & G. Jewett, "Pericyclic Differential", Univ. of Connecticut, Dept. of Mechanical Eng., Sr. Design Project, April 2004.
- [7] Lemanski A.J, Monahan, T.J. , "Non-Traction Pericyclic CVT's," 2004 International Continuously Variable and Hybrid Transmission Conference University of California – Davis, September 23-25, 2004.
- [8] White, G., Department of Mechanical Engineering, University of Technology, Loughborough Leics, England, “A Two-Path Variable Ratio Transmission With an Extended Range of Ratios”, The American Society of Mechanical Engineers, Paper No. 76-DET-37, 1976.
- [9] Parker, Richard J., Loewenthal, Stuart H., Fischer, George K., National Aeronautics and Space Administration, Lewis Research Center, “Design Studies of Continuously Variable Transmissions for Electric Vehicles”, Society of Automotive Engineers Congress, Detroit, Michigan, DOE/NASA/1044-12, NASA TM-81642, February 23-27, 1981.
- [10] Sauer, Georg, Institute of Agricultural Machinery, Technical University of Munich, Germany, “Continuously Variable Transmissions for Tractor Drive Line”, Report No 94-D-020, AGENG, Milano 1994.
- [11] R.C. Strawn and R. Biswas “Numerical Simulations of Helicopter Aerodynamics and Acoustics,” Journal of Computational and Applied Mathematics, 1996, Vol, 66 (1-2), pp. 471- 483.
- [12] P.P. Friedmann and T.A. Millott, “Vibration Reduction in Rotorcraft Using Active Control – Comparison of Various Approaches,” Journal of Guidance Control and Dynamics, 1995, Vol. 18, No. 4, pp. 664-673.
- [13] R.E. Brown, “Rotor Wake Modeling for Flight Dynamic Simulation of Helicopters,” AIAA Journal, 2000, Vol. 38, No. 1 pp. 57-83.
- [14] G. Lehmann, “The Effect of Higher Harmonic Control (HHC) on a 4-Bladed Hingeless Model Rotor,” Vertica, 1985 Vol. 9, No. 3, pp. 273-284.
- [15] Krothapalli, K.R., J.V.R. Prasad, D.A. Peters (2001) Helicopter Rotor Dynamic Inflow Modeling for Maneuvering Flight. Journal of the American Helicopter Society, 46: 129-139.
- [16] Morillo, J.A., and D.A. Peters (2002) Velocity Field Above A Rotor Disk by A New Dynamic Inflow Model. Journal of Aircraft, 39: 731-738.
- [17] Asokanthan, S. F. and Hwang, M. C., 1996, “Torsional Instabilities in a System Incorporating a Hooke’s Joint,” Journal of Vibration Acoustics, Vol. 118, pp. 386-374.
- [18] Chen, L. W. and Chen, H. K., 1995, “Whirl Speed and Stability of Rotating Shaft Subjected to End Loads,” AIAA Journal, Vol. 33, No. 9.
- [19] Iwatsubo, T. and Saigo, M., 1984, “Transverse Vibration of a Rotor System Driven by a

- Cardan Joint,” *Journal of Sound and Vibration*, Vol. 95, pp. 9-18.
- [20] Mazzei, A. J., Jr., Argento, A. and Scott, R. A., 1999, “Dynamic Stability of a Rotating Shaft Driven through a Universal Joint,” *Journal of Sound and Vibration*, Vol. 222, pp. 19-47.
- [21] DeSmidt, H. A., Wang, K. W. and Smith, E. C., 2002, “Coupled Torsion-Lateral Stability of A Shaft-Disk System Driven Through A Universal Joint,” *ASME Journal of Applied Mechanics*, Vol. 69, No. 3, pp. 261-273.
- [22] Kirk, R. G., Mondy, R. E. and Murphy, R. C., 1984, “Theory and Guidelines to Proper Coupling Design for Rotor Dynamics Considerations,” *Journal of Vibration, Acoustics, Stress, and Reliability in Design*, Vol. 106, pp. 129-138.
- [23] H. A. DeSmidt, K. W. Wang, and E. C. Smith, ”Stability of a Segmented Supercritical Driveline with Non-Constant Velocity Couplings Subjected to Misalignment and Torque,” *Journal of Sound and Vibration* Vol. 277, No. 4-5, pp. 895-918, 2004.
- [24] H. A. DeSmidt, *Robust-Adaptive Active Vibration Control of Alloy and Flexible Matrix Composite Rotorcraft Drivelines via Magnetic Bearings: Theory and Experiment*, Ph.D. Thesis, The Pennsylvania State University, May 2005.
- [25] M.G. Ballin, “A High Fidelity Realtime Simulation of a Small Turboshaft Engine,” NASA TM 100991, July 1988.
- [26] C. Evans, D. Rees, and A. Borell, “Identification of aircraft gas turbine dynamics using frequency-domain techniques,” *Control Engineering Practice*, 2000, Vol. 8 No. 4 pp. 457–467.
- [27] K. Vazquez, “System applied strategies applied to aircraft gas turbine engines,” *Control Engineering Practice*, 2001, Vol. 9 No. 2, pp. 135–148.
- [28] O.M. Boaghe, S.A. Billings, L.M. Li and F.J. Lui, “Time and Frequency Domain Identification and Analysis of a Gas Turbine Engine,” *Control Engineering Practice*, 2002, Vol. 10, pp. 1347-1356.
- [29] A.S. Hopkins, G.C. Ruzicka and R.A. Ormiston, “Analytical Investigations of Coupled Rotorcraft/Engine/Drive Train Dynamics,” *Proc. of the American Helicopter Society 2nd Interational Region Aero Mechanics Specialists’ Conf.*, Bridgeport, CT, Oct. 11-13, 1995.
- [30] L.C. Jaw and A.E. Bryson, Jr., “Modeling Rotor Dynamics With Rotor Speed Degree of Freedom for Drive Train Torsional Stability Analysis,” *Proc. of 16th the European Rotorcraft Forum*, Glasgow Scotland, Sept. 21 1990.
- [31] K. Liu, M. Mittal, J.V.R. Prasad, C.J. Scholz, “A Study of Coupled Engine/Rotor Dynamic Behavior,” *Proc. of the 51st Annual Forum of the American Helicopter Society*, Fort Worth, TX, May. 9-11, 1995.
- [32] M. Roa, S.K. Biswas, B.P. Butz and D.G. Miller, “Dynamic Modeling and Feedback Control of a Side-by-Side Rotor Tandem Helicopter,” *IEEE Paper Number TH0333-5/90/0000/0780*, 1990, pp. 780-785.

CHAPTER 2

- [1] Walsh, P. P., and Fletcher, P., 1998, Gas Turbine Performance, Blackwell Science, Oxford, Chap. 8, p. 468.
- [2] Smith, D. L., and Stammetti, V. A., 1990, "Sequential Linearization as an Approach to Real Time Marine Gas Turbine Simulation," J. Eng. Gas Turbines Power, 112, pp. 187–191.
- [3] Visser, P. J., Broomhead, M. J., and van der Vorst, J., 2001, "TERTS, A Generic Real-Time Gas Turbine Simulation Environment," ASME Paper No. 2001-GT-0446.
- [4] Stamatis, A., Mathioudakis, K., Ruiz, J., and Curnock, B., 2001, "Real Time Engine Model Implementation for Adaptive Control & Performance Monitoring of Large Civil Turbofans," ASME Paper No. 2001-GT-0362.
- [5] Camporeale, S. M., Fortunato, B., and Dumas, A., 1998, "Dynamic Modeling and Control of Regenerative Gas Turbines," ASME Paper No. 98-GT-172
- [6] Agresti, M., Camporeale, S. M., and Fortunato, B., 2000, "An Object-Oriented Program for the Dynamic Simulation of Gas Turbines," ASME Paper No. 2000-GT-42.
- [7] "Industrial Engine Performance-Natural Gas Fuel," 1997, GE Report available from "www.ge.com."
- [8] Spector, R. B., and Miller, A. A., 1983, "GE LM 2500 Aircraft-Derivative Gas Turbine System," General Electric Company Report GER 343.
- [9] Schobeiri, M. T., Attia, M., and Lippe, C., 1994, "GETRAN: A Generic Modularly Structured Computer Code for Simulation of Dynamic Behavior of Aero- and Power Generation Gas Turbine Engines," Trans. ASME: J. Eng. Gas Turbines Power, 116, pp. 483–494.
- [10] Kim, J. H., Song, T. W., Kim, T. S., and Ro, S. T., 2000, "Model Development and Simulation of Transient Behaviour of Heavy Duty Gas Turbines," ASME Paper No. 2000- GT-0548.
- [11] Camporeale, S. M., Fortunato, B., and Mastrovito, M. 2006, "A Modular Code for Real Time Dynamics Simulation of Gas Turbines in Simulink," Trans. ASME: J. Eng. Gas Turbines Power, 128, pp. 506-517.
- [12] Sekhon, R., Bassily, H., Wagner, J., and Gaddis, J.. 2006, "Stationary Gas Turbines – A Real Time Dynamic Model with Experimental Validation," Proc. of the 2006 American Control Conference, Minneapolis, Minnesota, USA, June 14-16, 2006.
- [13] Veres J. P., 2009, "Compressor Study to Meet Large Civil Tilt Rotor Engine Requirements," AHS International, 65th Annual Forum & Technology Display, Grapevine, Texas, May 27–29, 2009.
- [14] Snyder, C.A., and Thurman, D.R., "Gas turbine characteristics for a Large Civil Tilt-Rotor (LCTR)," AHS International, 65th Annual Forum & Technology Display, Grapevine, Texas, May 27–29, 2009.

CHAPTER 3

- [1] Johnson, W., Yamauchi, G.K., and Watts, M.E., "NASA Heavy Lift Rotorcraft Systems Investigation", NASA/TP-2005-213467, Dec. 2005
- [2] Acree, C.W., Yeo, H., and Sinsay, J.D., "Performance Optimization of the NASA Large Civil Tiltrotor", International Powered Lift Conference, London, UK, Jul. 22-24, 2008.
- [3] Goi, T., Kawakami, K., Yamakawa, E., and Tanaka, H., "Variable Rotor Speed Transmission with High Speed Traction Drive", American Helicopter Society 55th Annual Forum, Montreal, Quebec, Canada, May 25-27, 1999.

- [4] Kish, J., "Vertical Lift Drive System Concept Studies Variable Speed / Two-Speed Transmissions", NASA Contractor Report CR-2002-211564, Army Research Laboratory Contractor Report ARL-CR-0495, Grant NAG3-2570, Jun. 2002.
- [5] Bossler, R.B., "Vertical Lift Drive System Concept Studies", NASA Contractor Report CR-2002-211563, Army Research Laboratory Contractor Report ARL-CR-0496, Grant NAG3-2570, Jun. 2002.
- [6] Ai, X., Mohr, T., and Anderson, S., "An Electro-Mechanical Infinitely Variable Speed Transmission", SAE 2004 World Congress, Detroit, MI, Mar. 8-11, 2004.
- [7] Saribay, Z., Smith, E., Lemanski, A., Bill, R., Wang, K.W., and Rao, S., "Compact Pericyclic Continuously Variable Speed Transmission Systems: Design Features and High-Reduction Variable Speed Case Studies", American Helicopter Society 63rd Annual Forum, Virginia Beach, VA, May 1-3, 2007.
- [8] Stevens, M.A., Handschuh, R.F., and Lewicki, D.G., "Variable/Multispeed Rotorcraft Drive System Concepts", NASA TM-2009-215456, Army Research Laboratory Report ARL-TR-4758, Mar. 2009.
- [9] Hong, K., Yang, K., and Lee, K., "An Object-Oriented Modular Simulation Model for [9] Integrated Gasoline Engine and Automatic Transmission Control", SAE transactions, Vol.108, No. 6, Part 1, pp. 1349-1357, 1999.
- [10] Haj-Fraj, A., and Pfeiffer, F., "Optimization of Gear Shift Operations in Automatic Transmissions", Proceedings of the 6th International Workshop on Advanced Motion Control, Nagoya, Japan, pp. 469-473, 2000.
- [11] Jung, G., Cho, B., and Lee, K., "Dynamic Analysis and Closed-Loop Shifting Control of EF-Automatic Transmission with Proportional Control Solenoid Valves", FISITA World Automotive Congress, Seoul, Korea, pp. 12-15, 2000.
- [12] Gong, J., Zhao, D., Chen, Y., and Chen, N., "Study on Shift Schedule Saving Energy of Automatic Transmission of Ground Vehicles", Journal of Zhejiang University-Science A, Vol. 5, No. 7, pp. 878-883, 2004.
- [13] Watechagit, S., "Modeling and Estimation for Stepped Automatic Transmission with Clutch-to-Clutch Shift Technology", PhD Dissertation, The Ohio State University, Department of Mechanical Engineering, 2004.
- [14] Kim, D., Peng, H., Bai, S., and Maguire, J., "Control of Integrated Powertrain with Electronic Throttle and Automatic Transmission", IEEE Transactions on Control Systems Technology, Vol. 15, No. 3, pp. 474, 2007.
- [15] Lu, X., Xu, X., and Liu, Y., "Simulation of Gear-Shift Algorithm for Automatic Transmission Based on MATLAB", Proceedings of the 2009 World Research Institute World Congress on Software Engineering, pp. 476-480, May 19-21, 2009.
- [16] Lin, C., Peng, H., Grizzle, J., and Kang, J., "Power Management Strategy for a Parallel Hybrid Electric Truck", IEEE Transactions on Control Systems Technology, Vol. 11, No.6, pp. 839-849, 2003.
- [17] Yamamoto, M., Wakahara, T., Okahara, H., and Oshita, H., "Hydraulic System, Shift and Lock-Up Clutch Controls Developed for a Large Torque Capacity CVT", International Continuously Variable and Hybrid Transmission Congress, Paper No. 04CVT-07, 2004.
- [18] Lu, Z., "Acceleration Simulation of a Vehicle with a Continuously Variable Power Split Transmission", Master's Thesis, West Virginia University, Department of Mechanical Engineering, 1998.
- [19] Wicke, V., Brace, C., and Vaughan, N., "The Potential for Simulation of Driveability of CVT Vehicles", SAE Transactions, Vol. 109, No. 6, pp. 1205-1210, 2000.
- [20] Yamamoto, M., Wakahara, T., Okahara, H., and Oshita, H., "Hydraulic System, Shift and Lock-Up Clutch Controls Developed for a Large Torque Capacity CVT", 2004
- [21] International Continuously Variable and Hybrid Transmission Congress, Paper No 04CVT-07, 2004.

- [22] Klaassen, T., et al., "Modeling and Simulation of an Electro-Mechanically Actuated Pushbelt Type Continuously Variable Transmission", Mechatronic Systems 2004: A Proceedings Volume From the 3rd IFAC Symposium, Sydney, Australia, Sep. 2004.
- [23] Togai, K., and Koso, M., "Dynamic Scheduling Control for Engine and Gearshifts: Consolidation of Fuel-Economy Optimization and Reserve Power", Mitsubishi Motors Technical Review No. 18, 2006.
- [24] Anthony, J., Moskwa, J., and Danielson, E., "Powertrain Simulation of the M1A1 Abrams Using Modular Model Components", SAE International Congress & Exposition, Detroit, MI, Feb. 1998.
- [25] Assanis, D., et al., "Validation and Use of SIMULINK Integrated, High Fidelity, Engine-In-Vehicle Simulation of the International Class VI Truck", SAE Transactions, Vol. 109, No. 3, pp. 384-399, 2000.
- [26] Fathy, H., Ahlawat, R., and Stein, J., "Proper Powertrain Modeling for Engine-in-the Loop Simulation", Proceedings of the 2005 ASME International Mechanical Engineering Congress and Exposition, Orlando, FL, 2005.
- [27] Lewicki, D.G., DeSmidt, H.A., Smith, E.C., and Bauman, S.W.. "Two-Speed Gearbox Dynamic Simulation Predictions and Test Validation," Proc. 66th American Helicopter Society Annual Forum, Phoenix, AZ., May 2010.

CHAPTER 4

- [1] W. Johnson, G. K. Yamauchi and M.E. Watts "NASA Heavy Lift Rotorcraft Systems Investigation." NASA 213467, December 2005.
- [2] Z. Saribay, A. Lemanski, M. Elmoznino, "Pericyclic Non-Traction Continuously Variable Speed Transmission (P-CVT): Rotorcraft Applications", AHS International 62nd Annual Forum and Technology Display, Phoenix, AZ, May 9 – 11, 2006.
- [3] J. Kish, "Vertical Lift Drive System Concept Studies Variable Speed/Two-Speed Transmissions," NASA CR -2002-211564, 2002.
- [4] Acree, C.W., Yeo, H., and Sinsay, J.D., "Performance Optimization of the NASA Large Civil Tiltrotor", International Powered Lift Conference, London, UK, Jul. 22-24, 2008.

APPENDIX

Off nominal steady state operation analysis code.

```

clear all
format long g

%%%%%%%%%%%%%%%%%%%%%%%%%%%%%%%%%%%%%%%%%%%%%%%%%%%%%%%%%%%%%%%%%%%%%%%%
%
% Gas Turbine Engine: Gas-Generator/Power Turbine/Load
% Off-nominal steady-state operation analysis
%
%
% Station: 1  2  3  4  5  6  7
%
% Pa, Ta | \ | | | | | | | Pa
%         | \ | | | | | | |
%         | \ "cp" "cc" | / | "tp" | / |
% ----> | \ | | | | | | |
%         | |-----| | | | | | | JL, TL
%         | |-----| | | | | | |
% ----> | / | | | | | | |
%         | / | | | | | | |
%         | / | | | | | | |
%
% "a"  "c"                "ggt"  "pt"  "L"
%
% Element:                Stations:
% "a"  == ambient
% "c"  == compressor (igv/comp/egv)  "1-2"
% "cp" == compressor plenum          "2-3"
% "cc" == combustion chamber         "3-4"
% "ggt" == gas generator turbine      "4-5"
% "tp" == turbine plenum              "5-6"
% "pt" == power turbine               "6-7"
% "L"  == load
%
%%%%%%%%%%%%%%%%%%%%%%%%%%%%%%%%%%%%%%%%%%%%%%%%%%%%%%%%%%%%%%%%%%%%%%%%
% global dr rd rs2hz hz2rs rs2rpm rpm2rs m2ft ft2m m2in in2m in2mil
% mil2in m2mil mil2m mil2um um2mil m2um um2m m2mm mm2m
% global hp2w w2hp knots2ms ms2knots lbf2kg kg2lbf lbf2n n2lbf ftlb2nm
% nm2ftlb psi2pa pa2psi pa2atm atm2pa
% global gaccel p_AL E_AL G_AL v_AL SMAX_AL p_FE E_FE G_FE v_FE SMAX_FE
%
% overall engine
% global cp_air R_air gamma_air P2T T2P ga lambda
% global Pa Ta
% global mdot_n Pr_cn Pr_ccn eta_cn PWR_ptn
% global LHV DT0_ccn mfdot_n eta_tn
% global A P0_n T0_n P_n T_n rho_n C_n Ca_n alpha_n Ma_n
% global DT0_cn DT0_ggtn DT0_ptn
%
% compressor (igv/rotors/stators/egv)
% global Ca_in alpha1_in alpha2_in C1_in C2_in
% global T01_in T1_in T02_in T2_in P01_in P1_in P02_in P2_in
% global rho1_in rho2_in A1_i A2_i
% global Ca_cn U_cn OMEGA_cn Ns_c alpha_cn
% global Rm_c Rhr_c Rtr_c Rhs_c Rts_c A1_c A2_c A3_c

```



```

global T01_cn T02_cn T03_cn P01_cn P02_cn P03_cn
global T1_cn T2_cn T3_cn P1_cn P2_cn P3_cn M1_cn M2_cn M3_cn
global alpha1_cn alpha2_cn alpha3_cn beta1_cn beta2_cn beta3_cn DHr_cn
global C1_cn C2_cn C3_cn DHs_cn

global Ca_en alpha1_en alpha2_en C1_en C2_en
global T01_en T1_en T02_en T2_en P01_en P1_en P02_en P2_en
global rho1_en rho2_en A1_e A2_e

% compressor map
global beta_cmap OMEGA_cmap mdot_cmap Pr_cmap eta_cmap
global OMEGA_data mdot_data Pr_c_data eta_c_data
global mdot_c_surge Pr_c_surge mdot_c_stonewall Pr_c_stonewall
global Nbeta beta_cmax beta_cmin beta_cnom

%%%%%%%%%%%%%%%%%%%%%%%%%%%%%%%%%%%%%%%%%%%%%%%%%%%%%%%%%%%%%%%%%%%%%%%%
%%%%%%%%%%%%%%%%%%%%%%%%%%%%%%%%%%%%%%%%%%%%%%%%%%%%%%%%%%%%%%%%%%%%%%%%

if 1==1

% load conversion factors & physical constants
conversionfactors;
physicalconst;

% abbreviations
P2T=(gamma_air-1)/gamma_air;
T2P=gamma_air/(gamma_air-1);
ga=gamma_air;

% Intake
Ta=288; % atmospheric temperature, K
Pa=1.01*atm2pa; % atmospheric pressure, N/m^2
LHV=43.1*1e6; % lower heating value of fuel, J/kg

% engine design parameters
mdot_n=13.5; % engine mass flow, kg/sec
Pr_cn=28; % compressor pressure ratio
eta_cn=1; % compressor efficiency (must be 1)
Ca_cn=150 % compressor axial velocity, m/sec
Ns_c=8; % number of compressor stages
U_cn=330 % compressor mean line speed, m/sec
OMEGA_cn=26500*rpm2rs; % compressor rotation speed, rad/sec
alpha_cn=37*dr; % compressor entrance flow angle, rad
Pr_ccn=0.85; % combustion chamber pressure drop
PWR_ptn=7500*hp2w; % power turbine power (load power)

% two speed gas turbine engine design
TwoSpoolGTE_design; % cycle calculations and flow areas

% Compressor Design (IGV\Rotor-Statots\EGV)
compressor_design;

% compressor map

```

```

OMEGA_data=linspace(OMEGA_cn*0.6,OMEGA_cn*1.25,15); % rotation speed
mdot_data=linspace(mdot_n*0.25,mdot_n*1.25,1000); % mass flow

OMEGA_data=unique(sort([OMEGA_data,OMEGA_cn]));
mdot_data=unique(sort([mdot_data,mdot_n]));

P01=Pa;
T01=Ta;

[Pr_c_data,eta_c_data,mdot_c_surge,Pr_c_surge,mdot_c_stonewall,Pr_c_sto
newall]=comp_map(P01,T01,mdot_data,OMEGA_data);

% Power Turbine (Choking Parameter)
lambda=sqrt(gamma_air/R_air*(1+(gamma_air-1)/2)^((gamma_air+1)/(1-
gamma_air)));

% PLOTS
figure(1),plot(mdot_data,Pr_c_data,'b'), hold on
figure(1),plot(mdot_c_surge,Pr_c_surge,'k'), hold on
figure(1),plot(mdot_c_stonewall,Pr_c_stonewall,'k'), hold on

figure(2),plot(mdot_data,eta_c_data,'b'), hold on

% beta lines -----
Nbeta=15; % number of beta lines

Xsurge=mdot_c_surge(:);
Ysurge=Pr_c_surge(:);
beta_cmax=Ysurge'*Xsurge.^2/(Xsurge'.^2*Xsurge.^2);
beta_cmax=beta_cmax*2;

Xstonewall=mdot_c_stonewall(:);
Ystonewall=Pr_c_stonewall(:);
beta_cmin=Ystonewall'*Xstonewall.^2/(Xstonewall'.^2*Xstonewall.^2);

beta_cnom=Pr_cn/mdot_n^2; % nominal compressor beta

beta_cmap=linspace(beta_cmin,beta_cmax,Nbeta);
beta_cmap=unique(sort([beta_cmap,beta_cnom]));

iindex=0;
for i = 1:length(OMEGA_data)

    jindex=find(isnan(Pr_c_data(i,:))==0);

    if isempty(jindex)==0

Pr_data_extrap=interp1(mdot_data(jindex),Pr_c_data(i,jindex),mdot_data,
'linear','extrap');

```

```

eta_data_extrap=interp1(mdot_data(jindex),eta_c_data(i,jindex),mdot_data,
a, 'linear', 'extrap');

figure(100),plot(mdot_data,Pr_c_data(i,:)), hold on
figure(101),plot(mdot_data,eta_c_data(i,:)), hold on

iindex=iindex+1;
OMEGA_cmap(iindex)=OMEGA_data(i);
for k = 1:length(beta_cmap)
[error,sindex]=sort(abs(beta_cmap(k)*mdot_data.^2-Pr_data_extrap));

mdot_cmap(iindex,k)=mdot_data(sindex(1)); % take nearest value....
Pr_cmap(iindex,k)=Pr_data_extrap(sindex(1));
eta_cmap(iindex,k)=eta_data_extrap(sindex(1));
figure(100),plot(mdot_data,beta_cmap(k)*mdot_data.^2), hold on
end

end

end

figure(100),plot(mdot_cmap,Pr_cmap,'kd'), hold on,
axis([min(mdot_data),max(mdot_data),0,50])
figure(101),plot(mdot_cmap,eta_cmap,'kd'), hold on

figure(12),plot(beta_cmap,mdot_cmap)
xlabel('beta'),ylabel('mdot')

figure(13),plot(beta_cmap,Pr_cmap)
xlabel('beta'),ylabel('Pr')

figure(14),plot(beta_cmap,eta_cmap)
xlabel('beta'),ylabel('eta')

figure(31),surf(OMEGA_cmap*rs2rpm,beta_cmap,mdot_cmap')
figure(32),surf(OMEGA_cmap*rs2rpm,beta_cmap,Pr_cmap')
figure(33),surf(OMEGA_cmap*rs2rpm,beta_cmap,eta_cmap')

% check nominals
interp2(beta_cmap,OMEGA_cmap,mdot_cmap,beta_cnom,OMEGA_cn)
interp2(beta_cmap,OMEGA_cmap,Pr_cmap,beta_cnom,OMEGA_cn)
interp2(beta_cmap,OMEGA_cmap,eta_cmap,beta_cnom,OMEGA_cn)

% save off-nominal engine parameters
save TwoSpoolGTE_offnominal.mat cp_air R_air gamma_air lambda ga ...
Pa Ta mdot_n Pr_cn OMEGA_cn Rm_c Rhr_c
Rtr_c Rhs_c Rts_c eta_cn Pr_ccn LHV
mfdot_n A P0_n T0_n P_n T_n rho_n C_n
Ca_n alpha_n Ma_n eta_tn PWR_ptn
beta_cmap OMEGA_cmap mdot_cmap Pr_cmap
eta_cmap OMEGA_data mdot_data Pr_c_data

```

```

eta_c_data    mdot_c_surge    Pr_c_surge
mdot_c_stonewall    Pr_c_stonewall    Nbeta
beta_cmax    beta_cmin    beta_cnom

end

if 1~=1

close all
clear all

% load off-nominal engine parameters
load TwoSpoolGTE_offnominal

figure(1),plot(mdot_data,Pr_c_data,'b'), hold on
figure(1),plot(mdot_c_surge,Pr_c_surge,'m'), hold on
figure(1),plot(mdot_c_stonewall,Pr_c_stonewall,'m'), hold on

% find operating line -----
'////////// now computing operating line //////////'

% operating point
PWR_LOAD=linspace(PWR_ptn,0.5*PWR_ptn,50);

options=optimset('MaxFunEvals',1000,'MaxIter',1000,'TolX',1e-
5,'TolFun',1e-5);

X0=[OMEGA_cn,beta_cnom,mfdot_n];
for i = 1:length(PWR_LOAD)

    i
    PWR_L=PWR_LOAD(i);
    X=fminsearch(@fcn_gteop,X0,options,PWR_L);
    X0=X;

    OMEGA_c(i)=X(1);
    beta_c(i)=X(2);
    mfdot(i)=X(3);

mdot(i)=interp2(beta_cmap,OMEGA_cmap,mdot_cmap,beta_c(i),OMEGA_c(i));
Pr_c(i)=interp2(beta_cmap,OMEGA_cmap,Pr_cmap,beta_c(i),OMEGA_c(i));
eta_c(i)=interp2(beta_cmap,OMEGA_cmap,eta_cmap,beta_c(i),OMEGA_c(i));

end

figure(1),plot(mdot,Pr_c,'k'), hold on

end

```

OFF-NOMINAL PARAMETERS

```
function TwoSpoolGTE_params

% conversion factors
global dr rd rs2hz hz2rs rs2rpm rpm2rs m2ft ft2m m2in in2m in2mil
mil2in m2mil mil2m mil2um um2mil m2um um2m m2mm mm2m
global hp2w w2hp knots2ms ms2knots lbf2kg kg2lbf lbf2n n2lbf ftlb2nm
nm2ftlb psi2pa pa2psi pa2atm atm2pa
global gaccel p_AL E_AL G_AL v_AL SMAX_AL p_FE E_FE G_FE v_FE SMAX_FE

% paramaters defined in 'TwoSpoolGTE_offnominal.mat'
global cp_air R_air gamma_air lambda ga
global Pa Ta Pr_cn mdot_n A P0_n T0_n P_n T_n rho_n C_n Ca_n alpha_n
Ma_n eta_tn
global Rhr_c Rtr_c Rhs_c Rts_c eta_cn Rm_c m_c J_c
global PWR_ptn
global Pr_ccn LHV mfdot_n
global beta_cmap OMEGA_cmap mdot_cmap Pr_cmap eta_cmap
global OMEGA_data mdot_data Pr_c_data eta_c_data
global mdot_c_surge Pr_c_surge mdot_c_stonewall Pr_c_stonewall
global Nbeta beta_cmax beta_cmin beta_cnom

% off-nominal model parameters
load TwoSpoolGTE_offnominal;

% additional paramaters for transient simulation -----
----
global OMEGA_cn mdot_cn PWR_cn m_c J_c
global OMEGA_ggtn mdot_ggtn PWR_ggtn Rt_ggt Rh_ggt Rm_ggt m_ggt J_ggt
global OMEGA_ptn mdot_ptn PWR_ptn Rt_pt Rh_pt Rm_pt m_pt J_pt
global tau_cc Vol_cp Vol_tp

% compressor 1-2
mdot_cn=mdot_n; % mass flow, kg/m
PWR_cn=mdot_cn*cp_air*(T0_n(2)-T0_n(1)); % power, watts
m_c=200*lbf2kg; % mass, kg
J_c=0.5*m_c*Rm_c^2; % rotational inertia, kg*m^2

% compressor plenum 2-3
Vol_cp=0.1; % volume, m^3

% combustion chamber 3-4
tau_cc=10; % time constant, sec

% gas generator turbine 4-5
OMEGA_ggtn=OMEGA_cn; % rotation speed, rad/sec
mdot_ggtn=mdot_cn; % mass flow, kg/m
PWR_ggtn=mdot_ggtn*cp_air*(T0_n(4)-T0_n(5)); % power, watts
htratio_ggt=0.65; % hub-to-tip ratio
Rt_ggt=sqrt(A(5)/(pi*(1-htratio_ggt^2))); % tip radius
Rh_ggt=Rt_ggt*htratio_ggt; % hub radius
Rm_ggt=(Rt_ggt+Rh_ggt)/2; % mean radius
m_ggt=50*lbf2kg; % mass, kg
J_ggt=0.5*m_ggt*Rm_ggt^2; % rotational inertia
```

```

% turbine plenum 5-6
Vol_tp=0.1; % volume, m^3

% power turbine 6-7
OMEGA_ptn=12500*rpm2rs; % rotation speed, rad/sec
mdot_ptn=mdot_ggtn; % mass flow, kg/m
htratio_pt=0.65; % hub-to-tip ratio
Rt_pt=sqrt(A(7)/(pi*(1-htratio_pt^2))); % tip radius
Rh_pt=Rt_pt*htratio_pt; % hub radius
Rm_pt=(Rt_pt+Rh_pt)/2; % mean radius
m_pt=150*lb2kg; % mass, kg
J_pt=0.5*m_pt*Rm_pt^2; % rotational inertia

```

Two Spool Gas Turbine Engine Design

```
function TwoSpoolGTE_design
```

```

% paramaters and stations 1 and 2 -----
%
% Station: 1 2 3 4 5 6 7
%
% Pa, Ta | \ | | | | | | | Pa
%         | \ "cp" "cc" | / | "tp" | / |
% ----> | \ ----- | / | ----- | | JL, TL
%         | | ----- | | | ----- | |
% ----> | / ----- | \ | ----- | \ |
%         | / ----- | \ | ----- | \ |
%         | / ----- | \ | ----- | \ |
%
% "a" "c" "ggtn" "pt" "L"
%
%*****
global cp_air R_air gamma_air P2T T2P
global Pa Ta
global mdot_n Pr_cn Pr_ccn PWR_ptn
global LHV DT0_ccn mfdot_n eta_tn
global Ca_cn
global A P0_n T0_n P_n T_n rho_n C_n Ca_n alpha_n Ma_n
global DT0_cn DT0_ggtn DT0_ptn
%*****

% cycle calculations
P0_n(1)=Pa;
T0_n(1)=Ta;

P0_n(2)=Pr_cn*P0_n(1);
DT0_cn=T0_n(1)*(Pr_cn^P2T-1);

```

```

T0_n(2)=T0_n(1)+DT0_cn;

P0_n(3)=P0_n(2);
T0_n(3)=T0_n(2);

P0_n(4)=Pr_ccn*P0_n(3);
DT0_ccn=(PWR_ptn-Ta*cp_air*mdot_n*(1-Pr_ccn^(-P2T)))/(cp_air*mdot_n*(1-
(Pr_ccn*Pr_cn)^(-P2T)));
T0_n(4)=T0_n(3)+DT0_ccn;

DT0_ggtn=T0_n(1)*(Pr_cn^P2T-1);
T0_n(5)=T0_n(4)-DT0_ggtn;
P0_n(5)=P0_n(4)*(T0_n(5)/T0_n(4))^T2P;

P0_n(6)=P0_n(5);
T0_n(6)=T0_n(5);

DT0_ptn=PWR_ptn/(cp_air*mdot_n);
T0_n(7)=T0_n(6)-DT0_ptn;
P0_n(7)=P0_n(6)*(T0_n(7)/T0_n(6))^T2P;
%should be identically equal to Pa !!!

% fuel rate & efficiency -----
mfdot_n=mdot_n*cp_air*DT0_ccn/LHV;    % fuel flow rate, kg/sec
Q_ccn=mfdot_n*LHV;                    % heat in, Watts
eta_tn=PWR_ptn/Q_ccn;                 % total efficiency

% station flow state and areas -----

% compressor entrance
i=1;

Ca_n(i)=Ca_cn;
alpha_n(i)=0;

C_n(i)=Ca_n(i)/cos(alpha_n(i));
T_n(i)=T0_n(i)-C_n(i)^2/(2*cp_air);
P_n(i)=P0_n(i)*(T_n(i)/T0_n(i))^T2P;
rho_n(i)=P_n(i)/(R_air*T_n(i));
Ma_n(i)=C_n(i)/sqrt(gamma_air*R_air*T_n(i));
A(i)=mdot_n/(rho_n(i)*Ca_n(i));

% compressor exit
i=2;

Ca_n(i)=Ca_n(i-1);
alpha_n(i)=0;

C_n(i)=Ca_n(i)/cos(alpha_n(i));
T_n(i)=T0_n(i)-C_n(i)^2/(2*cp_air);
P_n(i)=P0_n(i)*(T_n(i)/T0_n(i))^T2P;
rho_n(i)=P_n(i)/(R_air*T_n(i));
Ma_n(i)=C_n(i)/sqrt(gamma_air*R_air*T_n(i));
A(i)=mdot_n/(rho_n(i)*Ca_n(i));

```

```

% combustion chamber entrance
i=3;

Ca_n(i)=Ca_n(i-1);
alpha_n(i)=0;

C_n(i)=Ca_n(i)/cos(alpha_n(i));
T_n(i)=T0_n(i)-C_n(i)^2/(2*cp_air);
P_n(i)=P0_n(i)*(T_n(i)/T0_n(i))^T2P;
rho_n(i)=P_n(i)/(R_air*T_n(i));
Ma_n(i)=C_n(i)/sqrt(gamma_air*R_air*T_n(i));
A(i)=mdot_n/(rho_n(i)*Ca_n(i));

% gas generator turbine entrance
i=4;

Ma_n(i)=0.99;           % inlet choking
alpha_n(i)=0;

C_n(i)=Ma_n(i)*sqrt(gamma_air*R_air*T0_n(i)/(1+(gamma_air-
1)/2*Ma_n(i)^2));

Ca_n(i)=C_n(i)*cos(alpha_n(i));
T_n(i)=T0_n(i)-C_n(i)^2/(2*cp_air);
P_n(i)=P0_n(i)*(T_n(i)/T0_n(i))^T2P;
rho_n(i)=P_n(i)/(R_air*T_n(i));
A(i)=mdot_n/(rho_n(i)*Ca_n(i));
Ma_n(i)=C_n(i)/sqrt(gamma_air*R_air*T_n(i));  %%%%%%%%%%%%%%

% gas generator turbine exit
i=5;

Ca_n(i)=Ca_n(i-1);
alpha_n(i)=0;

C_n(i)=Ca_n(i)/cos(alpha_n(i));
T_n(i)=T0_n(i)-C_n(i)^2/(2*cp_air);
P_n(i)=P0_n(i)*(T_n(i)/T0_n(i))^T2P;
rho_n(i)=P_n(i)/(R_air*T_n(i));
Ma_n(i)=C_n(i)/sqrt(gamma_air*R_air*T_n(i));
A(i)=mdot_n/(rho_n(i)*Ca_n(i));

% power turbine entrance
i=6;

Ma_n(i)=0.99;           % inlet choking
alpha_n(i)=0;

C_n(i)=Ma_n(i)*sqrt(gamma_air*R_air*T0_n(i)/(1+(gamma_air-
1)/2*Ma_n(i)^2));

Ca_n(i)=C_n(i)*cos(alpha_n(i));

```



```

T_n(i)=T0_n(i)-C_n(i)^2/(2*cp_air);
P_n(i)=P0_n(i)*(T_n(i)/T0_n(i))^T2P;
rho_n(i)=P_n(i)/(R_air*T_n(i));
A(i)=mdot_n/(rho_n(i)*Ca_n(i));
Ma_n(i)=C_n(i)/sqrt(gamma_air*R_air*T_n(i)); %%%%%%%%%%%

```

```

% power turbine exit
i=7;

```

```

Ca_n(i)=Ca_n(i-1);
alpha_n(i)=0;

```

```

C_n(i)=Ca_n(i)/cos(alpha_n(i));
T_n(i)=T0_n(i)-C_n(i)^2/(2*cp_air);
P_n(i)=P0_n(i)*(T_n(i)/T0_n(i))^T2P;
rho_n(i)=P_n(i)/(R_air*T_n(i));
Ma_n(i)=C_n(i)/sqrt(gamma_air*R_air*T_n(i));
A(i)=mdot_n/(rho_n(i)*Ca_n(i));

```

Compressor Design

```

function compressor_design

```

```

% load conversion factors & physical constants
conversionfactors;
physicalconst;

```

```

% Intake & IGV -----
Ca_in=Ca_cn;
alpha1_in=alpha_n(1);

```

```

% IGV flow entrance angle
C1_in=Ca_in/cos(alpha1_in);

```

```

T01_in=T0_n(1);
T1_in=T01_in-C1_in^2/(2*cp_air);

```

```

P01_in=P0_n(1);
P1_in=P01_in*(T1_in/T01_in)^(gamma_air/(gamma_air-1));
rho1_in=P1_in/(R_air*T1_in);
A1_i=mdot_n/(rho1_in*Ca_in);
alpha2_in=alpha_cn;

```

```

% IGV flow exit angle
C2_in=Ca_in/cos(alpha2_in);
T02_in=T01_in;
T2_in=T02_in-C2_in^2/(2*cp_air);
P02_in=P01_in*(T02_in/T01_in)^(gamma_air/(gamma_air-1));
P2_in=P02_in*(T2_in/T02_in)^(gamma_air/(gamma_air-1));
rho2_in=P2_in/(R_air*T2_in);
A2_i=mdot_n/(rho2_in*Ca_in);

```

```

% compressor rotor and stators stages -----
DT0s_cn=DT0_cn/Ns_c*ones(1,Ns_c); % stage stag. temp rise

% stagnation temps
T01_cn=T0_n(1)+[0,cumsum(DT0s_cn(1:end-1))]; % rotor entrance stag temp
T02_cn=T0_n(1)+cumsum(DT0s_cn); % rotor exit stag temp
T03_cn=T02_cn; % stator exit stag temp

% stagnation pressures
P01_cn=P0_n(1)*(T01_cn./T0_n(1)).^(gamma_air/(gamma_air-1));
% rotor entrance stag. pres
P02_cn=P0_n(1)*(T02_cn./T0_n(1)).^(gamma_air/(gamma_air-1));
% rotor exit stag. pres
P03_cn=P0_n(1)*(T03_cn./T0_n(1)).^(gamma_air/(gamma_air-1));
% stator entrance stag. pres

% absolute angles
alpha1_cn=alpha2_in*ones(1,Ns_c); % rotor entrance angle, rad
alpha2_cn=atan(cp_air*DT0s_cn./(U_cn*Ca_cn)+tan(alpha1_cn));
% rotor exit angle, rad
alpha3_cn=alpha1_cn; % stator exit angle, rad

% relative angles
beta1_cn=atan(U_cn/Ca_cn-tan(alpha1_cn)); % rotor entrance angle, rad
beta2_cn=atan(U_cn/Ca_cn-tan(alpha2_cn)); % rotor exit angle, rad
beta3_cn=atan(U_cn/Ca_cn-tan(alpha3_cn)); % stator exit angle, rad

% absolute velocities
C1_cn=Ca_cn./cos(alpha1_cn); % rotor entrance velocity, m/s
C2_cn=Ca_cn./cos(alpha2_cn); % rotor exit velocity, m/s
C3_cn=Ca_cn./cos(alpha3_cn); % stator exit velocity, m/s

% temperatures
T1_cn=T01_cn-C1_cn.^2/(2*cp_air);
T2_cn=T02_cn-C2_cn.^2/(2*cp_air);
T3_cn=T03_cn-C3_cn.^2/(2*cp_air);

% pressures
P1_cn=P01_cn.*((T1_cn./T01_cn).^(gamma_air/(gamma_air-1)));
P2_cn=P02_cn.*((T2_cn./T02_cn).^(gamma_air/(gamma_air-1)));
P3_cn=P03_cn.*((T3_cn./T03_cn).^(gamma_air/(gamma_air-1)));

% densities
rho1_cn=P1_cn./(R_air*T1_cn);
rho2_cn=P2_cn./(R_air*T2_cn);
rho3_cn=P3_cn./(R_air*T3_cn);

% Areas
A1_c=mdot_n./(rho1_cn*Ca_cn);
A2_c=mdot_n./(rho2_cn*Ca_cn);
A3_c=mdot_n./(rho3_cn*Ca_cn);

% mach numbers
M1_cn=C1_cn./sqrt(gamma_air*R_air*T1_cn);

```

```

M2_cn=C2_cn./sqrt(gamma_air*R_air*T2_cn);
M3_cn=C3_cn./sqrt(gamma_air*R_air*T3_cn);

% de Haller numbers
DHr_cn=cos(beta1_cn)./cos(beta2_cn);           % rotor, DH = V2/V1
DHS_cn=cos(alpha2_cn)./cos(alpha3_cn);       % stator, DH = C3/C2

% radii
Rm_cn=U_cn/OMEGA_cn;                          % mean radius, m

Rh1_cn=Rm_cn-A1_cn/(4*pi*Rm_cn);
Rh2_cn=Rm_cn-A2_cn/(4*pi*Rm_cn);
Rh3_cn=Rm_cn-A3_cn/(4*pi*Rm_cn);

Rt1_cn=2*Rm_cn-Rh1_cn;
Rt2_cn=2*Rm_cn-Rh2_cn;
Rt3_cn=2*Rm_cn-Rh3_cn;

Rhr_cn=(Rh1_cn+Rh2_cn)/2;
Rtr_cn=(Rt1_cn+Rt2_cn)/2;

Rhs_cn=(Rh2_cn+Rh3_cn)/2;
Rts_cn=(Rt2_cn+Rt3_cn)/2;

% EGV -----
Ca_en=Ca_cn;

alpha1_en=alpha3_cn(Ns_cn);
% egv flow entrance angle
C1_en=Ca_en/cos(alpha1_en);

T01_en=T03_cn(Ns_cn);
T1_en=T01_en-C1_en^2/(2*cp_air);

P01_en=P03_cn(Ns_cn);
P1_en=P01_en*(T1_en/T01_en)^(gamma_air/(gamma_air-1));

rho1_en=P1_en/(R_air*T1_en);
A1_e=mdot_n/(rho1_en*Ca_in);

alpha2_en=0;                                  % egv flow exit angle
C2_en=Ca_en/cos(alpha2_en);

T02_en=T01_en;
T2_en=T02_en-C2_en^2/(2*cp_air);

P02_en=P01_en*(T02_en/T01_en)^(gamma_air/(gamma_air-1));
P2_en=P02_en*(T2_en/T02_en)^(gamma_air/(gamma_air-1));

rho2_en=P2_en/(R_air*T2_en);
A2_e=mdot_n/(rho2_en*Ca_en);

```

```

% check design
if min(alpha1_cn) < 0, '//////// Warning alpha1_cn<0 //////////', pause, end
if min(alpha2_cn) < 0, '//////// Warning alpha2_cn<0 //////////', pause, end
if min(alpha3_cn) < 0, '//////// Warning alpha3_cn<0 //////////', pause, end

if min(beta1_cn) < 0, '//////// Warning beta1_cn<0 //////////', pause, end
if min(beta2_cn) < 0, '//////// Warning beta2_cn<0 //////////', pause, end
if min(beta3_cn) < 0, '//////// Warning beta3_cn<0 //////////', pause, end

```

Compressor Map

```

function [Pr_c, eta_c, mdot_c_surge, Pr_c_surge, mdot_c_stonewall, Pr_c_stonewall] = comp_map(P01, T01, mdot, OMEGA)

```

```

% compressor map
global cp_air R_air gamma_air
global Ns_c

for j = 1:length(mdot)

    j

    % igv (no work, no losses)

    [Ca2_i(j), alpha2_i(j), T02_i(j), P02_i(j), Ma2_i(j)] = igv_stage(P01, T01, mdot(j));

    for i = 1:length(OMEGA)

        % stage 1

        [Ca3(1, i, j), alpha3(1, i, j), T03(1, i, j), P03(1, i, j), Ma(:, 1, i, j)] = comp_stage(1, OMEGA(i), mdot(j), Ca2_i(j), alpha2_i(j), T02_i(j), P02_i(j));

        % stage 2 - N
        for snum = 2:Ns_c

            [Ca3(snum, i, j), alpha3(snum, i, j), T03(snum, i, j), P03(snum, i, j), Ma(:, snum, i, j)] = comp_stage(snum, OMEGA(i), mdot(j), Ca3(snum-1, i, j), alpha3(snum-1, i, j), T03(snum-1, i, j), P03(snum-1, i, j));
            end

        % egv (no work, no losses)

        [Ca2_e(i, j), alpha2_e(i, j), T02_e(i, j), P02_e(i, j), Ma2_e(i, j)] = egv_stage(P03(Ns_c, i, j), T03(Ns_c, i, j), mdot(j));

    end
end

```

```

end

% overall igv/compressor/egv

% exit stagnation temp
T02=T02_e;

% exit stagnation pressure
P02=P02_e;

% pressure ratio
Pr_c=P02/P01;

% isentropic efficiency
eta_c=((P02/P01).^((gamma_air-1)/gamma_air)-1)./(T02/T01-1);

eta_c=real(eta_c);

% surge line
[Pr_c_surge,index_surge]=max(Pr_c');
mdot_c_surge=mdot(index_surge);
index=find(isnan(Pr_c_surge)==0);
Pr_c_surge=Pr_c_surge(index);
mdot_c_surge=mdot_c_surge(index);

[tmp,index_stonewall]=max(diff(isnan(Pr_c')));
for i =1:length(index_stonewall)
    Pr_c_stonewall(i)=Pr_c(i,index_stonewall(i));
end
mdot_c_stonewall=mdot(index_stonewall);

Compressor Stage
function
[Ca3,alpha3,T03,P03,Ma]=comp_stage(snum,OMEGA,mdot,Ca1,alpha1,T01,P01)

%%%%%%%%%%%%%%%%%%%%%%%%%%%%%%%%%%%%%%%%%%%%%%%%%%%%%%%%%%%%%%%%%%%%%%%%
%%%%%%%%
global cp_air gamma_air R_air
global Rm_c alpha1_cn alpha2_cn alpha3_cn beta1_cn beta2_cn beta3_cn
global A1_c A2_c A3_c
%%%%%%%%%%%%%%%%%%%%%%%%%%%%%%%%%%%%%%%%%%%%%%%%%%%%%%%%%%%%%%%%%%%%%%%%
%%%%%%%%
if isnan(Ca1)==1

    Ca3=nan;
    alpha3=nan;
    T03=nan;
    P03=nan;
    TQ=nan;
    psi=nan;
    phi=nan;
    Ma=[nan,nan,nan];
    return

```

```

end

U=OMEGA*Rm_c; % mean-line rotor velocity

beta2n=beta2_cn(snum);
alpha3n=alpha3_cn(snum);

beta1=atan(U/Ca1-tan(alpha1));

A1=A1_c(snum);
A2=A2_c(snum);
A3=A3_c(snum);

C1=Ca1/cos(alpha1);
T1=T01-C1^2/(2*cp_air);

% rotor -----
-
% Ca2^(12/5) + a1*Ca2^(2/5) + a2 = 0
a1=(2*Ca1*U*tan(alpha1)-U^2-2*cp_air*T01)*cos(beta2n)^2;
a2=2*cp_air*T1*cos(beta2n)^2*(Ca1*A1/A2)^(gamma_air-1);

Xa2_solns=roots([1,0,0,0,0,a1,a2]); % re-map:
Xa2^6+a1*Xa2+a2=0 with Xa2=Ca2^(2/5)
Ca2_solns=Xa2_solns.^(5/2);
Ca2_solns=Ca2_solns(find(imag(Ca2_solns)==0)); % keep only real
solutions

[deltaC,index]=min(abs(Ca2_solns-Ca1)); % extract Ca2 solution
(the closest value to Ca1)
Ca2=Ca2_solns(index);

if isempty(Ca2)==1

    Ca3=nan;
    alpha3=nan;
    T03=nan;
    P03=nan;
    TQ=nan;
    psi=nan;
    phi=nan;
    Ma=[nan,nan,nan];
    return

end

alpha2=atan(U/Ca2-tan(beta2n));
C2=Ca2/cos(alpha2);
T2=T1*(A1/A2*Ca1/Ca2)^(gamma_air-1);
T02=T2+C2^2/(2*cp_air);

```

```

% stator -----
-----
%  $Ca3^{(12/5)} + b1*Ca3^{(2/5)} + b2 = 0$ 
b1=-2*cp_air*T02*cos(alpha3n)^2;
b2=2*cp_air*T2*cos(alpha3n)^2*(Ca2*A2/A3)^(gamma_air-1);

Xa3_solns=roots([1,0,0,0,0,b1,b2]); % re-map:
Xa3^6+b1*Xa3+b2=0 with Xa3=Ca3^(2/5)
Ca3_solns=Xa3_solns.^(5/2);
Ca3_solns=Ca3_solns(find(imag(Ca3_solns)==0)); % keep only real
solutions

[deltaC,index]=min(abs(Ca3_solns-Ca1)); % extract Ca3 solution
(the closest value to Ca1)
Ca3=Ca3_solns(index);

if isempty(Ca3)==1

    Ca3=nan;
    alpha3=nan;
    T03=nan;
    P03=nan;
    TQ=nan;
    psi=nan;
    phi=nan;
    Ma=[nan,nan,nan];
    return

end

alpha3=alpha3n;
C3=Ca3/cos(alpha3);
T3=T2*(A2/A3*Ca2/Ca3)^(gamma_air-1);
T03=T3+C3^2/(2*cp_air); % identically T03=T02

% isentropic stage efficiency
eta=1-0.6*abs(betal1-betal_cn)/betal_cn;

% stator exit pressure
P03=P01*(eta*(T03/T01-1)+1)^(gamma_air/(gamma_air-1));

% absolute mach numbers
Ma(1)=C1/sqrt(gamma_air*R_air*T1);
Ma(2)=C2/sqrt(gamma_air*R_air*T2);
Ma(3)=C3/sqrt(gamma_air*R_air*T3);

```

Inlet Guide Vane Stage

```

function [Ca2,alpha2,T02,P02,Ma2]=igv_stage(P01,T01,mdot)

global cp_air gamma_air R_air

```

```

global alpha1_in alpha2_in
global A1_i A2_i

alpha2=alpha2_in; % igv flow exit angle

T02=T01; % igv does no work
P02=P01;

% Ca2^(12/5) + b1*Ca2^(2/5) + b2 = 0
b1=-2*cp_air*T02*cos(alpha2)^2;
b2=2*cp_air*cos(alpha2)^2*(T02^gamma_air)*(mdot*R_air/(P02*A2_i))^(gamma
a_air-1);

Xa2_solns=roots([1,0,0,0,0,b1,b2]);
% re-map: Xa2^6+b1*Xa2+b2=0 with Xa2=Ca2^(2/5)
Ca2_solns=Xa2_solns.^(5/2);
Ca2_solns=Ca2_solns(find(imag(Ca2_solns)==0));
% keep only real solutions

[deltaC,index]=min(abs(Ca2_solns));
Ca2=Ca2_solns(index);

if isempty(Ca2)==1

    Ca2=nan;
    Ma2=nan;
    T02=nan;
    P02=nan;
    return

end

C2=Ca2/cos(alpha2);
T2=T02-C2^2/(2*cp_air);

% igv exit mach number
Ma2=C2/sqrt(gamma_air*R_air*T2);

```

Exit Guide Vanes

```

function [Ca2,alpha2,T02,P02,Ma2]=egv_stage(P01,T01,mdot)

global cp_air gamma_air R_air
global alpha1_en alpha2_en
global A1_e A2_e

if isnan(P01)==1

    Ca2=nan;
    alpha2=nan;
    T02=nan;
    P02=nan;

```



```

    Ma2=nan;
    return

end

alpha2=alpha2_en; % egv flow exit
angle

T02=T01; % egv does no work
P02=P01;

% Ca2^(12/5) + b1*Ca2^(2/5) + b2 = 0
b1=-2*cp_air*T02*cos(alpha2)^2;
b2=2*cp_air*cos(alpha2)^2*(T02^gamma_air)*(mdot*R_air/(P02*A2_e))^(gamma
a_air-1);

Xa2_solns=roots([1,0,0,0,0,b1,b2]);
% re-map: Xa2^6+b1*Xa2+b2=0 with Xa2=Ca2^(2/5)
Ca2_solns=Xa2_solns.^(5/2);
Ca2_solns=Ca2_solns(find(imag(Ca2_solns)==0));
% keep only real solutions

[deltaC,index]=min(abs(Ca2_solns));
Ca2=Ca2_solns(index);

if isempty(Ca2)==1

    Ca2=nan;
    Ma2=nan;
    T02=nan;
    P02=nan;
    return

end

C2=Ca2/cos(alpha2);
T2=T02-C2^2/(2*cp_air);

% egv exit mach number
Ma2=C2/sqrt(gamma_air*R_air*T2);

```

Single Path Continuously Variable Transmission System Model

```

function [sys,x0,str,ts] = Single_Path_CVT_Plant(t,x,u,flag)

%%%%%%%%%%%%%%%%%%%%%%%%%%%%%%%%%%%%%%%%%%%%%%%%%%%%%%%%%%%%%%%%%%%%%%%%
global dr rd rs2hz hz2rs rs2rpm rpm2rs m2ft ft2m m2in in2m in2mil
mil2in m2mil mil2m mil2um um2mil m2um um2m
global hp2w w2hp knots2ms ms2knots lbf2kg kg2lbf lbf2n n2lbf ftlb2nm
nm2ftlb m2mm mm2m psi2pa pa2psi
global gaccel p_AL E_AL G_AL v_AL SMAX_AL p_FE E_FE G_FE v_FE SMAX_F

```

```

global J_pt Jg1 Jg2 JMR ni nf ks1 ks2 viscs OMEGA_ptn
global ph1_0 ph2_0
%%%%%%%%%%%%%%%%%%%%%%%%%%%%%%%%%%%%%%%%%%%%%%%%%%%%%%%%%%%%%%%%%%%%%%%%

switch flag,

    % Initialization:
    % Return the sizes, initial conditions, and sample times for the S-
    function.
    case 0,

        sizes=simsizes;
        sizes.NumContStates = 6;           % number of continuous states,
        x=[pe;ph1;ph2;ped;ph1d;ph2d]
        sizes.NumDiscStates = 0;          % number of discrete states
        sizes.NumOutputs = 6;             % number of outputs,
        y=[pMR;ph1;ph2;pMRd;ph1d;ph2d]
        sizes.NumInputs = 4;              % number of inputs,
        u=[TPT,ncvtd,ncvt,TMR]
            sizes.DirFeedthrough = 0;      % direct feedthrough flag
            sizes.NumSampleTimes = 1;

        sys = simsizes(sizes);

        x0=[0 -ph1_0 -ph2_0 OMEGA_ptn 0 0]'; % initial conditions

        str = [];
        ts = [0 0];                        % sample time

        % Derivatives
        % Return the derivatives for the continuous states.

    case 1,
        % Inputs
        TPT=u(1);                            % Engine torque, N-m
        ncvtd=u(2);                           % CVT Shift Rate, ncvtd=dnvtd/dt
        ncvt=u(3);                             % CVT Speed Ratio, ncvt=W1/W0
        TMR=u(4);                              % Rotor Load Torque, N-m

        % Coordinates & velocities
        q=x([1:3],1);                          % q=[pPT;ph1;ph2]
        qd=x([1:3]+3,1);                       % qd=[pPTd;ph1d;ph2d]

        % System Matricies
        JLa=Jg2+JMR*nf^2;
        JLa=Jg1+JLa*ncvt^2;

        M=[J_pt+JLb*ni^2                ni*JLb                JMR*nf^2*ni*ncvt
           ni*JLb                       JLb                    JMR*nf^2*ncvt
           JMR*nf^2*ni*ncvt             JMR*nf^2*ncvt         JMR*nf^2];

        Cnd=ncvtd*[2*JLa*ni^2*ncvt      2*JLa*ni*ncvt      JMR*nf^2*ni
                  2*JLa*ni*ncvt         2*JLa*ncvt          JMR*nf^2];

```

```

                JMR*nf^2*ni                JMR*nf^2    0];

K=[0          0          0
   0          ks1       0
   0          0         ks2];

Csd=viscs*K;

F=[TPT-nf*ni*ncvt*TMR
   -nf*ncvt*TMR
   -nf*TMR];

% System Response
qdd=inv(M)*(-(Csd+Cnd)*qd-K*q+F);

% store xd
sys=[qd
     qdd];

% Outputs
% Return the block outputs.

case 3,
    sys=x;      % outputs

% Unhandled flags
case { 2, 4, 9 },
    sys=[];

% Unexpected flags
otherwise
    error(['Unhandled flag = ',num2str(flag)]);

end

```

Physical constants

```

function physicalconst

%%%%%%%%%%%%%%%%%%%%%%%%%%%%%%%%%%%%%%%%%%%%%%%%%%%%%%%%%%%%%%%%%%%%%%%%
%%%%%%%%%%%%%%%%%%%%%%%%%%%%%%%%%%%%%%%%%%%%%%%%%%%%%%%%%%%%%%%%%%%%%%%%
% Define physical constants. All values in SI units.
%
%%%%%%%%%%%%%%%%%%%%%%%%%%%%%%%%%%%%%%%%%%%%%%%%%%%%%%%%%%%%%%%%%%%%%%%%
%%%%%%%%%%%%%%%%%%%%%%%%%%%%%%%%%%%%%%%%%%%%%%%%%%%%%%%%%%%%%%%%%%%%%%%%
global gaccel
global p_AL E_AL G_AL v_AL SMAX_AL
global p_FE E_FE G_FE v_FE SMAX_FE
global p_kapton E_kapton G_kapton v_kapton CTE_kapton SMAX_kapton
global p_pvdf E_pvdf G_pvdf v_pvdf SMAX_pvdf
global p_air cp_air R_air gamma_air

```

%%
%%

% Acceleration of Gravity
gaccel=9.81; % m/sec^2

% Material Properties -----

% Aluminum (Alloy 2014-T6)
p_AL=2800; % Density, kg/m^3
E_AL=75*1e9; % Elastic Modulus, N/m^2
G_AL=27*1e9; % Shear Modulus, N/m^2
v_AL=E_AL/(2*G_AL)-1; % Poission's Ratios
SMAX_AL=230*1e6; % Yield Shear Stress, N/m^2

% Steel (ASTM-A242)
p_FE(1)=7870; % Density, kg/m^3
E_FE(1)=200*1e9; % Elastic Modulus, N/m^2
G_FE(1)=77*1e9; % Shear Modulus, N/m^2
v_FE(1)=E_FE(1)/(2*G_FE(1))-1; % Poission's Ratios
SMAX_FE(1)=205*1e6; % Yield Shear Stress, N/m^2

% Steel (ANSI-302, Stainless)
p_FE(2)=7920; % Density, kg/m^3
E_FE(2)=190*1e9; % Elastic Modulus, N/m^2
G_FE(2)=75*1e9; % Shear Modulus, N/m^2
v_FE(2)=E_FE(2)/(2*G_FE(2))-1; % Poission's Ratios
SMAX_FE(2)=150*1e6; % Yield Shear Stress, N/m^2

% Kapton
p_kapton=1420; % Density, kg/m^3
E_kapton=2.5*1e9; % Elastic Modulus, N/m^2
G_kapton=0.93*1e9; % Shear Modulus, N/m^2
v_kapton=0.34; % Poission's Ratios
CTE_kapton=20e-6; % Coefficient of thermal expansion,
ppm/C
SMAX_kapton=172*1e6; % Tension Yield Stress, N/m^2 **
was at 69 MPa but now using value from Jenkins pp. 19

% PVDF
p_pvdf=1780; % Density, kg/m^3
E_pvdf=2.27*1e9; % Elastic Modulus, N/m^2
G_pvdf=0.69*1e9; % Shear Modulus, N/m^2
v_pvdf=0.225; % Poission's Ratios
SMAX_pvdf=41*1e6; % Tension Yield Stress, N/m^2 **

% Air
p_air=1.225; % Density, kg/m^3
cp_air=1.005*1e3; % specific heat (constant
pressure), J/(kg*K)
R_air=0.286*1e3; % ideal gas constant, J/(kg*K)
gamma_air=1.4; % specific heat ratio, cp/cv

Continuously Variable Speed Rotorcraft Propulsion Model

```

clear all
format long g

%%%%%%%%%%%%%%%%%%%%%%%%%%%%%%%%%%%%%%%%%%%%%%%%%%%%%%%%%%%%%%%%%%%%%%%%
%%%%%%%%
%
% Gas Turbine Engine: Gas-Generator/Power Turbine/Load
% Transient Model
%
%
% Station: 1      2      ___  3      ___  4      5      ___  6      7
%
% Pa,Ta  | \ | |___| |___| |___| | | |___| | Pa
%        | \ | "cp" | "cc" | | / | | "tp" | | / | |
% ----> | \ | |-----| | | | |-----| | JL, TL
%        | | |-----| | | | |-----| |
% ----> | / | | | | | | | | | | | | | |
%        | / | | | | | | | | | | | | |
%        | / | | | | | | | | | | | |
%
% "a"    "c"                                "ggt"    "pt"    "L"
%
%
% Element:                                Stations:
% "a"    == ambient
% "c"    == compressor (igv/comp/egv)    "1-2"
% "cp"   == compressor plenum           "2-3"
% "cc"   == combustion chamber          "3-4"
% "ggt"  == gas generator turbine        "4-5"
% "tp"   == turbine plenum              "5-6"
% "pt"   == power turbine                "6-7"
% "L"    == load
%
%%%%%%%%%%%%%%%%%%%%%%%%%%%%%%%%%%%%%%%%%%%%%%%%%%%%%%%%%%%%%%%%%%%%%%%%
%%%%%%%%

% conversion factors
global dr rd rs2hz hz2rs rs2rpm rpm2rs m2ft ft2m m2in in2m in2mil
mil2in m2mil mil2m mil2um um2mil m2um um2m m2mm mm2m
global hp2w w2hp knots2ms ms2knots lbf2kg kg2lbf lbf2n n2lbf ftlb2nm
nm2ftlb psi2pa pa2psi pa2atm atm2pa
global gaccel p_AL E_AL G_AL v_AL SMAX_AL p_FE E_FE G_FE v_FE SMAX_FE

```

```

% GTE paramaters
global cp_air R_air gamma_air lambda ga Pa Ta
% air
global Pr_cn eta_cn mdot_n A P0_n T0_n P_n T_n rho_n C_n Ca_n alpha_n
Ma_n eta_tn          % overall engine
global OMEGA_cn mdot_cn PWR_cn Rhr_c Rtr_c Rhs_c Rts_c Rm_c m_c J_c
% compressor
global OMEGA_ggtn mdot_ggtn PWR_ggtn Rt_ggt Rh_ggt Rm_ggt m_ggt J_ggt
% gas generator turbine
global OMEGA_ptn mdot_ptn PWR_ptn Rt_pt Rh_pt Rm_pt m_pt J_pt
% power turbine
global Pr_ccn LHV mfdot_n tau_cc
% combustion chamber
global Vol_cp Vol_tp
% plenum

global beta_cmap OMEGA_cmap mdot_cmap Pr_cmap eta_cmap
% compressor map
global OMEGA_data mdot_data Pr_c_data eta_c_data
global mdot_c_surge Pr_c_surge mdot_c_stonewall Pr_c_stonewall
global Nbeta beta_cmax beta_cmin beta_cnom
global mdot_plot pr_plot

global Jg1 Jg2 ni nf ks1 ks2 viscs

global J_pt JMR Rb sigma acL cD0 rho_air

global ph1_0 ph2_0

global vc_set vc_new vc_slope

% load conversion factors & physical constants
conversionfactors;
physicalconst;

% Two Spool GTE parameters (design, off-nominal & transient)
TwoSpoolGTE_params

% Compressor Beta Regulation
KI_beta=100/Pr_cn;          % integrator gain

% Engine Fuel Control
kp_fuel=1e-1;              % Proportional gain, N-m/(rad per
sec)
kd_fuel=0.01*kp_fuel;     % Derivative gain, N-m-sec/(rad per
sec)
ki_fuel=1e-1;             % Integrator gain, N-m/sec/(rad per
sec)

mfdot_min=0;              % min fuel rate
mfdot_max=mfdot_n*1.5;   % max fuel rate

```

```

% plots -----
----

if 1~=1
%figure(1),plot(mdot(:,1),P0(:,2)./P0(:,1),'k')
end

if 1~=1
% find operating line -----
----
'////////// now computing operating line //////////'

% operating point
PWR_LOAD=linspace(PWR_ptn,0.7*PWR_ptn,50);

options=optimset('MaxFunEvals',1000,'MaxIter',1000,'TolX',1e-
6,'TolFun',1e-6);

% optimset(Display, TolX, TolFun, MaxFunEvals, MaxIter.

X0=[OMEGA_cn,beta_cnom,mfdot_n];
for i = 1:length(PWR_LOAD)

    i
    PWR_L_ss=PWR_LOAD(i);
    [X,err(i)]=fminsearch(@fcn_gteop,X0,options,PWR_L_ss);
    X0=X;

    OMEGA_c_ss(i)=X(1);
    beta_c_ss(i)=X(2);
    mfdot_ss(i)=X(3);

mdot_ss(i)=interp2(beta_cmap,OMEGA_cmap,mdot_cmap,beta_c_ss(i),OMEGA_c_
ss(i));

Pr_c_ss(i)=interp2(beta_cmap,OMEGA_cmap,Pr_cmap,beta_c_ss(i),OMEGA_c_ss
(i));

eta_c_ss(i)=interp2(beta_cmap,OMEGA_cmap,eta_cmap,beta_c_ss(i),OMEGA_c_
ss(i));

end

end

```

```

% conversion factors & physical constants
conversionfactors;
physicalconst;

% engine -----

% closed-loop engine PID speed control gains

kp_fuel=9e-3; % Proportional gain, kg
kd_fuel=0.03*kp_fuel; % Derivative gain, kg-sec
ki_fuel=1e-2; % Integrator gain, kg/sec
kb_fuel=100; % anti-windup gain (back calculation gain)

% shafts and gearboxes -----
Jg1=5;
Jg2=5;

ni=1/1.87;
nb=1/4;
nf=1/37;

viscs=1e-5;

ks1=40000;
ks2=40000;

% main rotor -----
ncvt_n=1;
WR_n=OMEGA_ptn*(ni*ncvt_n*nf); % nominal rotor speed, rad/sec
cd_n=PWR_ptn/WR_n^3; % nominal rotor drag
OMEGA_at_ks1=OMEGA_ptn*ni;
Torque_at_ks1=PWR_ptn/OMEGA_at_ks1;
OMEGA_at_ks2=OMEGA_ptn*ni*ncvt_n;
Torque_at_ks2=PWR_ptn/OMEGA_at_ks2;
ph1_0=Torque_at_ks1/ks1;
ph2_0=Torque_at_ks2/ks2;

%main Rotor
MainRotor_params;

rho_air=1.225; % Density, kg/m^3
Aw=1001*ft2m^2;
CD=0.0267;
CD0w=0.012/4;
mv=107500*1bf2kg; % vehicle mass, kg (based on gross vehicle weight)

```



```

teta_p_initial=5*dr;
vc_initial=200*knots2ms;

% Forward Speed Control (blade pitch control, regulating horizontal
velocity)
kp_pitch=0.125/6;
ki_pitch=0.001;
kd_pitch=0.001;

th_pitch_min=-8*dr;
th_pitch_max=8*dr;

close all

figure(15),plot(mdot_data,Pr_c_data,'b'), hold on
figure(15),plot(mdot_c_surge,Pr_c_surge,'--k','LineWidth',2), hold on
figure(15),plot(mdot_n,Pr_cn,'r*'), hold on
figure(15),plot(mdot_plot,pr_plot,'k'), hold on

%CASESSSSSSSSSSSS-----

%.....
vc_set_initial=200*knots2ms;
vc_new=225*knots2ms;

t1=25;
t2=40;
DeltaT=t2-t1;
vc_slope1=(vc_new-vc_set_initial)/(t2-t1);
%vc_slope1=0;

ton_downshift=25;    %start of downshift
ton_upshift=60;     %start of upshift

ncvt_init_downshift=1;
ncvt_final_downshift=0.75;

t3=60;
t4=75;
vc_slope2=(vc_set_initial-vc_new)/(t4-t3);

nd_value=(ncvt_final_downshift-ncvt_init_downshift)/DeltaT;

```

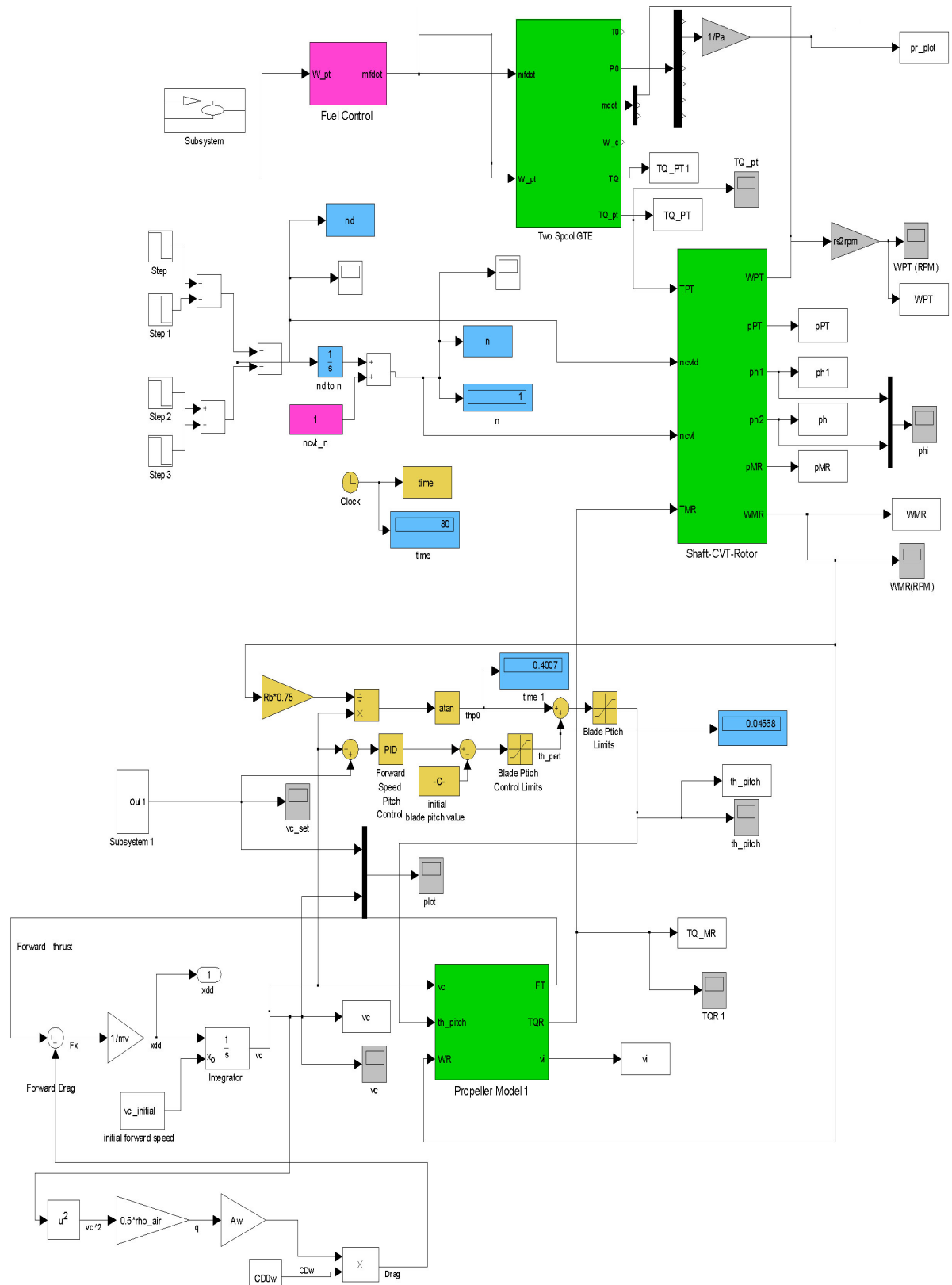
```
toff_downshift=ton_downshift+DeltaT;      %end of shifting
toff_upshift=ton_upshift+DeltaT;

ncvt_init_upshift=0.75;
ncvt_final_upshift=1.;

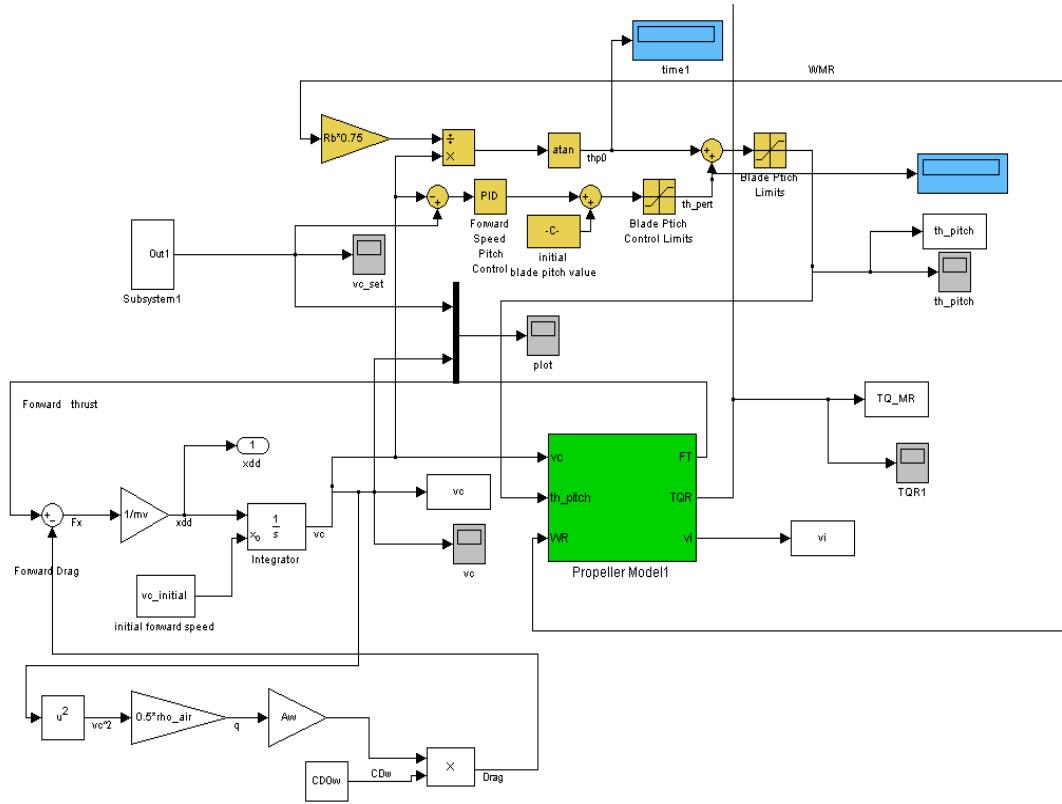
TT=80;

% save 10_trial_const_nd.mat
```

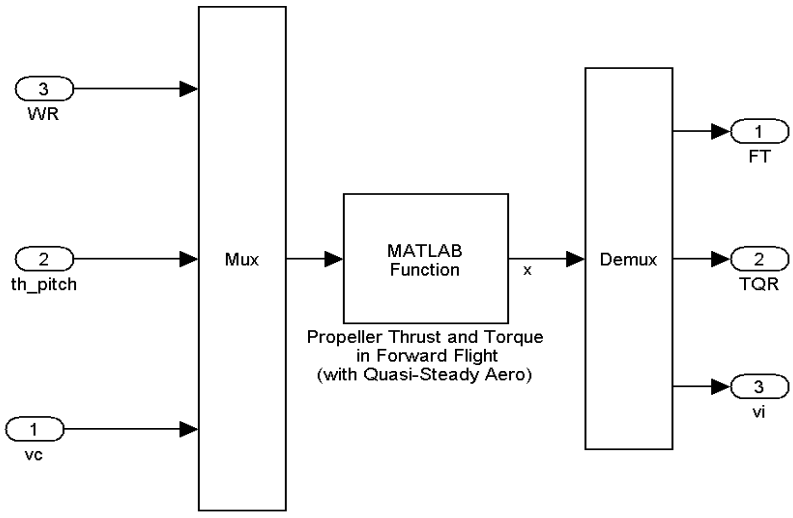
SIMULINK MODELS



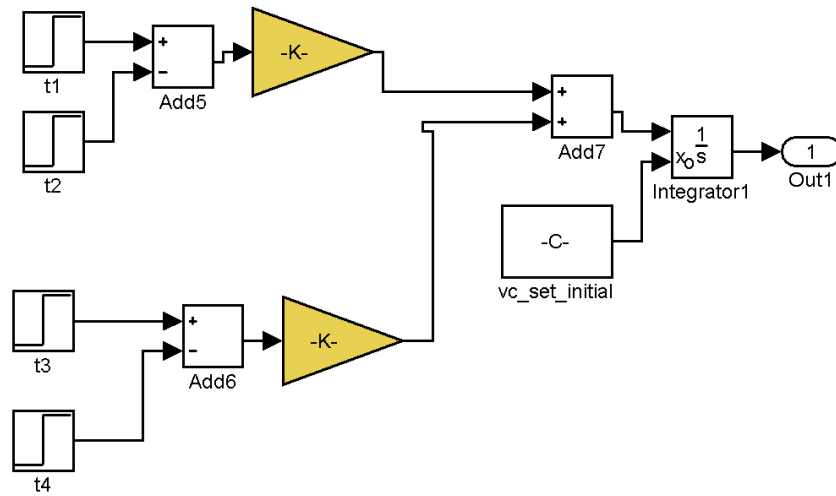
CVSRPM with a complete flight control block



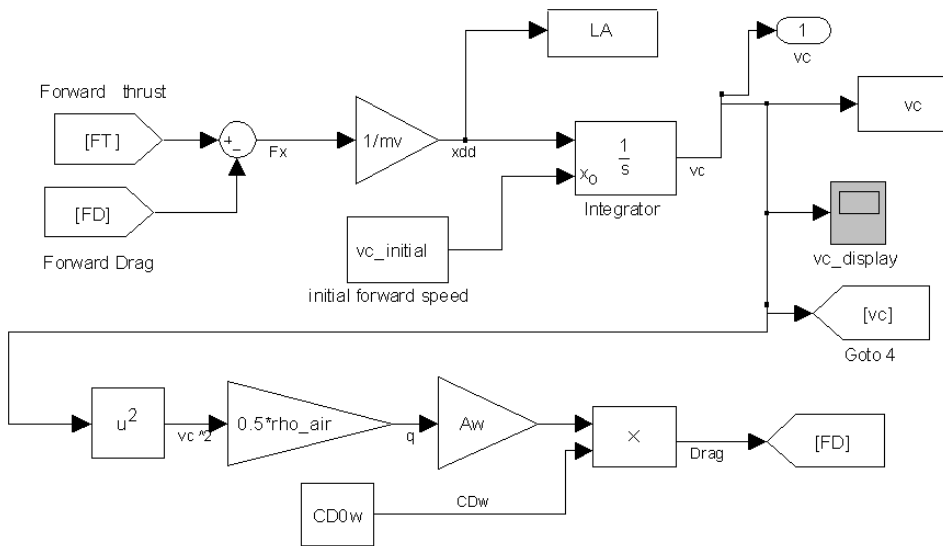
Forward speed subsystem and trim control in a propeller block



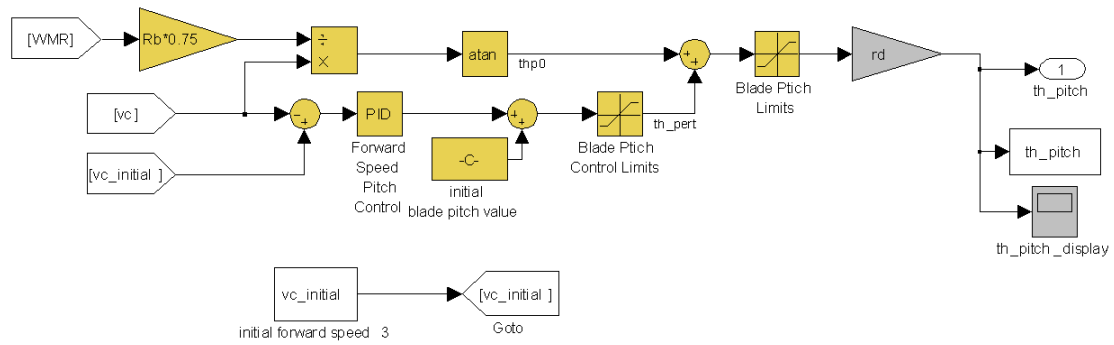
Propeller Block



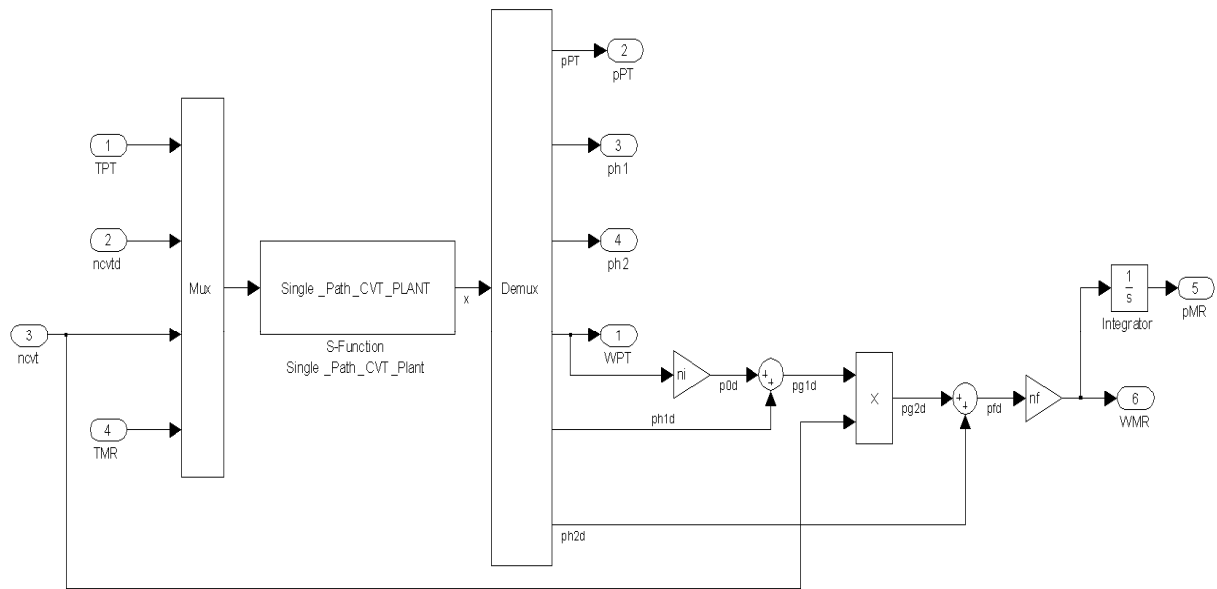
Set point speed subsystem block



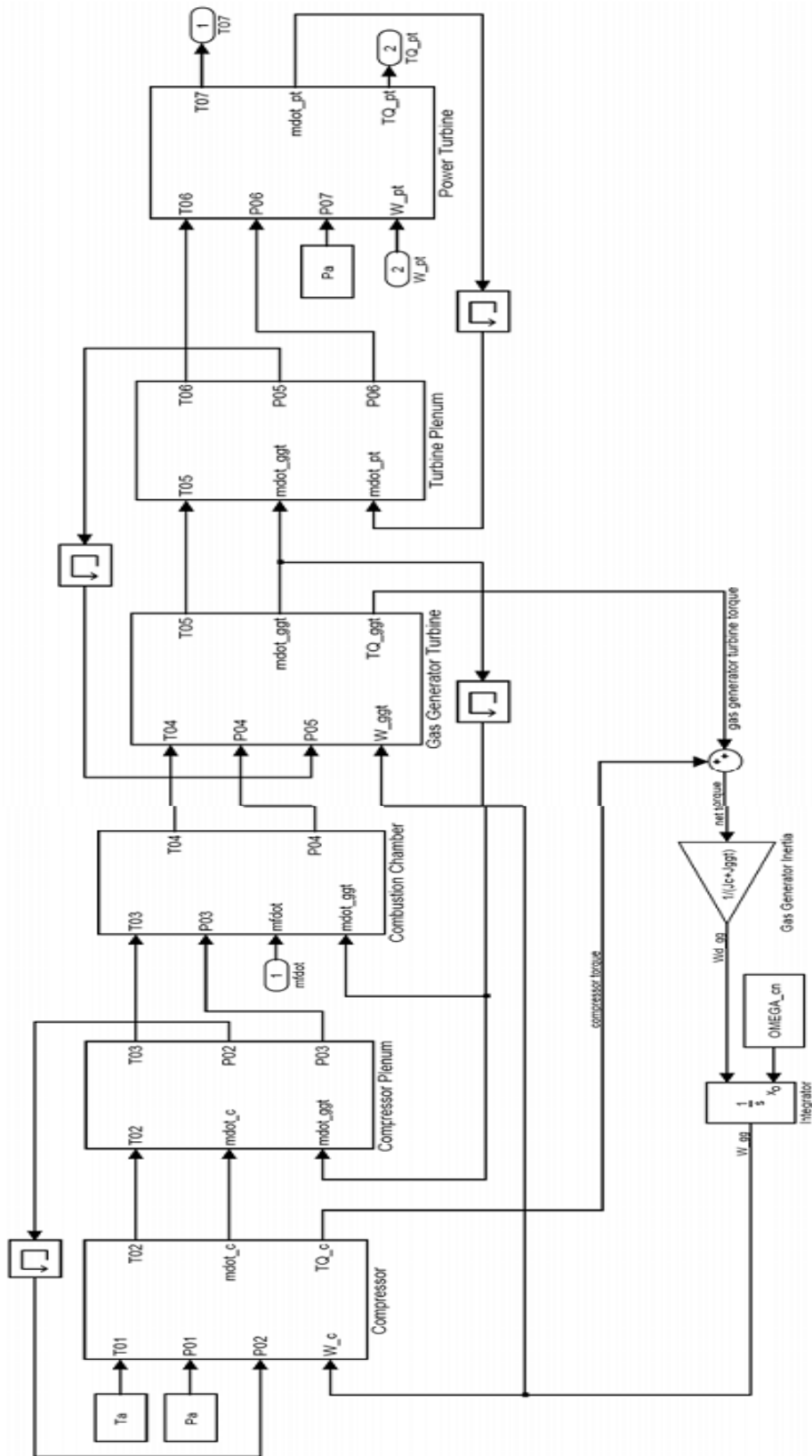
Forward Speed Controller Block



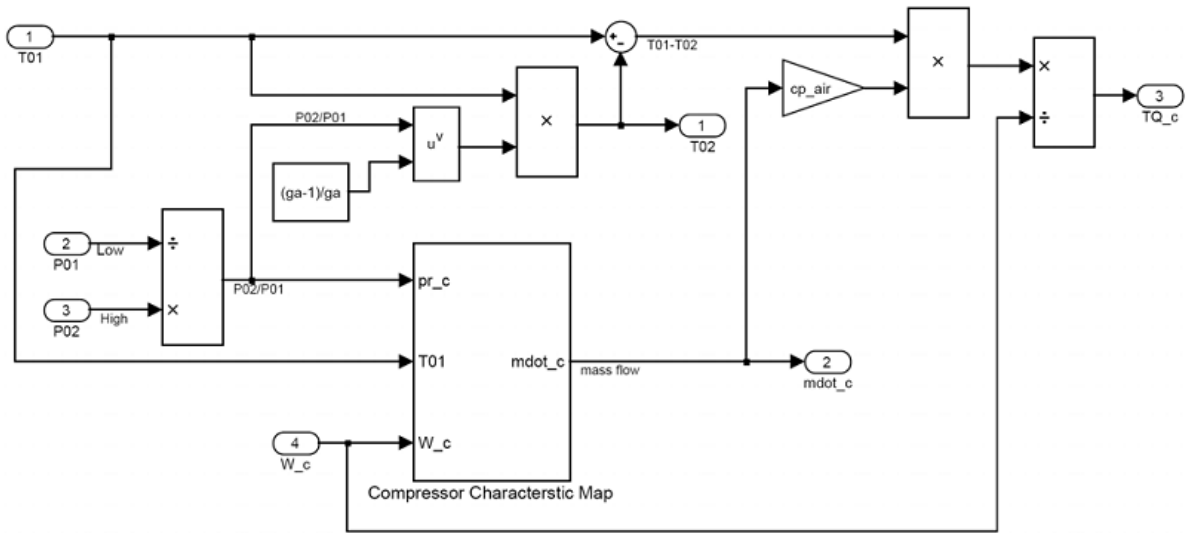
Theta pitch Controller Block



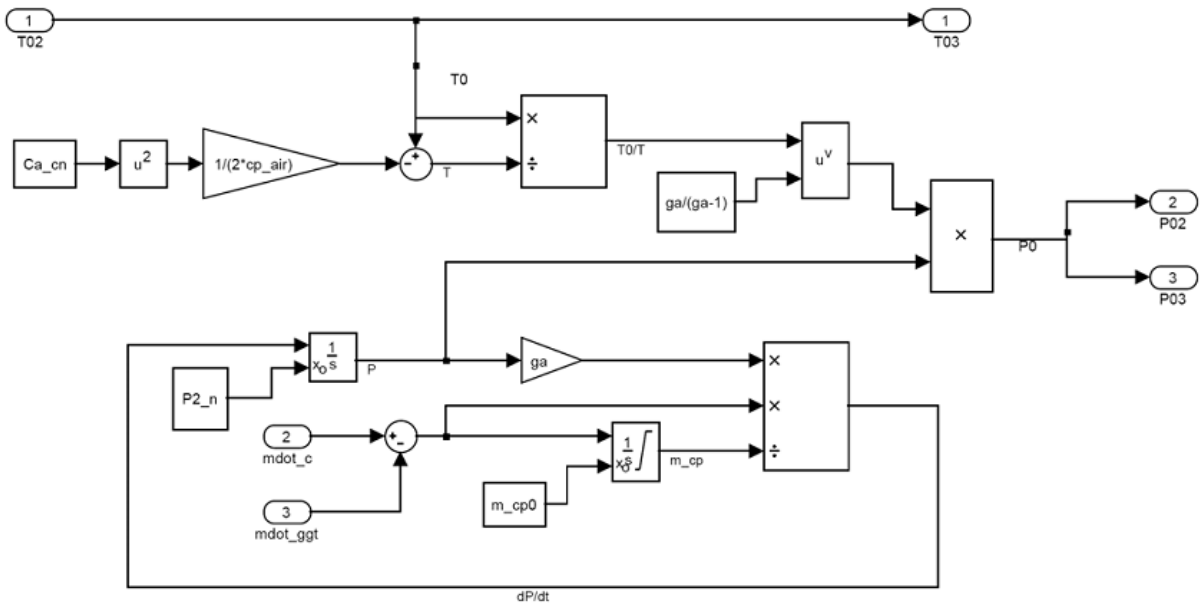
Continuously variable transmission block



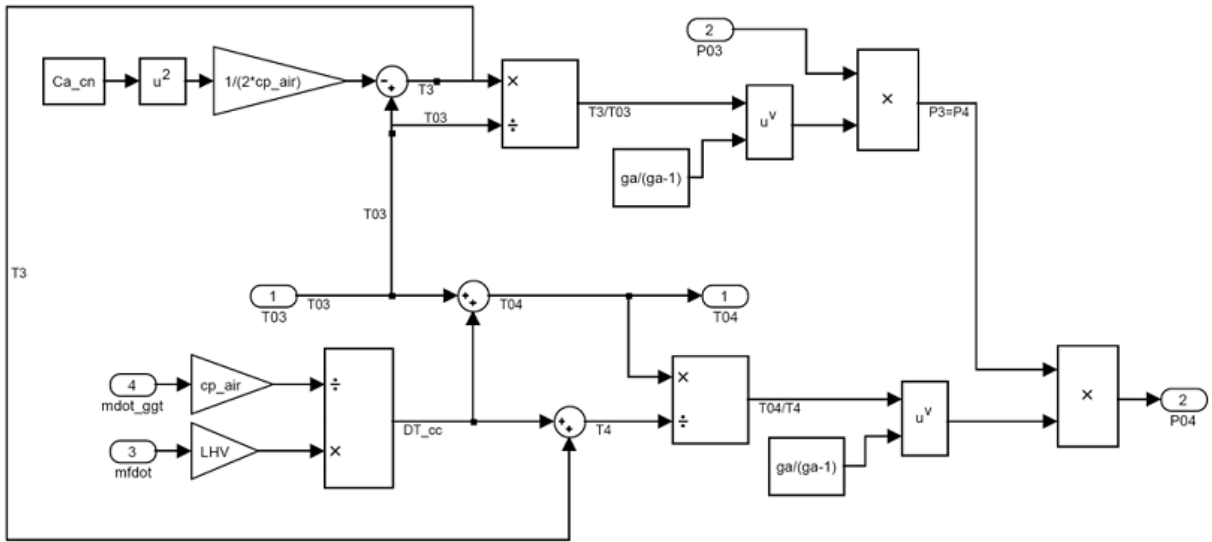
Two Spool gas turbine engine simulation block



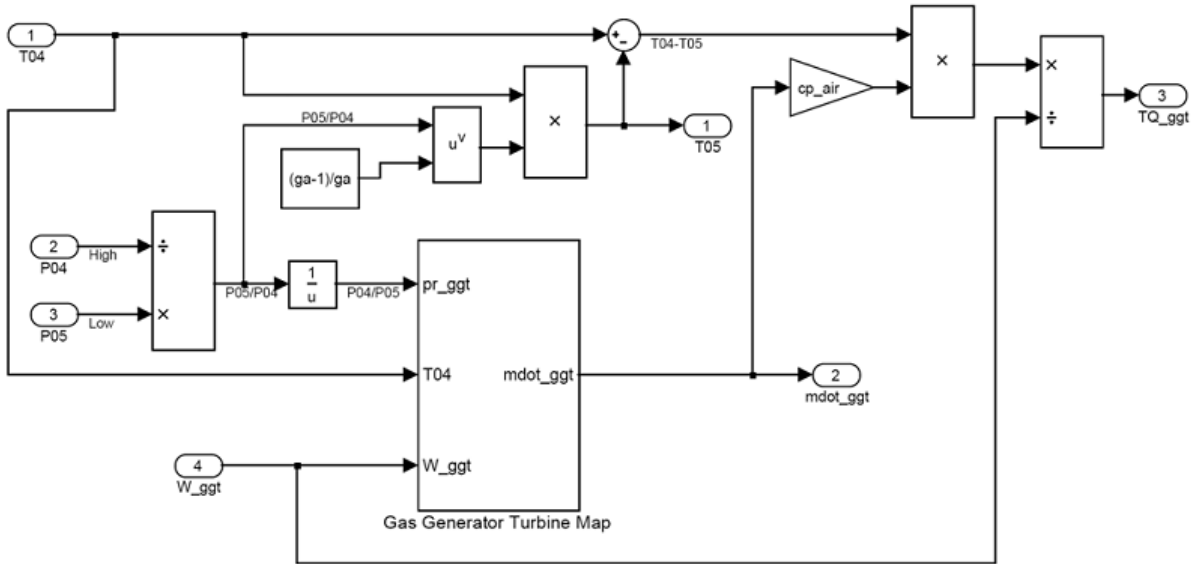
Compressor Simulation Block



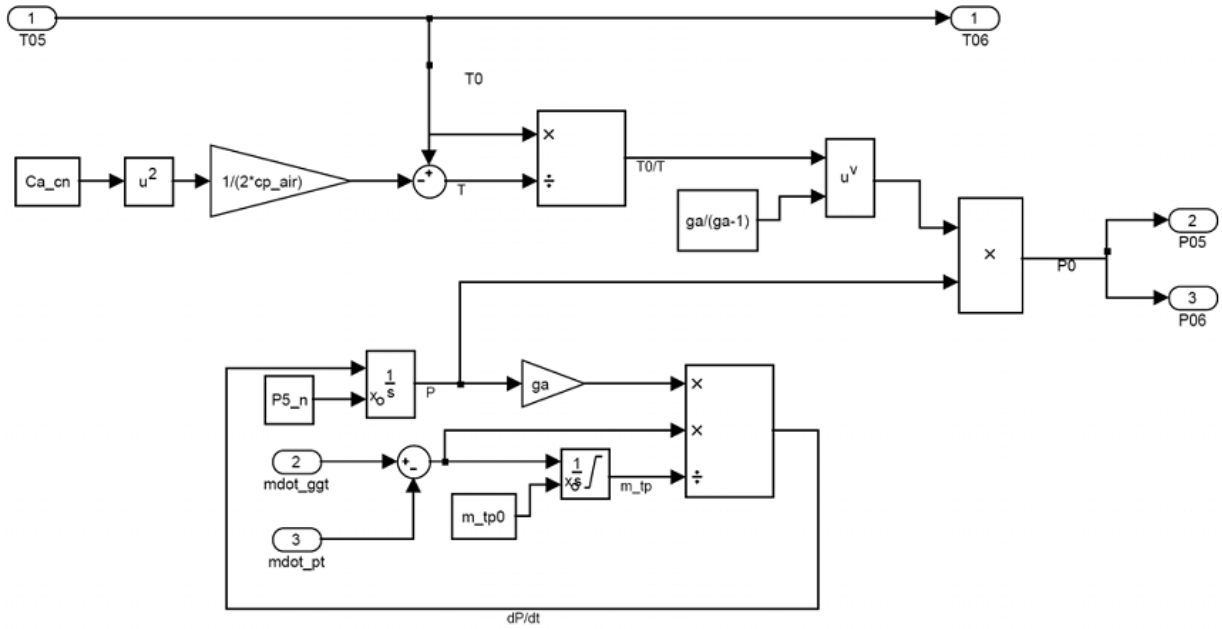
Inter compressor/combustion chamber plenum



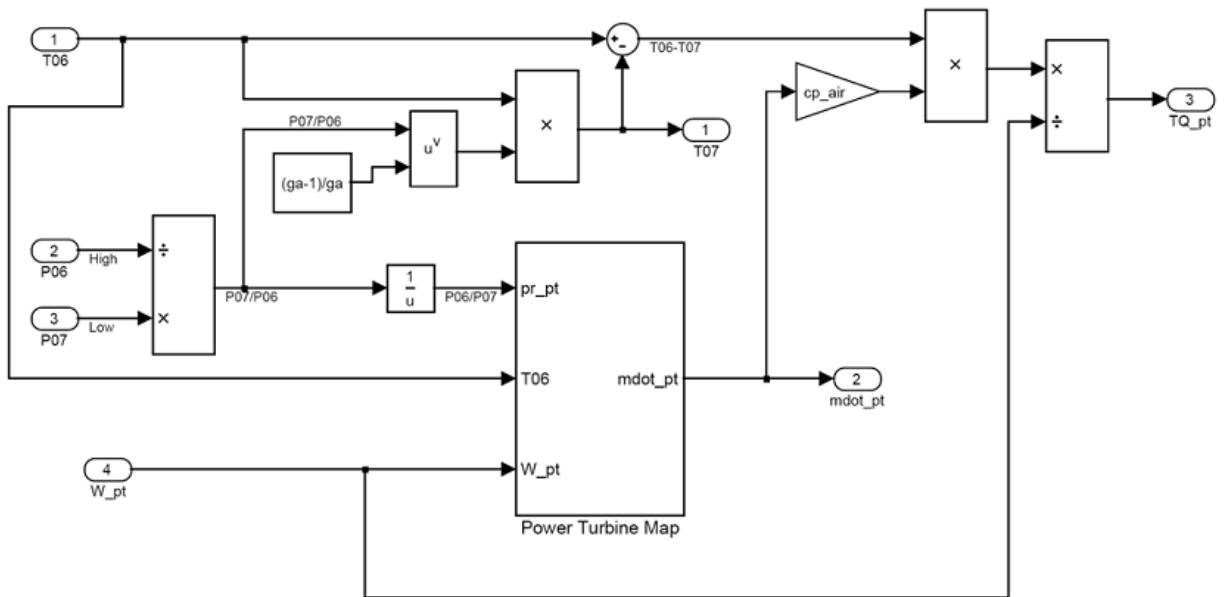
Combustion chamber simulation block



Gas generator turbine simulation block



Inter turbine plenum



Power turbine simulation block

VITA

Naveen Kumar Vallabhaneni was born in Avanigadda a small town in Andhra Pradesh, India on December 19, 1987. He is son of V.Satyanarayana Rao and Radha Yanamadala. He grew up in Hyderabad, capital of Andhra Pradesh state where he attended primary and secondary schools. He then went to the Jawaharlal Nehru Technological University in Hyderabad, where he graduated with a Bachelor of Science degree in Aeronautical Engineering in May 2008 being a summa cum laude. In August of 2008, he entered the Aerospace Engineering program at the University of Tennessee, Knoxville for his graduate studies. He will conclude his Master of Science degree in Aerospace Engineering in August 2011.